Aus dem Zentrum für Innere Medizin der Universität zu Köln

Klinik und Poliklinik für Innere Medizin I

Direktor: Universitätsprofessor Dr. med. M. Hallek

An autochthonous mouse model of *Myd88*- and *BCL2*-driven diffuse large B-cell lymphoma reveals actionable molecular vulnerabilities

Ein autochthones Mausmodell des *Myd88*- und *BCL2*-getriebenen diffusen großzelligen B-Zell Lymphoms zeigt relevante molekulare Vulnerabilitäten

Inaugural-Dissertation zur Erlangung der Doktorwürde

der Medizinischen Fakultät

der Universität zu Köln

vorgelegt von

Tim Rehkämper

aus Düsseldorf

promoviert am 11. August 2022

Dekan:　　　　Universitätsprofessor Dr. med. G. R. Fink
1. Gutachter:　Universitätsprofessor Dr. med. H. C. Reinhardt
2. Gutachter:　Universitätsprofessor Dr. med. R. Thomas
3. Gutachter:　Privatdozent Dr. med. U. Schnetzke

Erklärung
Ich erkläre hiermit, dass ich die vorliegende Dissertationsschrift ohne unzulässige Hilfe Dritter und ohne Benutzung anderer als der angegebenen Hilfsmittel angefertigt habe; die aus fremden Quellen direkt oder indirekt übernommenen Gedanken sind als solche kenntlich gemacht.[1]

Bei der Auswahl und Auswertung des Materials sowie bei der Herstellung des Manuskriptes habe ich Unterstützungsleistungen von folgenden Personen erhalten:

Universitätsprofessor Dr. med. Hans Christian Reinhardt

Weitere Personen waren an der Erstellung der vorliegenden Arbeit nicht beteiligt. Insbesondere habe ich nicht die Hilfe einer Promotionsberaterin/eines Promotionsberaters in Anspruch genommen. Dritte haben von mir weder unmittelbar noch mittelbar geldwerte Leistungen für Arbeiten erhalten, die im Zusammenhang mit dem Inhalt der vorgelegten Dissertationsschrift stehen.

Die Dissertationsschrift wurde von mir bisher weder im Inland noch im Ausland in gleicher oder ähnlicher Form einer anderen Prüfungsbehörde vorgelegt.

Die Experimente, die dieser Arbeit und der Publikation zu Grunde liegen, sind im größten Teil von Dr. rer. nat. Gero Knittel, Dr. med. Ruth Flümann, Pascal Nieper und mir unter der Supervision durch Universitätsprofessor Dr. med. Hans Christian Reinhardt durchgeführt worden.

Im Folgenden ist dargestellt, welche wesentlichen Beiträge ich in der täglichen Betreuung des Projektes geleistet habe:

Am Anfang des Projektes betreute ich die MRT Studien (Abbildung 1B,C) sowie die durchflusszytometrische Charakterisierung der B-Zell Subspezies (Figure 1D-F).
Im Folgenden lag mein Hauptverantwortungsbereich in der Betreuung der $Cd19^{Cre/wt}$ (C)-, $Cd19^{Cre/wt};Myd88^{c-p.L252P/wt}$ (MC)- und $Cd19^{Cre/wt;}Rosa26^{LSL.BCL2.IRES.GFP/wt};Myd88^{c-p.L252P/wt}$ (MBC)-Mäuse. Neben Sichtkontrollen, Zuchtstrategie und -organisation war meine Hauptaufgabe die autoimmunologische, durchflusszytometrische und immunhistochemische Charakterisierung der Phänotypen zu unterschiedlichen Zeitpunkten (Abbildung 2 A-D).
Darüber hinaus war es meine Aufgabe, die terminalen Phänotypen histologisch und immunhistochemisch zu charakterisieren (Abbildung 4 A-D) und Zelllinien für Compound-Screens (Abbildung 5 A-G) und das Transplantationsmodell (Abbildung 4 F) zu generieren (Abbildung 4 A-C, Zelllinien aus Abbildung 6).
Weiterführend etablierte ich durch MRT-Studien den Startpunkt für eine Behandlung der Mausmodelle und war an der Durchführung der Behandlung beteiligt (Abbildung 6 D-F).
An der Diskussion der Befunde in der Arbeitsgruppe mit Blick auf die Fragestellung war ich maßgeblich beteiligt.

Köln, den 20.04.2021

Unterschrift: ....

[1]Bei kumulativen Promotionen stellt nur die eigenständig verfasste Einleitung und Diskussion die Dissertationsschrift im Sinne der Erklärung gemäß dieser Erklärung dar.

Erklärung zur guten wissenschaftlichen Praxis:
Ich erkläre hiermit, dass ich die Ordnung zur Sicherung guter wissenschaftlicher Praxis und zum Umgang mit wissenschaftlichem Fehlverhalten (Amtliche Mitteilung der Universität zu Köln AM 132/2020) der Universität zu Köln gelesen habe und verpflichte mich hiermit, die dort genannten Vorgaben bei allen wissenschaftlichen Tätigkeiten zu beachten und umzusetzen.

Köln, den 20.04.2021

Unterschrift: ....

Acknowledgements

I would like to thank the following people, without whom I would not have been able to complete this dissertation.

First, I would like to thank my dissertational thesis advisor Universitätsprofessor Dr. med. Hans Christian Reinhardt for his enthusiasm for this project, for his support, encouragement and guidance reaching beyond this project.

I would also like to say a special thank you to Dr. rer. nat. Gero Knittel for teaching me a lot throughout my dissertation, for his continued support and for making the work more enjoyable.

My biggest thanks to my parents, Ursula von Lewicki-Rehkämper and Universitätsprofessor Dr. rer. nat. Gerd Rehkämper, who always supported me so tirelessly over so many years and in so many ways.

Special thanks to my brother, Dr. med. Jan Rehkämper, for his valuable advice and for always helping me out.

Lastly, I would like to thank my wife Friederike Rehkämper, thanks for all her unconditional support, her patience and her encouragement in the last very intense years.

Inscription

Table of Contents

I   Abbreviations

3´ UTR	Three prime untranslated region
ABC	Activated B-cell-like
AKT	Serine-threonie protein kinase
ATM	Ataxia-telangiectasia mutated
ATP	Adenosintriphosphat
B-NHL	B-cell non-Hodgkin's lymphoma
BAK	A member of the bcl-2 family
BAX	A member of the bcl-2 family
BCL-$_{XL}$	Synonym for BCL2L1, standing for BCL2-like 1
BCL10	B-cell CLL/lymphoma 10
BCL2	B-cell CLL/lymphoma 2
BCL6	B-cell CLL/lymphoma 6
BCR	B-cell receptor
BCR-ABL1	Breakpoint cluster region protein-Abelson murine leukemia oncogene
BH3	Bcl2 homology domain 3
BID 3	BH3 interacting domain death agonist
BIM	Synonym for BCL2L11, BCL2-like 11
BL	Burkitt's lymphoma
BLIMP1	B-lymphocyte maturation protein 1 (transcriptional repressor, encoded by PRDM1)
BRCA1	Breast and ovarian cancer susceptibility genes 1
BRCA2	Breast and ovarian cancer susceptibility genes 2
BTK	Bruton's tyrosine kinase
bTrCP	Beta-transducin repeat containing protein
CAGS	Cytomegalovirus early enhancer/chicken βactin
CARD11	Caspase recruitment domain family member 11
CD10	Cluster of differentiation 10
CD19	Cluster of differentiation 19
CD79B	Cluster of differentiation 79 B
cFLIP	Cellular FADD-like IL-1β-converting enzyme inhibitory protein
cIAP1	Cellular inhibitor of apoptosis 1
cIAP2	Cellular inhibitor of apoptosis 2
CLL	Chronic lymphocytic leukemia
DAG	Diacylglycerol
DLBCL	Diffuse large B cell lymphoma
DTX1	Deltex E3 ubiquitin ligase 1
EGFR	Epidermal growth factor receptor
EZH2	Enhancer of zeste homolog 2
FL	Follicular lymphoma
FOXP1	Forkhead box P1
GCB	Geminal center B cell-like
GCET1	Germinal center B-cell expressed transcript 1

GEP	Gene expression profiling
GNA13	G protein subunit alpha 13
HCL	Hairy cell leukemia
HCV	Hepatitis C
hGHpA	Human Growth Hormone poly-adenylation
HL	Hodgkin´s lymphoma
Ig	Immunoglobulin
IgA	Immunoglobulin A
IgE	Immunoglobulin E
IgG	Immunoglobulin G
IgM	Immunoglobulin M
IkBa	Inhibitor of NFκB subunit a
IKK	IκB kinase
IRAK	IL1-Receptor-associated kinases
IRES-GFP	Internal ribosomal entry site-Green fluorescent protein
ITAM	Immunoreceptor tyrosine-based activation motif
JNK	c-Jun NH2-terminal kinase
Kmt2d	Histone-lysine N-methyltransferase 2D
MALT	Mucosa-associated lymphoid tissue
MALT1	Mucosa-associated lymphoid tissue lymphoma translocation protein 1
MAPK	Mitogen activated protein kinase
MCL	Mantle cell lymphoma
MDM2	Mouse double minute 2 homolouge
MUM1	Multiples Myelom-Onkogen-1
Myc	Myelocytomatosis oncogene
MYD88	Myeloid differentiation primary response gene 88
NFkB	Nuclear factor kappa-B
Nfkbia	NFκB Inhibitor Alpha
NHL	Non-Hodgkin´s lymphoma
NOXA	Phorbol-12-myristate-13-acetate-induced protein 1
p100	Precursor of p52NFKB2
p38	Mitogen-Activated Protein Kinase P38
p50^{NFKB1}	NFkB-subunit
p52	NFkB-subunit
p52^{NFKB2}	NFkB-subunit
p65^{RelA}	NFkB-subunit
PARP1	Poly(ADP-ribose) polymerase
PD-1	Programmed cell death protein 1
PD-L1	Programmed death-ligand 1
PENL	Primary extranodal lymphomas
PI3K	Phosphatidylinositol-4,5-bisphosphate 3-kinase
Pim1	Pim-1 Proto-Oncogene
PKCβ	Protein kinase Cβ

PLCγ	1-Phosphatidylinositol-4,5-bisphosphate phosphodiesterase gamma
PMBL	Primary mediastinal B-cell lymphoma
Pouf2f	Member of the POU transcription factor family
PRDM1	PR domain zinc finger protein 1
PUMA	p53 upregulated modulator of apoptosis
R-CHOEP	Rituximab, Cyclophosphamid, hydroxydaunorubicin, vincristin (oncovin), etoposide, prednisolone
R-CHOP	Rituximab, Cyclophosphamid, hydroxydaunorubicin, vincristin (oncovin) prednisolone
RAG	Recombination activating gene
Rag1	Recombination activating gene 1
RelB	NFkB-subunit
SGK1	Serum and glucocorticoid-regulated kinase 1
SMZL	Splenic marginal zone lymphoma
SPEN	Spen family transcription repressor
SPIB	Spi-B transcription factor
SYK	Spleen associated tyrosine kinase
T-NHL	T-cell non-Hodgkin Lymphoma
TAK1	Synonym for MAP3K7, Mitogen-activated protein kinase kinase kinase 7
TBL1XR1	Transducin (beta)-like 1X-linked Receptor 1
TD	Thymus dependent
TI	Thymus-independent
TIR	Toll-IL-1 receptor
TLR	Toll-like receptor
TLR	Toll-like receptor
TNFAIP3	Tumor Necrosis Factor Alpha-Induced Protein 3
TP53	Tumor protein 53
TRAF6	Tumor Necrosis Factor receptor associated factor 6
V	Variable
WHO	World Health Organization

1   Zusammenfassung

Das diffus großzellige B-Zell Lymphom (DLBCL) ist mit ca. 30-40% der Erstdiagnosen das am häufigsten diagnostizierte Lymphom in der Gruppe der Non-Hodgkin Lymphome. Das DLBCL kann in zwei Untergruppen unterteilt werden, nämlich erstens in das aktivierte B-Zell ähnliche (ABC) DLBCL, zweitens in das Keimzentrums B-Zell ähnliche (GCB). Die aktuellsten groß-angelegten Sequenzierungen legten eine Vielzahl an Überschneidungen zwischen ABC-und GCB-DLBCL offen. Aus diesem Grund wurde eine neue genetisch basierte Einteilung des DLBCL durch zwei Forschungsgruppen publiziert, welche die Erkrankung in verschiedene Cluster einteilten. Das MCD/C5-DLBCL zeigt den aggressivsten klinischen Verlauf und entwickelt häufig Resistenzen gegenüber der Erstlinientherapie. Das MCD/C5-DLBCL ist wesentlich durch zwei häufige genetische Veränderungen geprägt. Diese sind zum einen eine Amplifikation des *BCL2* und zum anderen Mutationen in *MYD88.*

In diesem Projekt konnten wir eine detaillierte Charakterisierung eines *Myd88-* und *BCL2-*getriebenen MCD/C5-DLBCL Mausmodells mittels Immunphäno-typisierung, RNA-Sequenzierung und Exom-Sequenzierung darstellen. Die Ergebnisse zeigen, dass unser Mausmodell genetische Eigenschaften des humanen MCD/C5-DLBCL widerspiegelt.

Die molekularen Alterationen in *Myd88* und *BCL2* induzieren eine Splenomegalie und eine Formierung von Keimzentren. Dies weist darauf hin, dass das onkogene *Myd88* und eine Überexpression von *BCL2* bei der Lymphom-Entwicklung zusammenspielen. Weiterführend konnten wir belegen, dass unsere murinen MCD/C5-DLBCL abhängig von *BCL2* sind. Diese Abhängigkeit konnten wir ebenfalls in humanen MCD/C5-DLBCL Zelllinien demonstrieren. Humane MCD/C5-DLBCL zeigten im Vergleich zu humanen nicht-MCD/C5-DLBCL eine höhere Expression von *PD-L1*. Aus diesem Grund führten wir an unserem MCD/C5-DLBCL Mausmodell eine Kombinationstherapie mit einer Blockade von BCL2 und PD-1 durch. Es zeigte sich ein signifikanter synergistischer Effekt im Vergleich zur Einzeltherapie oder zur Placebo-Kontrolle. Die hierbei als signifikant festgestellten Endpunkte waren das Gesamtüberleben und die Kontrolle des Tumorwachstums, welche mittels MRT-Kontrollen detektiert wurde.

Zusammenfassend zeigten wir, dass unser *Myd88/BCL2* getriebenes Mausmodell die humane Erkrankung MCD/C5-DLBCL widerspiegelt. Weitergehend konnten wir unser Mausmodell als vorklinische Plattform verwenden, um molekulare Angriffspunkte zu finden und diese mit neuen Therapieregimen zu behandeln. Basierend auf dem beobachteten Zusammenspiel des mutierten *Myd88* und der *BCL2* Überexpression in der murinen Lymphom-Entwicklung, konnten wir einen synergistischen Effekt bei der kombinierten Therapie mit einem BCL2- und einem PD-1 Hemmer nachweisen. Diese Daten zeigen, dass eine BCL2/PD-1 Blockierung möglicherweise eine sinnvolle Alternativtherapie für refraktäre oder rezidivierende MCD/C5-DLBCL im klinischen Alltag darstellt.

2 Summary

Diffuse large B-cell lymphoma is the most common non-Hodgkin`s lymphoma and accounts for 30-40% of newly diagnosed lymphoma. DLBCL can be subdivided in the activated B-cell-like (ABC) and the germinal center B-cell-like (GCB) DLBCL. Large-scale sequencing efforts showed a large overlap between ABC- and GCB-DLBCL. Therefore two research groups recently published new genetic based approaches to classify DLBCL into distinct clusters. The most aggressive cluster in regards to clinical outcome and resistance to first line treatment is the MCD/C5-DLBCL, enriched with former ascribed ABC-DLBCL cases. Two of the most common aberrations in MCD/C5-DLBCL are a copy-number gain of *BCL2* and a point mutation in *MYD88*.

In this study we present a detailed characterization of our *Myd88-* and *BCL2*-driven MCD/C5-DLBCL mouse model. We characterized the mouse model using immune phenotyping, RNA sequencing and whole exome sequencing. We could show that the lymphomas derived from our mouse model resemble genetic features of human MCD/C5-DLBCL.

We detected that *Myd88* and *BCL2* induce splenomegaly and germinal center formation *in vivo*. This indicates that the oncogenic *Myd88* and *BCL2* overexpression might cooperate in lymphomagenesis. Furthermore we could detect an actionable dependence of the murine MCD/C5-DLBCL model on *BCL2*. This *BCL2* dependence was also shown in human MCD/C5-DLBCL cell lines. Moreover, the human MCD/C5-DLBCL in comparison to the human non-MCD/C5-DLBCL showed a higher expression of *PD-L1*. Therefore we used our MCD/C5-DLBCL mouse model as preclinical tool to test a combined blockade of BCL2 and PD-1. We observed a significant synergistic effect of the combined treatment in comparison to the single agents and the vehicle control with regard to overall survival and tumor growth control, which could be shown by MRI monitoring.

Altogether, we demonstrated that our *Myd88/BCL2*-driven mouse model resembles many features of the human MCD/C5-DLBCL. Further we could use our MCD/C5-DLBCL mouse model as a preclinical tool to detect actionable molecular vulnerabilities and to test new treatment regimens. Based on the detected cooperation of mutant *Myd88* and *BCL2* in murine lymphomagenesis, we were able to show a synergistic effect of combined BCL2 and PD-1 blockade in murine MCD/C5-DLBCL. These data indicate that it could be a reasonable approach to test a combined BCL2/PD-1 blockade in relapsed or refractory patients.

3 Introduction

Cancer is a leading cause for mortality and morbidity worldwide. The latest statistics estimate 14.1 million new cases of cancer every year and 8.2 million cancer-related deaths per year[1]. Due to aging, population growth and rapid economic transition, the worldwide incidence of all cancer cases is estimated to increase from 12.1 million new cases back in 2008 to 22.2 million by 2030[2].

Surgery, chemotherapy and radiation have been the main standard treatment approaches for cancer patients. Over the last few decades, a more targeted approach emerged as an effective treatment approach for several cancer entities, such as leukemia, breast cancer, lung cancer and others[3-6]. These approaches include monoclonal antibodies against specific surface markers, as well as small molecule inhibitors, which block enzymatic activities of specific target proteins.

However, there are still cancer entities and subgroups lacking new therapeutic approaches. One of these sub-groups is the most common form of B-cell non-Hodgkin´s lymphoma (B-NHL): diffuse large B-cell lymphoma (DLBCL). New, targeted treatment approaches for these lymphomas are slowly integrated into the clinical area. Today, the standard treatment regimen for low-risk DLBCL-patients is a combined chemo-immunotherapy, called R-CHOP (anti-CD20 antibody (rituximab), combined with the following cytotoxic agents: cyclophosphamid, hydroxydaunorubicin, vincristin (oncovin) and prednisolone)[7,8]. The 10 year overall survival rate with this first line regimen in low-risk patients is nearly 90%[9]. Fit high-risk patients receive R-CHOP or R-CHOEP (R-CHOP plus etoposide) every 14 or 21 days, achieving a 5 year overall survival rate of approximately 70%[10,11].

There is a substantial need for new therapy approaches for DLBCL, as around 30% of the high-risk DLBCL patients succumb to their disease within the first 5 years and survival rates for relapsed and refractory patients are low. Among all DLBCLs, the subgroup of activated B-cell like (ABC) DLBCL seems to have the most aggressive clinical course with the least favorable outcome[7,12,13]. As recent large-scale sequencing efforts shed light on the genetics of DLBCL, potential targets for new treatment approaches were revealed[14-16]. The following introduction will give a broad overview on cancer biology, the evolution of treatment approaches and then highlights the most relevant aspects of lymphomagenesis in DLBCL.

3.1 Cancer evolution and biology

Cancer has always been an enormous burden on patients and on society. Ever since, cancer patients were stigmatized by their disease. From the early days on, there have been numerous theories on the biology of cancer, its origin and what might cause it.

The earliest documented case in the history of cancer, a breast cancer, can be found in the Edwin Smith Papyrus from approximately 3000BC[17]. Back then, it was described as a disease

with no treatment options[17]. Over the years numerous cancers were documented but there was no lasting breakthrough in understanding the biology of this group of diseases. The first major landmarks in understanding cancer biology have been set centuries later. Shortly after the invention of the microscope, the German Mattias Jacob Schleiden, professor of Botany, and the German physiologist Theodore Schwann formulated the "cell-theory" in 1838[18]. Their theory based on the idea that every living tissue consists of microscopic structures, the "cells"[19]. Another German, Rudolf Virchow, was dedicated to the pathology of cells and therefore also to cancer cells. In the mid 19th century the pathologist followed up on the cell-theory and outlined his views and the modified version of it in his two illustrated books "Die Cellularpathologie"(1858) and in "Die krankhaften Geschwulste"(1863). He firstly established the theory that the cells themselves are the origin for the deadly disease of cancer. Virchow described cancer as the uncontrolled proliferation of human cells and therefore paved the way for the modern understanding of cancer biology[19,20]. Furthermore, Virchow´s research ultimately lead to the definition of the microscopic differences between benign and malignant cells[20]. The ability to invade surrounding tissues or to spread to more distant organs via blood or lymphatic vessels is what distinguishes malignant tumors and benign tumors[19].

The discovery of the DNA structure by Francis Crick and James Watson in 1958 was groundbreaking and the starting point to shed light on the genomic nature of cancer[21]. Following the discovery of the DNA, new DNA-sequencing technologies were established over the last 50-60 years. These sequencing efforts revealed various genomic changes in the cancer genome[22,23]. The causes for these so-called mutations are variant: they can be inherited, be the result of random errors in DNA repair or replication or be induced by environmental factors[19,24].

Generally considered, cancer is a disease of the elderly. This implicates a very complex and relatively slow development of the majority of cancers. Cancer cells arise from normal cells, mostly one mutated cell, and accumulate genetic alterations to gain any kind of proliferation advantage[25]. Throughout the proliferation cancer cells go through a competition comparable to the principle "survival of the fittest" by Charles Darwin[19,25]. Therefore, cancer cells accumulate mutations that ultimately lead to a pro-survival benefit, resulting in a tumor build with mostly identical cells. Gaining alterations to outcompete other tumor lines (so-called clones) in terms of proliferation is an important factor in a multifactorial tumorigenesis[22]. This process is called clonal expansion/selection and mostly ends in one mainly monoclonal tumor[25]. Multiple myeloma can provide proof to this monoclonality of tumors. This hematological tumor derives from antibody producing B-cells (plasma cells). Each normal, healthy plasma cell expresses a very specific individual antibody as a result of immunoglobulin gene rearrangements. In multiple myeloma patients high levels of identical antibodies occur, indicating the monoclonality of the increased plasma cell population[19]. Hence, the theory of

monoclonality and the survival of the fittest clone is complicated by other factors. During tumor growth, tumor genomes become more and more unstable and the mutational rate outpaces the Darwinian selection[19]. Recent genomic studies underlined that and revealed that tumors are formed by several genetically heterogenous sub-clones[26-28]. These studies also showed that the tumor genome is in a constant progress, which allows tumors to adapt and potentially avoid new treatment approaches[19].

Hannahan *et al.* (2000) defined six principles as hallmarks of cancer that play a significant role in the multifactorial tumorigenesis: 1. Sustaining proliferative signaling, 2. Evading growth suppressors, 3. Activating invasion and metastasis, 4. Enabling replicative immortality, 5. Inducing angiogenesis, 6. Resisting cell death[22,23]. Further, large sequencing efforts revealed so-called driver mutations which effect signaling pathways that ultimately facilitate the hallmarks of cancers[3,22,24]. These mutations ultimately lead either to a gain of function, amplification and/or overexpression of key oncogenes or a loss of function, deletion and/or epigenetic silencing of key tumor suppressors[3]. Another category of critical genes in the tumorigenesis is the group of so-called proto-oncogenes[19]. These genes have the possibility to turn into oncogenes by mutation[19].

By revealing the importance of oncogenes and tumor suppressor genes in the tumorigenesis, the therapeutic targeting of these genes became a major field of interest.

3.2 Targeting oncogenes and tumor suppressors

Targeting oncogenes and tumor suppressors as a therapeutic approach showed great success. The first successful and clinically used approach was the inhibition of the receptor tyrosine kinase HER2/NEU, a member of the EGFR family, in breast cancer with the monoclonal antibody Trastuzumab[3,5]. The following breakthrough was Imatinib, an ATP-competitive small molecule kinase inhibitor, that was able to get through the cell membrane. Imatinib targets *BCR-ABL1* oncogene, which is a hallmark of chronic myelogenous leukemia[3,4,29]. Following Imatinib and its enormous success several highly targeted compounds like Erlotinib and Gefitinib (both targeting *EGFR)* and Ibrutinib (targeting Bruton´s Tyrosine kinase in B-cells) underlined the principle of targeted therapy[3-6,30].

Targeting oncogenes shows productive results, as they are gain-of-function mutations. However, targeting loss-of-function mutations of tumor suppressor genes remains a challenge. In several TP53 (tumor protein 53) mouse models the clinical use of tumor suppressor restoration as a potential therapeutic approach is well demonstrated [31-33]. One therapeutic approach is to restore the function of TP53 by gene delivery systems[31-33]. However, integrating the vector within the DNA is associated with the risk of insertional mutagenesis which can potentially result in secondary malignancies[34]. Therefore, gene delivery has no relevant part in cancer therapy[34].

Another therapeutic approach is to target proteins that control TP53 activity like MDM2 (mouse double minute 2 homolouge). MDM2 negatively regulates the transcriptional activity and stability of TP53[35]. Overexpression of MDM2 is found in many human tumors[35]. Therefore, there are several ongoing trails using MDM2-Inhibitors as monotherapy or in combination, but clinical experience remains limited[36].

A relatively new approach uses the concept of synthetic lethality in the context of aberrant pathways in cancer. Synthetic lethality is given, when the mutation of one gene is compatible with viability, but simultaneous mutation of another gene is lethal[37,38]. While cancer-driving mutations stimulate the malignant transformation, they are associated with specific dependencies that are absent in normal non-cancerous cells[37,38]. An example for synthetic lethality is the interaction between PARP1 (Poly(ADP-ribose) polymerase) and BRCA1 and BRCA2 (breast and ovarian cancer susceptibility genes 1 and 2)[39,40]. Both genes result in a defect in the repair of double strand breaks which ultimately result in increased genome instability[32,37]. The PARP1 inhibitor Olaparib is already in clinical use for ovarian cancer patients and prostate cancer patients with defective *BRCA 1/2* genes[41,42]. Most recently we demonstrated that Olaparib might also be a therapeutic option in ataxia-telangiectasia mutated (*ATM)* defective CLL patients[43].

3.3 Lymphoid neoplasms

Human tumors arise from various tissues. Independent of gender, age and region lung, prostate and breast cancer are the most frequently diagnosed cancers[1]. Non-Hodgkin lymphoma (NHL) accounts for an estimated 385.700 new cases and 199.700 deaths in 2012[1]. Therefore, it is among the ten most frequently diagnosed cancers worldwide[1].

Historically, lymphoid neoplasms are subdivided into two groups: Hodgkin´s lymphoma (HL) and non-Hodgkin´s lymphoma. Furthermore, NHL are subdivided into T-cell NHL (T-NHL) and B-cell NHL (B-NHL). This work will focus on the subgroup of B-NHL, representing the majority of NHL cases[44,45].

The World Health Organization (WHO) classification of lymphoid neoplasms separates B-NHL subtypes by using surface marker expression, genomic aberrations, histological features and gene expression profiles[44-46].

B-NHL can occur in several different entities and subgroups, such as follicular lymphoma (FL), chronic lymphocytic leukemia (CLL), hairy cell leukemia (HCL), mucosa-associated lymphoid tissue (MALT) lymphoma, Burkitt's lymphoma (BL), mantle cell lymphoma[31], primary mediastinal B-cell lymphoma (PMBL) and diffuse large B-cell lymphoma (DLBCL)[31]. While all these entities are derived from healthy B-cells, they are thought to derive from different stages in B-cell development.

B-cell development is a complex process and starts with a hematopoietic stem cell. Throughout the differentiation B-cells go through developmental stages defined by successive steps in the assembly and expression of functional antigen-receptor genes[47]. The first checkpoint for B-cells is the formation of a pre-B-cell receptor by rearrangement of the heavy-chain locus. If this rearrangement was successful, a μ heavy-chain is produced that, together with surrogate light chains, forms a pre-B-cell-receptor[47]. The production of the pre-B-cell receptor ultimately leads to pre-B-cell proliferation in which light-chain rearrangement takes place[47]. If light-chain rearrangement is successful, gene rearrangement ceases and a complete immunoglobulin B-cell receptor is formed[47]. B-cells with unproductive rearrangements undergo apoptosis. Those with a complete immunoglobulin B-cell receptor enter the next developmental stage and undergo tolerance to self-antigens[47]. The process of self-antigen tolerance begins in the bone marrow and continues for a short period after emigration to the periphery[47]. The final stage of development for most B-cells occur in the B-cell follicles of the spleen[47]. Activation of a B-cell requires binding of an antigen by the B-cell-receptor and the interaction with an antigen-specific helper T-cell[47]. Further interactions between T-cells and B-cells continue after the formation of a germinal center in the follicle[47]. Upon the stimulation of the T-cells, B-cells proliferate and differentiate into either antibody-secreting plasma cells or memory B-cells[47]. The expressed immunoglobulin genes in the germinal center reaction are diversified by somatic hypermutation and class switching[47]. During somatic hypermutation point mutations are inserted to provide a greater affinity for the antigen as the immune response proceeds[47]. Class switching increases the diversity of immunoglobulins (Ig) and leads to the production of IgG, IgA or IgE antibodies[47]. The class switching process does not change the antigen specificity but it provides distinct effector capacities[47].

Lymphoma subtypes often resemble a B-cell at a particular developmental stage of differentiation judged by the presence or absence of immunoglobulin variable (V) region mutations and by gene expression profiling[45]. This theory is known as the "cell-of-origin" theory[45].

For instance, the counterpart of most MCLs are represented by the *IgV*-unmutated pre-germinal center mature B cell[45,48,49]. In CLL two subtypes occur[48,49]. One group shows unmutated *IgV* regions indicating a pre-germinal center origin, the other one carries mutated *IgV* regions, likely arising from post-germinal center B-cells[45,48,49]. The germinal center B-cell is the normal counterpart of FL, BL, and GCB-DLBCL[45,50-52]. MALT lymphomas are extranodal in their origin and phenotypically related to post-germinal center marginal zone B-cells[45]. HCLs carry mutated *Ig* genes and *Ig* heavy chain class switching and are most possibly derived from post-germinal center memory B-cells[45,53,54]. ABC-DLBCL has been postulated to be derived from post germinal center plasmablasts, that went through the germinal center reaction[45,50,51,55]. The recent DLBCL reclassification based on mutational landscapes presents

an ABC-DLBCL subset with recurrent mutations in *TBL1XR1*[15,16,56,57]. This ABC-DLBCL subset shows manifest extranodal dissemination similar to primary extranodal lymphomas (PENLs)[56]. These data suggest that the true cells-of-origin for ABC-DLBCL might be aberrant memory B-cells[56].

Nevertheless, there is not necessarily a correlation between the phenotypic copying of certain B-cell developmental stages and the cell of origin for different lymphomas[45]. In fact, the malignant phenotype can be determined by additional oncogenic hits at later developmental stages, even though the initiating oncogenic aberration might be detected in early B-cell development. The translocation t(14;18), for instance, a rearrangement of the *BCL2* proto-oncogene on chromosome 18 with the immunoglobulin heavy chain region on chromosome 14, is the defining feature of FL[46,58]. In most cases the RAG recombinase, which is active particularly in pre-B-cells and silenced in mature B-cells, is responsible for this translocation[45,59]. These data show that the mis-regulation of *BCL2* expression does not necessarily lead to the full malignant transformation of pre-B-cells and that non-physiological *BCL2* expression does not result in a differentiation arrest at an early pre-B cell stage. This is also indicated by mouse models, where the overexpression of *BCL2* rarely leads to lymphoma development, but merely induced an autoimmune disease with lymphoproliferation and an increased antibody-producing cell population[60,61].

3.4   DLBCL classification by cell of origin

DLBCL is a very heterogeneous disease and shows high variation in the differentiation of the malignant cells, proliferation and response to treatment. By comparing the transcriptional profiles of DLBCL tumors to those of different healthy B-cell populations, Alizadeh *et al.* (2000) were able to describe two molecularly distinct forms of DLBCL which had gene expression patterns of either a germinal center cell or a post-germinal center cell[45,50,62]. The ABC-DLBCL subgroup shows expression patterns more similar to activated, post-germinal center B-cells and the GCB-DLBCL arises from a more germinal center like B-cell[45,50]. These two subgroups of DLBCL also show distinct outcomes and different prognosis. Whereas 60% of GCB-DLBCL patients achieve stable remission, only 20% of ABC-DLBCL do so[50]. Later on, the same group identified a expression-based predictor for the classification of DLBCL tumors to divide these lymphomas in the ABC and GCB sub-types[51](Figure 1).
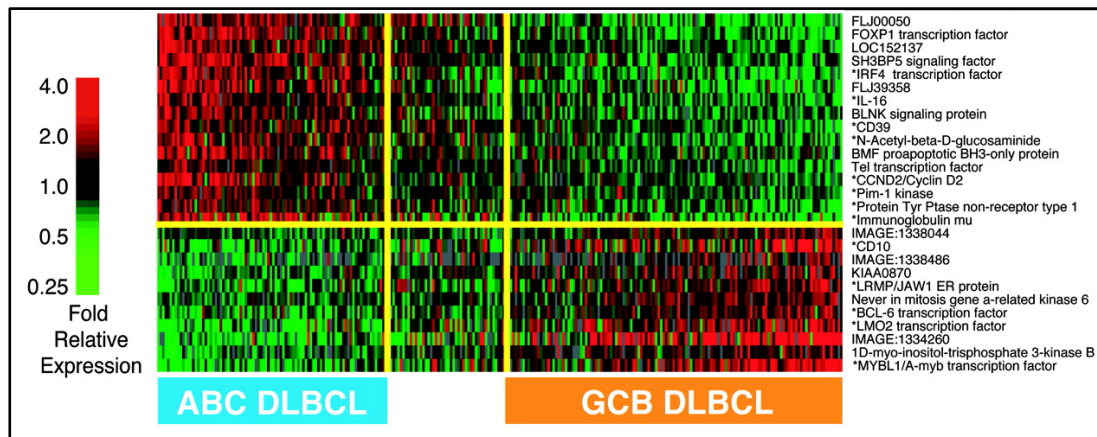
Figure 1: Expression-based DLBCL predictor for subtypes. Adapted from Wright et al., (2003)[51].

Since gene expression-based classification is not a practicable approach in clinical routine, there were different approaches to identify markers that resemble the subgroups of the disease by immunohistochemistry (IHC)[63]. The Hans algorithm was one approach to classify the DLBCLs by using CD10, BCL6 and MUM1 as immunohistochemical markers[64] (Figure 2). Later a second algorithm using GCET1 and FOXP1 as additional markers was published, achieving a better concordance (93%) with microarray data (gene expression profiling, GEP) than the Hans algorithm (86%)[65].
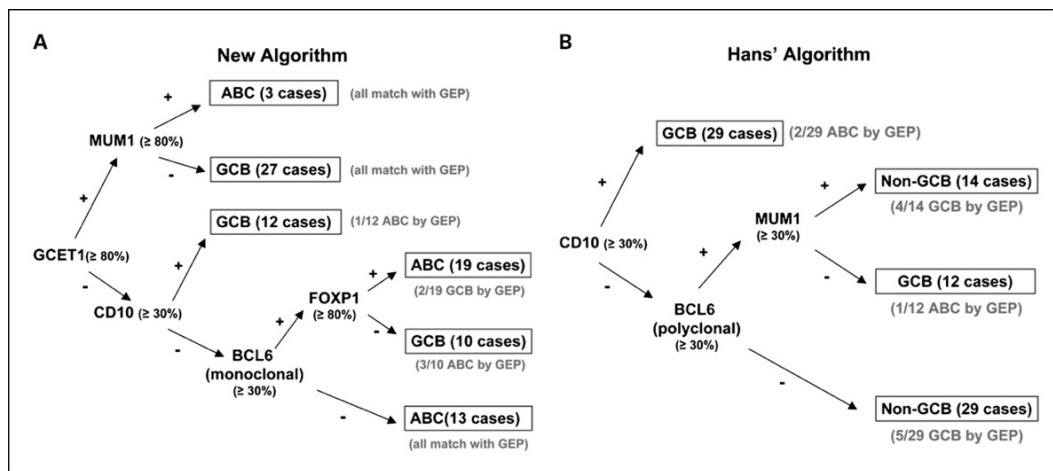

Figure 2: A: New Algorithm; B: Hans´ Algorithm. Adapted from Hans et al., 2004[64].

In fact, the classification into these two subgroups has been well-accepted in the scientific community and had an impact on the revised WHO classification of lymphoid neoplasms[46]. Nevertheless, the clinical significance is negligible, as the standard of care in both sub-groups remains R-CHOP/R-CHOEP depending on the risk evaluation[66]. However, the severe differences in the mutational spectrum among ABC-DLBCL and GCB-DLBCL result in different effects on the cellular pathways and therefore asking for different targeted treatment approaches[63].

3.5   DLBCL classification based on mutational landscape

The latest large-scale sequencing efforts have provided a new, more detailed insight in the genetics of DLBCL[14-16]. These data show that despite a great overlap in mutations between ABC and GCB sub-types, a subset of mutations is enriched in one of the two[63]. Whereas ABC is strongly enriched for mutations in the toll-like receptor (TLR) and the B-cell receptor (BCR), specifically in *CD79B, MYD88* and *CARD11*, the GCB subtype shows mutations in *EZH2, SGK1* and *GNA13* and translocations in *BCL2*[14,15]. The mutations found in the ABC sub-types lead to constitutive activation of NFκB, a hallmark of ABC-DLBCL[67].

Since the latest data show a large overlap of mutations between ABC and GCB, there have been new attempts to classify DLBCLs on a genetic level[15,16]. On the one hand Schmitz et al. (2018)[15] established four distinct clusters into which they classify approximately 50% of DLBCL cases, on the other hand Chapuy et al. (2018)[16] clustered all investigated 304 DLBCL samples into five groups[63] with distinct mutational profiles.

Cluster 5 by Chapuy et al. (2018)[16] is defined by amplifications of 18q, the chromosomal location of *BCL2,* and frequent mutations in *CD79B, MYD88,* gains in *3q, 19q13.42* and inactivation of *PRDM1.* Further cluster 5 was enriched with the prognostically significant *18p* copy gains[16]. The corresponding cluster identified by Schmitz et al. (2018)[15], termed MCD, also contains *MYD88* and *CD79B* mutations and gains or amplifications of *SPIB*[15]. Furthermore, a full plasmacytic differentiation is blocked in MCD by mutations that inactivate *BLIMP1 (PRMD1)*[15]. Both research groups could show that these two clusters are enriched for ABC DLBCL[15,16]. The ABCs from the MCD/C5 cluster show prominent extranodal dissemination and recurrent mutations in *TBL1XR1*, which is also mutated in PENLs[56].

Secondly Schmitz et al. (2018)[15] described a cluster, namely BN2, which is dominated by aberrations in the *NOTCH* pathway. BN2 lymphoma show a high rate of *NOTCH2* mutations and amplifications, *SPEN* mutations or mutations in *DTX1*[15]. Another main feature of this cluster is the alteration of *BCL6*[15]. This subgroup consists of ABC and unclassified DLBCL cases, but also gathers some GCB cases (41%, 40% and 19%)[15]. The correspondence in Chapuy et al. (2018)[16] to the BN2 cluster is cluster C1, which also contains *NOTCH2* mutations and *BCL6* fusions. Furthermore, both research groups describe *BCL10* and *TNFAIP3* mutations in these clusters, showing the importance of NFκB signaling[15,16].

Clusters C3 by Chapuy et al. (2018)[16] and EZB by Schmitz et al. (2018)[15] show a relevant overlap and are enriched for most genetic features previously ascribed to GCB-DLBCL, such as BCL2 translocations, EZH2 mutations, REL amplifications, as well as inactivation of tumor suppressors like CREBBP and KMT2D[15,16].

The remaining clusters of Chapuy et al. (2018)[16] C2, defined by *TP53* mutations and a set of chromosomal aberrations, and C4, defined by mutations effecting the BCR signaling cascade, do not match the fourth cluster of Schmitz et al. (2018)[15] (Figure 3). This cluster, termed N1,

stands for the predominance of mainly *NOTCH1* mutations and aberrations targeting transcriptional regulators of B-cell differentiation[15].
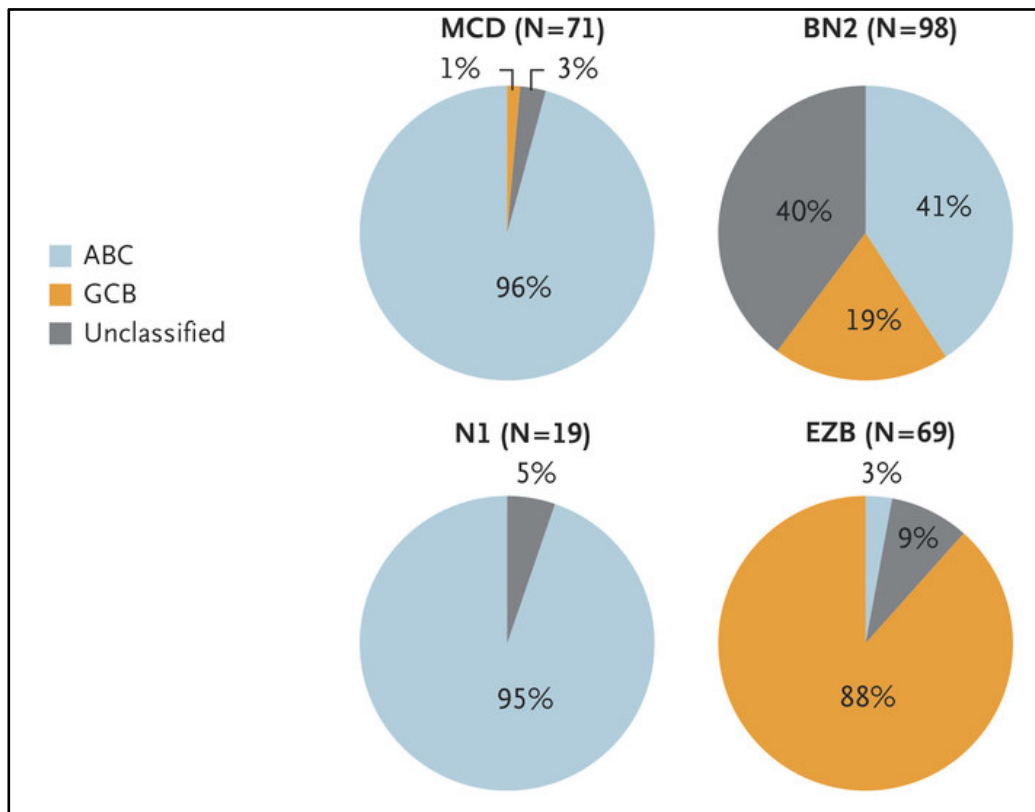

Figure 3: Distribution of gene-expression subroups within genetic subtypes. Adapted from Schmitz et al., 2018[15]. (N = number of DLBCL cases)

Altogether, the genetic differentiation of DLBCL and distribution into these clusters may predict a future clinical relevance in terms of treatment approaches[63]. The existence of subgroups with specific genetic profiles and therefore dependencies on specific pathways asks for a more targeted and more individualized therapy approach than R-CHOP/R-CHOEP. The MCD/C5 cluster is a good example for pathway dependencies, as it is defined by mutations that cause constitutively active NFκB signaling through activation of BCR and TLR signaling[67,68].

3.5.1 Inappropriate NFκB activation in DLBCL

Many genetic aberrations recurrently found in MCD/C5-DLBCL result in non-physiological NFκB activation. Besides MCD/C5-DLBCL, inappropriate NFκB activation is also found in MALT, PMBL, HL and multiple myeloma[7,45,69 70-73]. The NFκB family consists of transcription factors that form through homo- or hetero-dimerization of the sub-units $p65^{RelA}$, RelB, c-Rel, $p50^{NFKB1}$ and $p52^{NFKB2}$ [44,45,74-76]. There is a "classical" (also termed "canonical") NFκB signaling pathway and an "alternative" pathway to translocate NFκB sub-units to the nucleus[45,74-76].

In the classical pathway, multiple distinct upstream signaling cascades ultimately lead to IKKβ activation, which phosphorylates the inhibitory protein IκBα, marking it for ubiquitination by βTrCP and subsequent proteasomal degradation[44]. At ground state, IκBα sequesters p50$^{\text{NFKB1}}$/p65$^{\text{RelA}}$ and p50$^{\text{NFKB1}}$/c-Rel in the cytoplasmic compartment away from the nuclear chromatin[44,77]. Once liberated from IκBα, NFκB transmigrates from the cytoplasm to the nuclear chromatin where it transactivates numerous target genes, including the apoptosis-repressing *BCL2* family members *BCL2*, *BCL-XL*, *cFLIP*, *cIAP1* and *cIAP2*[44,77-79].

During activation through the alternative pathway, an IKK complex consisting of two IKKα subunits phosphorylates p100, which promotes proteolytic cleavage into the NFκB component p52[44]. p52 then engages into a complex with RelB and subsequently translocates to the nuclear compartment[44,45,77].

Especially in MCD/C5-DLBCL numerous recurrent genomic aberrations exist, that lead to inappropriate NFκB activation[44]. The CARD11/MALT1/BCL10 complex, MYD88 signaling and CD79-dependent B-cell receptor signaling are affected by these genomic aberrations (Figure 4)[44,45]. This constitutive NFκB activation in MCD/C5-DLBCL ultimately leads to cell proliferation[69]. NFκB inhibition introduced by retroviral transduction displays massive cytotoxicity in the MCD/C5, but not in non-MCD/C5-DLBCL-derived cells[69]. Constitutive NFκB activation, which has been shown to repress cytotoxicity upon chemotherapy, may also be the reason for the enhanced resistance of MCD/C5-DLBCL towards frontline-chemotherapy[7,44,77,80].
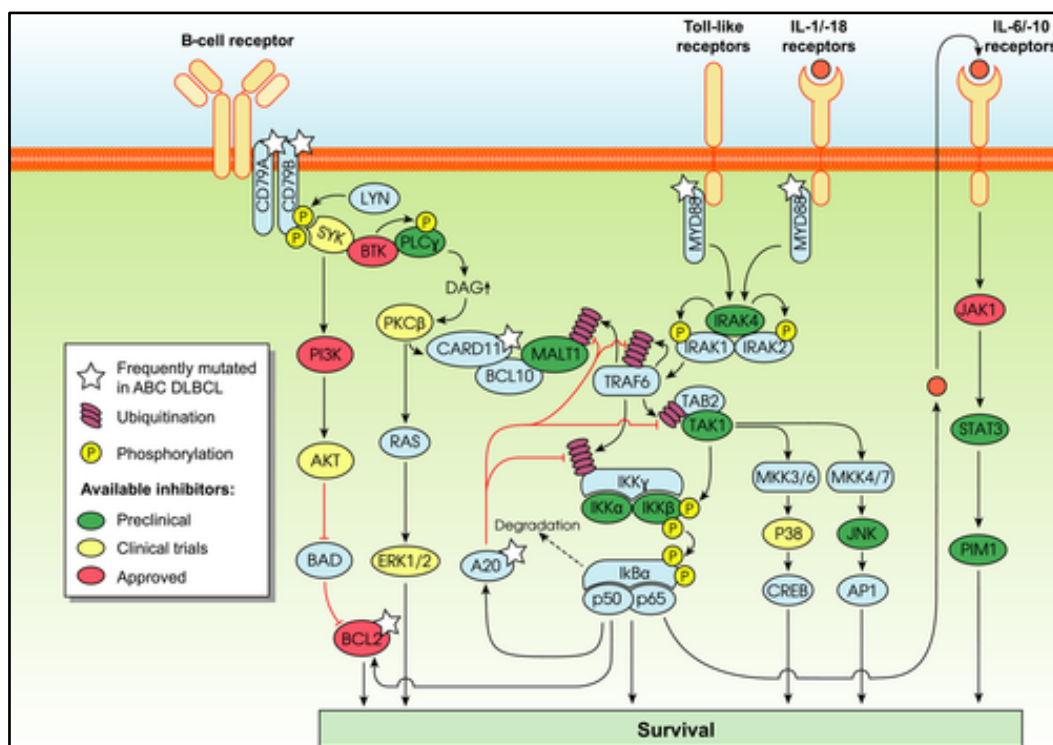

Figure 4: DLBCL relevant signaling pathways. Adapted from Knittel et al., 2016[44].

BCR expression is retained by most human B-cell lymphomas. The BCR´s light and heavy chain interact with CD79A/B, which regulates the receptor´s surface expression, endocytosis and signaling (Figure 4). The CD79A/B molecules harbor an ITAM (immunoreceptor tyrosine-based activation motif) in their intracellular domain[81]. Upon activation by phosphorylation of the ITAM motifs SYK is bound to the ITAM motifs, which in turn is activated by autophosphorylation[82,83]. BTK and PLCγ are activated[84], resulting in the generation of diacylglycerol (DAG) and through activation of PKCβ CARD11 is phosphorylated[85]. CARD11 initiates the formation of the CARD11/MALT10/BCL10 complex and activation of the NFκB pathway[86]. Additionally, PI3K is recruited by the BCR signaling complex and activates AKT via CD19[87].

Activation of the BCR pathway can be induced by antigenic stimulation[88], or it can be caused by mutations within the pathway. Recurrent mutations of the B-cell co-receptor *CD79B* are detected in 14% of DLBCL cases[16]. Furthermore, mutations in *CARD11* and *BCL10* are found in 11% and 5% of all DLBCL cases[16].

Another pathway for non-physiological NFκB activation is through Toll-like receptor (TLR) pathway signaling[44]. To date, nine TLRs have been identified to be shared by humans and mice and all of them, except TLR3, are linked to MYD88 to conduct downstream signaling[89,90]. Binding of a ligand to a TLR causes activation, allowing adaptor proteins like MYD88 to bind to the Toll-IL-1 receptor (TIR) domain at the intracellular part[91]. Upon ligand binding MYD88 forms the so-called "Myddosome" complex, consisting of MYD88 and the IL1-Receptor-associated kinases (IRAKs) IRAK1, IRAK2 and IRAK4[92,93]. Structural analyses of the MYD88-IRAK4-IRAK2 complex, which is formed by protein:protein interactions mediated by the death domains of MYD88 and IRAK kinases, revealed that the Myddosome forms a left-handed helical oligomer[44,92]. The assembly of the signaling super-complex is well structured and appears in a specific sequence. MYD88 first recruits IRAK4 and the MYD88:IRAK4 complex subsequently recruits IRAK2 or the related IRAK1 kinases which are substrates of IRAK4 kinase activity[44,92]. Subsequent phosphorylation of IRAK1 causes interaction with TRAF6, which ubiquitinates TAK1[94,95]. TAK 1 then phosphorylates and activates the IKK complex which finally results in a translocation of NFκB to the nucleus[96-98]. Additionally, TAK1 activates the JNK MAPK and p38 pathways[98-100].

Non-physiological TLR signaling has recently emerged as a potent driver of several lymphomas, such as CLL[101], Waldenström´s macroglobulinemia[102] and DLBCL[67]. Especially mutations in the adaptor protein MYD88 occur at a high frequency 18% in DLBCL[16], 3% in CLL[103] and even 91% in Waldenström´s Macroglobulinemia[102,104]. Specifically, the p.L265P mutation is by far the most recurrent variant of *MYD88* (60% of *MYD88* mutations in DLBCL)[15]. This mutation causes a disruption of the tertiary structure of the TIR domain[45]. This point mutation in the TIR domain of MYD88 has been shown to increase the frequency of

spontaneous formation of the Myddosome complex[105], suggesting that the increased NFκB activation by enhanced MYD88 signaling might be the reason for the recurrence of *MYD88* p.L265P in lymphoid cancer. In contrast to MCD/C5-DLBCL, the *MYD88* p.L265P mutation is only rarely detected in other clusters[15,16,67].

Altogether, these data show that MYD88-dependent oncogenic NFκB signaling is an important contributor to lymphomagenesis, especially in MCD/C5-DLBCL[44]. Furthermore, the observation that *MYD88*-mutant DLBCL are oncogene-addicted, strongly argues that MYD88 signaling might be a vital drug target for new therapeutic approaches of MCD/C5-DLBCL[44,67]. Moreover, *MYD88* mutations appear to cooperate with chronic active BCR signaling in MCD/C5-DLBCL lymphomagenesis, evidenced by a significant co-clustering of oncogenic *MYD88* and *CD79B* mutations in MCD/C5-DLBCL[15,16,44,67]. Recently, the strong interconnection between these pathways has been further elucidated by the discovery of the so-called My-T-BCR super-complex, consisting of MYD88, TLR9 and the BCR[106].

3.5.2 *BCL2* amplifications in DLBCL

BCL2 expression is often deregulated in various B-cell malignancies. The defining feature for FL for example is *BCL2* overexpression due to a *t(14;18)* translocation[107]. In DLBCL these translocations and additional amplifications are mainly found in EZB/C3-DLBCL former ascribed as GCB-DLBCL[15]. Further the MCD/C5-DLBCL shows increased expression in *BCL2* and amplification of its chromosomal location[15,16].

The BCL2 protein family is a group of intracellular proteins that regulate apoptosis[108]. Apoptosis regulation is mainly determined by interactions between three groups of the BCL2 family: 1. pro-survival family (BCL2, BCL-X_L and MCL1), 2. pro-apoptotic fraction of BH3-only proteins like BIM, PUMA and BID, 3. pro-apoptotic fraction of death effectors BAX and BAK[108]. At the beginning of the cascade, BH3-only proteins are induced upon a stress signal[63]. This could be due to activation of TP53, for example. TP53 is activated by several different noxious stresses such as DNA damage and then induces the transcription of BH3-only genes *NOXA* and *PUMA*[63,109,110]. After transcription the BH3-only proteins compete with the pro-apoptotic proteins of the BCL2 family (BAX, BAK) for the BH3 binding site of the pro-survival family (BCL2, BCL-$_{XL}$, MCL1)[63]. By increased BH3-only protein levels BAX and BAK are released from their inhibitors and cause permeabilization of the outer mitochondrial membrane, ultimately leading to cytochrome c release[63,108].

Over the years there have been numerous studies investigating *BCL2* overexpression in mice[60,111]. One group observed a prolonged survival of B cells *in vitro* induced by B-cell specific overexpression of *BCL2* cDNA under the control of a immunoglobulin enhancer *Eµ*[60]. Strasser *et al.* (1991) also detected increased B-cell populations in bone marrow, spleen and lymph nodes, indicating that these cells avoid apoptosis rather than proliferate[60]. Furthermore, the

older mice, even if they seemed to be healthy animals, showed elevated levels of anti-nuclear antibodies in their sera and showed amplified and prolonged immune response[60].

McDonnell *et al.* (1989) generated a mouse model by generating transgenic animals harboring a *BCL2-Ig* fusion minigene in order to model the effects of *t(14;18)* translocation. This *BCL2*-translocation is a defining feature for FL and is also found in 20% of DLBCL[107,111,112]. Similar to Strasser *et al.* the deregulated expression of *BCL2* lead to an expanded B-cell population, hypergammaglobulinemia and increased *in vitro* survival[111].

Interestingly, Strasser *et al.* could also show a synergy between *Eµ:BCL2* and *Myc* overexpression in lymphomagenesis[113]. These double transgenic mice showed hyperproliferation of B-cells and developed tumors way faster than the control groups[113]. In line with these findings goes that McDonnell *et al.* showed that animals carrying the *BCL2-Ig* develop DLBCL-like disease in some cases[111]. These DLBCL-like tumors showed *Myc*-rearrangements in half of the cases[111]. The subset of DLBCLs with translocations of both *MYC* and *BCL2* is associated with a poor outcome in patients treated with R-CHOP[114,115].

3.6   Genetically engineered mouse model of DLBCL

Genetically engineered mouse models play a significant role in the process of understanding cancer biology. Tumors derived from advanced mouse models closely mimic the histopathological and molecular features of their human counterparts, display genetic heterogeneity and grow in a natural immune-proficient microenvironment[116]. They have been proven useful in identifying cancer genes and tumor biomarkers, validating gene functions, gaining insight into molecular and cellular mechanisms and developing novel therapeutic approaches[117].

In the last years an autochthonous mouse model was generated, in which *Cd19:Cre*-mediated recombination drives the conditional expression of *Myd88* p.L252P (the orthologous position of the human *MYD88* p.L265P mutation) from the endogenous promoter, specifically in B cells[61]. The *Myd88* allele was generated by flanking the wildtype exons 2-6, including the entire 3´ UTR with *LoxP* sites (Figure 5)[61]. An additional poly-adenylation signal (hGHpA: human Growth Hormone poly-adenylation signal) was inserted between the 3' UTR and the distal LoxP site, in order to prevent downstream transcription of the mutated exon 5[61]. Exons 2-6, including the splice acceptor site of intron 1 were duplicated and inserted downstream of the distal LoxP site[61]. The p.L252P mutation was introduced into the duplicated exon 5[61]. Thus, Cre-mediated recombination leads to the excision of the wildtype sequence (exons 2-6) and allows splicing into the mutant exons 2-6[61]. *Cd19*[Cre/wt];*Myd88*[c.-p.L252P/wt] animals developed a lympho-proliferative disease, and occasional transformation into clonal DLBCL[61].
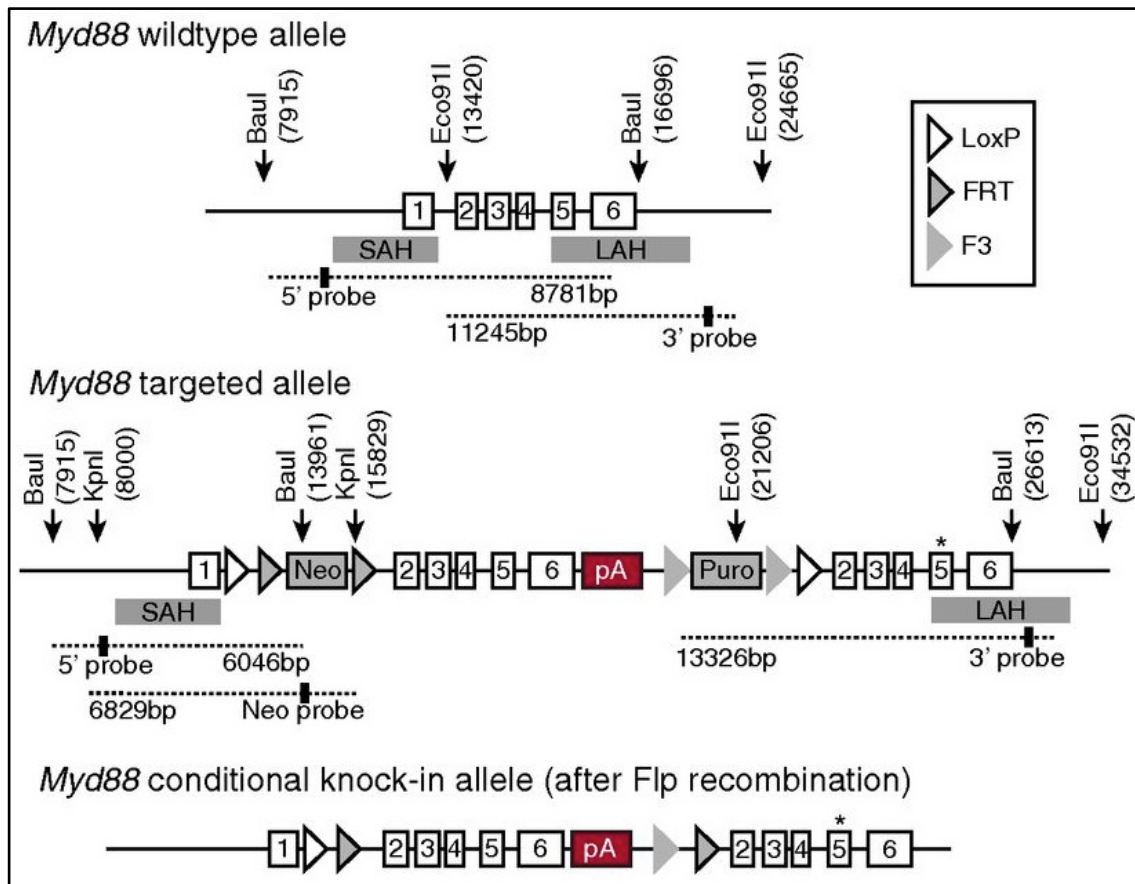
Figure 5: Construction of the conditional *Myd88* p.L252P allele. Adapted from Knittel et al., 2016[61].

Furthermore this mouse model was extended by conditional *BCL2* (*Rosa26*[LSL.BCL2.IRES.GFP]) knock-in mice[61]. The *Rosa26* locus-targeting vector was generated in which CAGS (CMV early enhancer/chicken β actin) promoter-driven expression of the transgene (*BCL2*) and downstream *IRES-GFP* (as a reporter for *Cre*-mediated recombination) is prevented by a *LoxP*-flanked STOP cassette[61]. The transgenic mice express the transgenes only after Cre-mediated excision of the *LoxP*-flanked STOP cassette.

This advanced mouse model expresses the *Myd88* mutant from the endogenous locus upon Cre-mediated recombination in a B-cell specific manner. Additionally, this mouse model carries an allele, which mediates conditional overexpression of BCL2[61]. These alterations mimic closely the human *MYD88* mutation and the *BCL2* overexpression which are both defining genetic characteristics of MCD/C5-DLBCL[15,16].

3.7   Prospects to the publication

As MCD/C5-DLBCL remains a difficult-to-treat clinically entity, especially in the relapsed setting[7], there is an urgent need for new therapeutic approaches that attack the molecular vulnerabilities. As mentioned above, MCD/C5-DLBCL shows several recurrent genetic aberrations that could possibly be targeted by novel therapeutics. *Myd88* p.L252P (the murine orthologue of human p.L265P) and *BCL2* overexpression cooperate in lymphomagenesis in a published mouse model[61].

In this project, we could reveal that the previously mentioned mouse model mimics human MCD/C5-DLBCL morphologically and transcriptionally. Moreover, we could detect a druggable dependence on BCL2 in murine cell lines and tumors, as well as in human MCD/C5-DLBCL cell lines, but not in human non-MCD/C5-DLBCL lines. Furthermore, we observed a single-agent response to PD-1 blockade by the *Myd88*-driven lymphomas, which occurred to be augmented with concurrent BCL2 inhibition, *in vivo*. Altogether these data implicate a biological rationale for the use of a combined PD-1 and BCL2 inhibition for the treatment of MCD/C5-DLBCL.

4 Publication

An Autochthonous Mouse Model of *Myd88*- and *BCL2*-Driven Diffuse Large B-cell Lymphoma Reveals Actionable Molecular Vulnerabilities

Ruth Flümann[1,2,3,4], Tim Rehkämper[1,2,3,4], Pascal Nieper[1,2,3,4], Pauline Pfeiffer[1,2,3,4], Alessandra Holzem[1,2,3,4], Sebastian Klein[5], Sanil Bhatia[6], Moritz Kochanek[1,2,3,4], Ilmars Kisis[1,2,3,4], Benedikt W. Pelzer[1,2,3,4], Heinz Ahlert[6], Julia Hauer[7,8], Alexandra da Palma Guerreiro[1,2,4], Jeremy A. Ryan[9], Maurice Reimann[10], Arina Riabinska[1,2,3,4], Janica Wiederstein[4], Marcus Krüger[4], Martina Deckert[2,11], Janine Altmüller[12], Andreas R. Klatt[13], Lukas P. Frenzel[1,2,4], Laura Pasqualucci[14], Wendy Béguelin[15], Ari M. Melnick[15], Sandrine Sander[16], Manuel Montesinos-Rongen[2,11], Anna Brunn[2,11], Philipp Lohneis[2,3,5], Reinhard Büttner[2,3,5], Hamid Kashkar[3,4,17], Arndt Borkhardt[6], Anthony Letai[9], Thorsten Persigehl[2,18], Martin Peifer[2,3,19], Clemens A. Schmitt[10,20], Hans Christian Reinhardt[21], and Gero Knittel[1,2,3,4]

ABSTRACT

Based on gene expression profiles, diffuse large B-cell lymphoma (DLBCL) is subdivided into germinal center B-cell–like (GCB) and activated B-cell–like (ABC) DLBCL. Two of the most common genomic aberrations in ABC-DLBCL are mutations in *MYD88* as well as *BCL2* copy-number gains. Here, we employ immune phenotyping, RNA sequencing, and whole-exome sequencing to characterize a *Myd88*- and BCL2-driven mouse model of ABC-DLBCL. We show that this model resembles features of human ABC-DLBCL. We further demonstrate an actionable dependence of our murine ABC-DLBCL model on BCL2. This BCL2 dependence was also detectable in human ABC-DLBCL cell lines. Moreover, human ABC-DLBCLs displayed increased *PD-L1* expression compared with GCB-DLBCL. *In vivo* experiments in our ABC-DLBCL model showed that combined venetoclax and PD-1 blockade significantly increased the overall survival of lymphoma-bearing animals, indicating that this combination may be a viable option for selected human ABC-DLBCL cases harboring *MYD88* and *BCL2* aberrations.

SIGNIFICANCE: Oncogenic *Myd88* and *BCL2* cooperate in murine DLBCL lymphomagenesis. The resulting lymphomas display morphologic and transcriptomic features reminiscent of human ABC-DLBCL. Data derived from our *Myd88*/*BCL2*-driven autochthonous model demonstrate that combined BCL2 and PD-1 blockade displays substantial preclinical antilymphoma activity, providing preclinical proof-of-concept data, which pave the way for clinical translation.

INTRODUCTION

Diffuse large B-cell lymphoma (DLBCL) is the most common lymphoid neoplasm in adults and accounts for approximately 35% of all B-cell non-Hodgkin lymphomas (1). DLBCL is a morphologically, biologically, and clinically heterogeneous disease that has historically been subdivided into germinal center B-cell–like (GCB) and activated B-cell–like (ABC) DLBCL using gene expression profiling (1–3). This cell of origin (COO)–based classifier separates subentities with distinct biology, pathogenesis, and clinical response to frontline chemoimmunotherapy (3–5). GCB-DLBCL has been proposed to originate from light-zone GCBs (6), whereas ABC-

DLBCL likely derives from postgerminal center plasmablasts (3, 6–8). To capture additional molecular heterogeneity in DLBCL, two independent comprehensive genomic analyses of human DLBCL cases were recently completed and led to the discovery of partially overlapping genetically defined DLBCL categories (9, 10). One group classified approximately 50% of the primary cases in a supervised approach to four genetically defined DLBCL subtypes (10). These were based on COO-associated alterations and identified tumors with co-occurring *MYD88*- and *CD79B* mutations (MCD), *BCL6* rearrangements and *NOTCH2* mutations (BN2), *EZH2* mutations and *BCL2* rearrangements (EZB), as well as *NOTCH1* mutations (N1; ref. 10). An independent analysis first defined

[1]University of Cologne, Faculty of Medicine and University Hospital Cologne, Clinic I of Internal Medicine, Cologne, Germany. [2]Center for Integrated Oncology, University of Cologne, Cologne, Germany. [3]Center for Molecular Medicine, University of Cologne, Cologne, Germany. [4]Cologne Excellence Cluster on Cellular Stress Response in Aging-Associated Diseases (CECAD), University of Cologne, Cologne, Germany. [5]Faculty of Medicine and University Hospital Cologne, Institute of Pathology, University of Cologne, Cologne, Germany. [6]Medical Faculty, Department of Pediatric Oncology, Hematology and Clinical Immunology, Heinrich Heine University Düsseldorf, Düsseldorf, Germany. [7]Department of Pediatrics, Pediatric Hematology and Oncology, University Hospital Carl Gustav Carus, Technische Universität Dresden, Dresden, Germany. [8]National Center for Tumor Diseases (NCT), Dresden, Germany. [9]Dana-Farber Cancer Institute, Harvard Medical School, Boston, Massachusetts. [10]Charité Universitätsmedizin Berlin, Medical Department of Hematology, Oncology and Tumor Immunology, and Molekulares Krebsforschungszentrum - MKFZ, Virchow Campus, Berlin, Germany. [11]Faculty of Medicine and University Hospital Cologne, Institute of Neuropathology, University of Cologne, Cologne, Germany. [12]Cologne Center for Genomics (CCG), University of Cologne, Cologne, Germany. [13]Faculty of Medicine and University Hospital Cologne, Institute of Clinical Chemistry, University of Cologne, Cologne, Germany. [14]Department of Pathology and Cell Biology, Institute for Cancer Genetics and the Herbert Irving Comprehensive Cancer Center, Columbia University, New York, New York. [15]Division of Hematology/Oncology, Department of Medicine, Weill Cornell Medicine, Cornell University, New York, New York.

[16]Adaptive Immunity and Lymphoma Group, German Cancer Research Center/National Center for Tumor Diseases Heidelberg, Heidelberg, Germany. [17]Faculty of Medicine and University Hospital Cologne, Institute for Medical Microbiology, Immunology and Hygiene, University of Cologne, Cologne, Germany. [18]Faculty of Medicine and University Hospital Cologne, Department of Radiology and Interventional Radiology, University of Cologne, Cologne, Germany. [19]Department of Translational Genomics, University of Cologne, Cologne, Germany. [20]Kepler Universitätsklinikum, Medical Department of Hematology and Oncology, Johannes Kepler University, Linz, Austria. [21]Department of Hematology and Stem Cell Transplantation, University Hospital Essen, University Duisburg-Essen, German Cancer Consortium (DKTK Partner Site Essen), Essen, Germany.

Note: Supplementary data for this article are available at Blood Cancer Discovery Online (https://bloodcancerdiscov.aacrjournals.org/).

R. Flümann, T. Rehkämper, and P. Nieper contributed equally to this article.

H.C. Reinhardt and G. Knittel contributed equally to this article.

Corresponding Author: Hans Christian Reinhardt, University Hospital Essen, Hufelandstr. 55, 45147 Essen, Germany. Phone: 49-201-723-3136; Fax: 49-201-723-5961; E-mail: christian.reinhardt@uk-essen.de

recurrent genetic drivers in DLBCL and used a non-negative matrix factorization consensus clustering approach, allowing classification of 98% of cases into five clusters with specific coordinate genetic signatures (9). These clusters were defined by: (i) *BCL6* structural variants in combination with *NOTCH2* aberrations (C1 DLBCL); (ii) biallelic *TP53* inactivation (*TP53* mutations and *17p* copy-number losses) in combination with haploinsufficiencies of *9p21.13/CDKN2A* and *13q14.2/RB1* (C2 DLBCL); (iii) *BCL2* mutations with concordant *BCL2* structural variants in combination with *EZH2*, *CREBBP*, and *KMT2D* mutations and additional activating alterations of the PI3K pathway (C3 DLBCL); and (iv) mutations in linker and core histone genes in combination with aberrations in immune evasion molecules, NF-κB, and RAS/JAK/STAT signaling molecules (C4 DLBCL; ref. 9). An additional cluster was defined by *18q* gains in combination with *MYD88* and *CD79B* mutations (C5 DLBCL; ref. 9). These large datasets, together with the recently published whole-exome sequencing results of 1,001 DLBCL cases, have established a framework for the identification of potentially druggable genomic aberrations in human DLBCL (11). In this context, it is important to note that frontline chemoimmunotherapy using R-CHOP, or R-CHOP–like regimens, achieves cure rates of more than 60% (9, 12, 13). However, relapsed or refractory disease represents a major clinical challenge, as these patients are often difficult to salvage, and even high-dose chemotherapy regimens with autologous stem cell support frequently do not provide long-term disease control (14–17). Thus, there is a pressing need for the development and preclinical validation of therapeutic strategies for the treatment of relapsed/refractory disease, as well as strategies to treat elderly and frail patients that do not qualify for intensive chemoimmunotherapy.

A powerful tool to assess the biological effects of targeted therapeutic agents are autochthonous mouse models, which are genetically engineered to carry genomic aberrations that precisely match those observed in the corresponding human disease. The advent of next-generation sequencing technologies has enabled the fine-grained cross-validation of mouse models and human disease. Here, we report the detailed molecular characterization and cross-species comparison of an autochthonous mouse model of *Myd88*-driven ABC-DLBCL. Note that 29% of human ABC-DLBCLs harbor the p.L265P mutation in the hydrophobic core of the MYD88 TIR domain (18, 19). In contrast, the *MYD88* p.L265P mutation is exceedingly rare in non–ABC-DLBCLs (18). To assess the role of *MYD88*[p.L265P] in B-cell lymphomagenesis, we recently generated a *Myd88*[p.L252P] allele (*Myd88*[c-p.L252P]) that is expressed from the endogenous locus upon Cre-mediated deletion of

the endogenous exons 2 to 6, together with the entire 3′ untranslated region (20). Of note, murine *Myd88*[p.L252P] is at the orthologous position of human *Myd88*[p.L265P] (20). When the *Myd88*[c-p.L252P] allele is crossed with an additional mutant strain that conditionally overexpresses *BCL2* from the *Rosa26* locus upon Cre-mediated deletion of a STOP cassette, the resulting *Myd88*[c-p.L252P/WT];*Rosa26*[LSL.BCL2.IRES.GFP/WT];*Cd19*[Cre/WT] (MBC) animals develop an aggressive lymphoma (20).

Here, we demonstrate that this MBC model resembles human ABC-DLBCL with respect to morphology, as well as on the transcriptomic and genomic level. In contrast, a *Kmt2d/Bcl2*-driven lymphoma model displayed more similarity with human GCB-DLBCL. Moreover, our analyses revealed a druggable dependence on BCL2 in murine and human ABC-DLBCL cell lines and tumors, which was not detected in human GCB-DLBCL cell lines. We further demonstrate that *Myd88*-driven lymphomas display a single-agent response to PD-1 blockade, which is synergistic with concurrent BCL2 inhibition, *in vivo*. Altogether, these data provide a detailed molecular and functional description of our *Myd88*-driven ABC-DLBCL model and provide a biological rationale for the use of combined BCL2 and PD-1 inhibition for the treatment of ABC-DLBCL.

RESULTS

Myd88[p.L252P] and *BCL2* Cooperate to Induce Splenomegaly and Germinal Center Formation *In Vivo*

Two of the most common genomic aberrations in human ABC-DLBCL are oncogenic *MYD88* mutations and *BCL2* copy-number gains (7, 9–11). Moreover, copy-number gains of 18q21.33, where the *BCL2* gene is localized, are significantly enriched in *MYD88* mutant DLBCL cases compared with *MYD88* wild-type (WT) cases (Supplementary Fig. S1A; ref. 9). To assess the *in vivo* effects of these aberrations, we performed longitudinal monitoring of WT, *Myd88*[c-p.L252P/WT]; *Cd19*[Cre/WT] (MC), *Rosa26*[LSL.BCL2.IRES.GFP/WT];*Cd19*[Cre/WT] (BC), and *Myd88*[c-p.L252P/WT];*Rosa26*[LSL.BCL2.IRES.GFP/WT];*Cd19*[Cre/WT] (MBC) animals using MRI scanning to monitor splenomegaly (Fig. 1A–C). Amplifications involving 18q21.33, the chromosomal location of *BCL2*, are associated with an overexpression of *BCL2* (Supplementary Fig. S1B), which is modeled by the *Rosa26*[LSL.BCL2.IRES.GFP] allele employed in this study. As shown in Fig. 1B and C, MBC animals displayed a significantly increased spleen volume, compared with WT, BC, and MC animals at 10, 20, and 30 weeks. Moreover, at the 20-, 30-, and 50-week time points, the spleen volume of BC animals was significantly larger than that of WT and MC mice (Fig. 1C;

Figure 1. Germinal center hyperplasia and increased plasma cell pools in MBC animals. **A,** Schematic illustrations of the employed alleles. Exons 2 to 6 of the endogenous *Myd88* locus were flanked by *loxP* sites (triangles). Downstream of the second *loxP* site, a second set of the exons 2 to 6 was inserted, harboring the L252P point mutation (asterisk). Read-through is prevented by a strong polyadenylation signal ("pA"). Human *BCL2* cDNA expression is controlled by a *CAGGs* promoter and prevented by a *lox*-stop-*lox* cassette. *GFP* expression is coupled to *BCL2* expression by an internal ribosomal entry site (IRES). The construct is a knock-in into the *Rosa26* locus. Both alleles have been previously published (20). The *Cd19*[Cre] allele is a knock-in into the *Cd19* locus and has been previously published (85). **B,** Exemplary axial MR images of 30-week-old animals. Spleens are outlined. **C,** Spleen volumes of WT (n = 5), MC (n = 5), BC (n = 7), and MBC (n ≥ 7) mice were quantified from MR images. **D,** IHC stainings for B220, PNA, and CD3 of splenic sections of 30-week-old WT, MC, BC, and MBC animals. **E,** The germinal center (GC) structures stained by PNA in splenic sections of 30-week-old WT (n = 8), MC (n = 4), BC (n = 5), and MBC animals (n = 5) were quantified. **F,** Splenocytes of 30-week-old WT (n ≥ 7), MC (n = 8), BC (n = 8), and MBC (n ≥ 7) were analyzed by flow cytometry, and the relative amounts of different B-cell developmental stages were quantified. Early PB, early plasmablasts; late PB/PC, late plasmablasts/plasma cells. **G,** Serum protein electrophoresis was performed with serum of 30-week-old WT, MC, BC, and MBC animals (n = 6 per genotype). **H,** Serum immunoglobulin levels of 30-week-old WT, MC, BC, and MBC animals (n ≥ 4 per genotype) were measured by ELISA. *, $P ≤ 0.05$; **, $P ≤ 0.01$; and ***, $P ≤ 0.001$; Welch unpaired two-tailed t test.
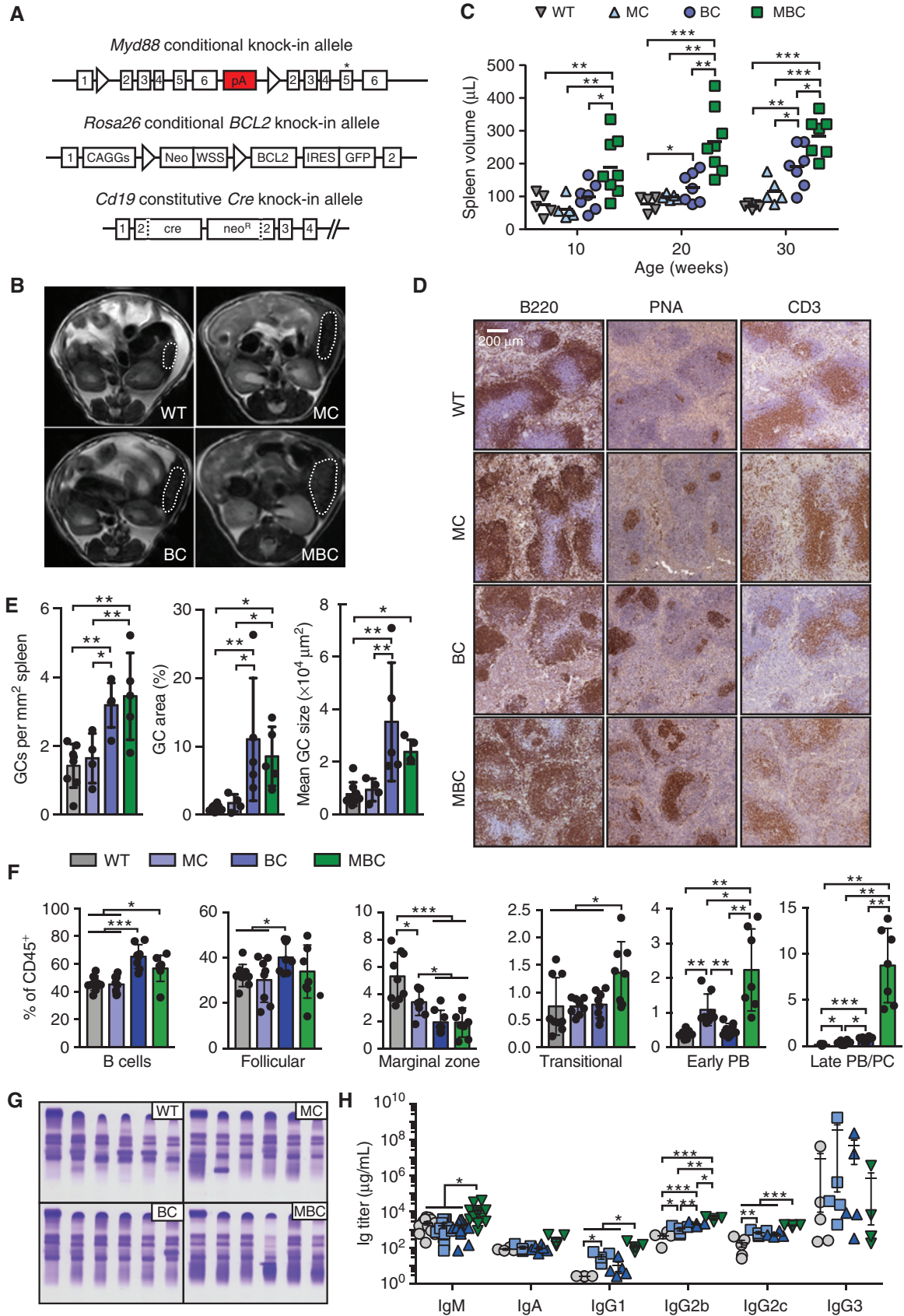
Supplementary Fig. S1C). We next performed a histologic assessment of spleen sections derived from WT, MC, BC, and MBC animals (Fig. 1D; Supplementary Fig. S1D). For that purpose, 30-week-old WT, MC, BC, and MBC animals were sacrificed, and spleens were stained with antibodies detecting CD3 (labeling the splenic T-cell zone) and B220 (labeling the splenic B-cell zone), as well as PNA (labeling the germinal center) on serial sections. Neither the number of germinal centers per spleen area nor the germinal center area per spleen area or the average size of the germinal centers differed significantly between WT and MC animals (Fig. 1D and E; Supplementary Fig. S1D). However, BC animals displayed significantly more and larger germinal centers than WT and MC animals (Fig. 1D and E). Similarly, MBC animals showed significantly more and larger germinal centers than MC mice and WT controls (Fig. 1D and E). Of note, we did not detect clonal lymphoma infiltrates in MBC spleens at this time point. Furthermore, the global splenic architecture was not disrupted in MBC mice. In a different set of experiments, we employed a BCL6 antibody to stain splenic germinal centers (Supplementary Fig. S1E). In these experiments, BC animals displayed slightly more and significantly larger germinal centers than WT animals (Supplementary Fig. S1E). Similarly, MBC animals showed significantly more and larger germinal centers than WT and MC controls (Supplementary Fig. S1E). Altogether, these data indicate that oncogenic *Myd88* and *BCL2* cooperate in enhancing reactive splenomegaly and germinal center formation *in vivo*.

Myd88[p.L252P] and *BCL2* Cooperate to Drive an Expansion of CD138-Positive Cells *In Vivo*

To gain further insight into the cellular composition underlying the germinal center hyperplasia that we observed in BC and MBC animals (Fig. 1D and E; Supplementary Fig. S1D and S1E), we next performed flow cytometry–based immune phenotyping (Fig. 1F; Supplementary Fig. S1F–S1H). We particularly assessed the representation of total B cells (B220^{+} of CD45^{+}), follicular B cells (B220^{+}/CD93^{−}/CD21^{low}/CD23^{+} of CD45^{+}), marginal zone B cells (B220^{+}/CD93^{−}/CD21^{high}/CD23^{−} of CD45^{+}), transitional B cells (B220^{+}/CD93^{+} of CD45^{+}), early plasmablasts (CD138^{+}/B220^{+}/MHCII^{+} of CD45^{+}), and late plasmablasts/plasma cells (CD138^{+}/B220^{−}/MHCII^{−} of CD45^{+}) from spleens and bone marrow (BM) of 30-week-old WT, MC, BC, and MBC animals (Fig. 1F; Supplementary Fig. S1F), as well as 50-week-old WT, MC, and BC mice (Supplementary Fig. S1G and S1H). As shown in Fig. 1F, the relative percentage of splenic B cells was significantly increased in BC and MBC mice compared with WT animals. A further subclassification of these B cells revealed that BC animals displayed significantly more follicular B cells compared with WT, MC, and MBC mice (Fig. 1F). Marginal zone B cells were significantly less prevalent in MC, BC, and MBC mice compared with WT animals (Fig. 1F). MBC mice displayed a significantly increased percentage of transitional B cells compared with WT, MC, and BC mice (Fig. 1F). The most striking differences were observed when the percentages of CD138^{+} cells were analyzed (Fig. 1F). MC animals displayed significantly more CD138^{+} cells compared with WT and BC mice, possibly indicating that oncogenic *Myd88* enhances germinal center transition (Fig. 1F). Moreover,

oncogenic *Myd88* and *BCL2* appear to cooperate in the accumulation of CD138^{+} early plasmablasts (Fig. 1F). Similarly, MBC mice harbor a significantly higher percentage of late plasmablasts/plasma cells in the spleen and BM compared with WT, MC, and BC mice (Fig. 1F; Supplementary Fig. S1F). The levels of CD138^{+} cells found in MBC animals at 30 weeks of age were not reached even by 50-week-old MC and BC mice (Supplementary Fig. S1G and S1H). To investigate whether these plasma cells passed through the germinal center reaction, or whether the engineered mutations preferentially drive the development of extrafollicular plasma cells, we performed full-length B-cell receptor (BCR) sequencing on CD138^{+} cells isolated from the spleens of 10-week-old WT and MBC animals (*n* = 4 per genotype; ref. 21). In short, each individual *Ig* cDNA molecule is uniquely labeled with a barcode (unique molecular identifier, UMI) during reverse transcription. This UMI allows the assignment of each sequencing read to a cDNA molecule of origin. Reads with identical UMI are grouped into a "molecular identifier group" (MIG), and a nearly error-free sequence is derived for each MIG by consensus assembly of the assigned reads. Analysis of the somatic hypermutation frequency of the derived V(D)J region sequences revealed a minor but significant shift toward mutated *Ighm* sequences (51.6% and 39.4% of *Ighm* sequences with more than one mutation for MBC and WT CD138^{+} cells, respectively; Supplementary Fig. S2A and S2B). No significant differences in the mutation rates of transcripts with *Ighg1, Ighg2c, Ighg3*, and *Igha* constant regions were observed (Supplementary Fig. S2A and S2B). *Ig* sequences recovered from CD138^{+} MBC cells showed a significant reduction of *Ighm* transcripts and a significant increase in *Ighg2c* and *Ighg3* isotypes compared with CD138^{+} WT cells (Supplementary Fig. S2C and S2D), in line with a role of Toll-like receptor (TLR) signaling in promoting class switch recombination (22–24). Altogether, these data indicate that the CD138^{+} cells, which accumulate in MBC mice, pass through the germinal center reaction with at least the same frequency as CD138^{+} WT cells. These observations further suggest a role of oncogenic *Myd88* in promoting the transition through the germinal center reaction, which may be augmented by the apoptosis-repressing effect of an increased *BCL2* gene dosage, ultimately leading to a substantial expansion of postgerminal center B-cell stages in non-lymphoma–bearing animals.

B-cell–Specific *Myd88*[p.L252P] and *BCL2* Expression Disrupts Self-tolerance *In Vivo*

Given the robust expansion of postgerminal center B-cell populations in MBC mice, we next asked whether MBC animals displayed increased serum immunoglobulin levels compared with WT, MC, and BC mice. To address this question, we initially performed electrophoreses with serum samples isolated from 30-week-old animals (Fig. 1G). Consistent with the massive expansion of early and late plasmablasts, as well as plasma cells in MBC mice, we observed a substantially increased gamma-globulin fraction in sera derived from MBC animals compared with WT, MC, and BC samples (Fig. 1G). The gamma-globulin levels of MC and BC animals were only mildly increased compared with WT mice (Fig. 1G). Of note, we detected a monoclonal gamma-globulin band in 1 out of 6 MC animals, whereas no monoclonal band could be detected in WT, BC, and MBC mice at this 30-week time point

($n = 6$ each; Fig. 1G). To further dissect this gammopathy, we next performed ELISA experiments to assess the contribution of IgM and the IgG subclasses IgG1, IgG2b, IgG2c, and IgG3 to the gamma-globulin fraction. As shown in Fig. 1H, MBC animals displayed significantly increased serum IgM, IgG1, IgG2b, and IgG2c concentrations compared with WT, MC, and BC animals, whereas there was no significant difference in IgG3 concentrations (Fig. 1H). These data are consistent with the reduced percentage of splenic marginal zone cells, which are a major source of IgG3 in response to T-cell–independent antigens (25). These results demonstrate that 30-week-old MBC animals display a marked polyclonal gammopathy, consisting of class-switched and nonclass-switched immunoglobulins.

Recent reports have provided evidence indicating that chromatin/DNA-associated as well as RNA and RNA-associated antigens can potently activate autoreactive B cells through sequential dual engagement of BCR and TLR/MYD88 signaling cascades (26–29). In brief, AM14 RF^{+} B cells that bind autologous IgG2a with low affinity can be driven into proliferation by *in vitro* exposure to affinity-purified IgG2a[j] monoclonal antibodies specific for nucleosomes (30). Using this system, it was shown that activation of RF^{+} B cells was driven by IgG2a:chromatin immune complexes, which was DNAse sensitive (26). Moreover, activation was dependent on the synergistic engagement of the BCR- and MYD88-dependent TLR signaling (26). The same BCR/TLR paradigm was shown to hold true for RNA-associated autoantigens, as well as CpG dsDNA antigens (27, 29). It is important to note that full activation of these autoreactive B cells was abolished in the absence of *Myd88* (26, 27, 29). Moreover, the constitutive B-cell–specific overexpression of BCL2 was recently shown to impair tolerance induction in a series of model systems and to induce a lupus-like serologic phenotype with antinuclear reactivity (31–37). Given the critical role of *Myd88* in promoting the activation of autoreactive B cells, as well as the impact of *BCL2* on tolerance induction, we next asked whether B-cell–specific expression of the *Myd88* p.L252P gain-of-function mutation and/or *BCL2* overexpression may promote the loss of self-tolerance. For that purpose, we assessed the presence or absence of autoreactive serum antibodies using the HEp-2 indirect immunofluorescence staining assay. As shown in Fig. 2A, WT and BC sera produced only a dim anti-IgM fluorescence signal in the HEp-2 assay, whereas MC and MBC animals displayed significantly higher levels of autoreactive IgM antibodies. The staining pattern obtained with MC and MBC sera was largely cytoplasmic, indicating that these antibodies may not recognize DNA or DNA-associated antigens (Fig. 2B). We next assessed the presence of IgG autoreactive antibodies. As shown in Fig. 2C, we observed a robust staining with sera derived from MC, BC, and MBC animals, whereas WT serum only produced faint signal. Of note, BC serum primarily reacted with nuclear antigens (Fig. 2D). Altogether, these data indicate that B-cell–specific expression of *Myd88*[p.L252P] overcomes self-tolerance. Of note, *Myd88*[p.L252P] expression primarily results in an increased presence of autoantibodies against cytoplasmic structures, mainly of the IgM isotype, whereas *BCL2* overexpression promotes the generation of predominantly antinuclear IgG immunoglobulins. MBC animals showed a mixed phenotype.

B-cell–Specific *Myd88*[p.L252P] and *BCL2* Expression Leads to an Enhanced B-cell Reactivity *In Vivo*

B-cell responses are subdivided into T-cell–dependent (TD) and T-cell–independent (TI) responses (38). TD antigens are proteins that are processed and presented on MHC-II surface molecules for detection by CD4^{+} T helper cells (38). Two types of TI antigens exist (38). TI-I antigens, such as lipopolysaccharide (LPS), CpG, and poly-IC, mediate polyclonal B-cell activation by engaging TLRs (38). TI-II antigens are typically polysaccharides that induce antigen-specific B-cell responses through BCR clustering (38). To ask whether B-cell–specific *Myd88*[p.L252P] expression and/or *BCL2* overexpression may affect the magnitude or persistence of the humoral immune response induced by TD or TI-II antigens, we immunized WT, MC, BC, and MBC mice with NP-CGG (TD) or NP-Ficoll (TI-II) and quantified the NP-specific IgM and IgG response 4, 7, 10, 21, and 40 days after the vaccination. The maximal IgM response to NP-Ficoll was increased 7.5- and 6.6-fold in MC and BC animals compared with WT, respectively (Fig. 2E). This effect was even more pronounced in MBC animals, where we observed a 14.8-fold increase compared with WT (Fig. 2E). The NP-Ficoll–induced IgG response was similarly enhanced in MC and MBC animals (23.0- and 36.3-fold, respectively), compared with WT (Fig. 2E). However, in contrast to the IgM response, the IgG response was only marginally (4.5-fold) increased in BC compared with WT animals, suggesting *BCL2* overexpression may not suffice in promoting class-switch recombination following TI-II–mediated B-cell activation (Fig. 2E). The humoral anti-NP response following exposure to the TD antigen NP-CGG differed from that observed for NP-Ficoll. Both BC and MBC animals displayed a massively enhanced maximal IgM (7.3- and 8.3-fold, respectively) and IgG response (67.7- and 80.6-fold) compared with WT controls (Fig. 2F). In contrast, MC animals displayed only a marginally enhanced IgM and IgG response (2.8- and 27.6-fold) compared with WT mice (Fig. 2F). These data, which are in line with previous reports on the analysis of an *Eμ:Bcl2* allele (35), indicate that *BCL2* overexpression particularly promotes the humoral response against TD antigens. The expression of *Myd88*[p.L252P] promotes class switch in response to TI-II antigen, in agreement with previous studies demonstrating the importance of TLR signaling for class switch to IgG in response to thymus-independent antigen (22, 39).

Expression of Oncogenic *Myd88* Drives the Formation of a Protein Supercomplex Containing BCR and Myddosome Components

Recent data from human lymphoma cell lines indicate that oncogenic BCR signaling in a subset of ABC-DLBCL cases is coordinated by a protein complex involving MYD88, TLR9, and IgM (40). This so-called My-T–BCR complex colocalizes with mTOR on endolysosomes, where it promotes NF-κB–mediated prosurvival signaling (40). This report prompted us to ask whether protein complexes involving BCR signaling components, as well as MYD88 and Myddosome components, also assemble in nontransformed *Myd88*-mutant cells. To this end, we performed proximity ligation assays (PLA), which label proteins that colocalize within a nanometer distance (41). We isolated naïve B cells from WT and MC animals to explore the
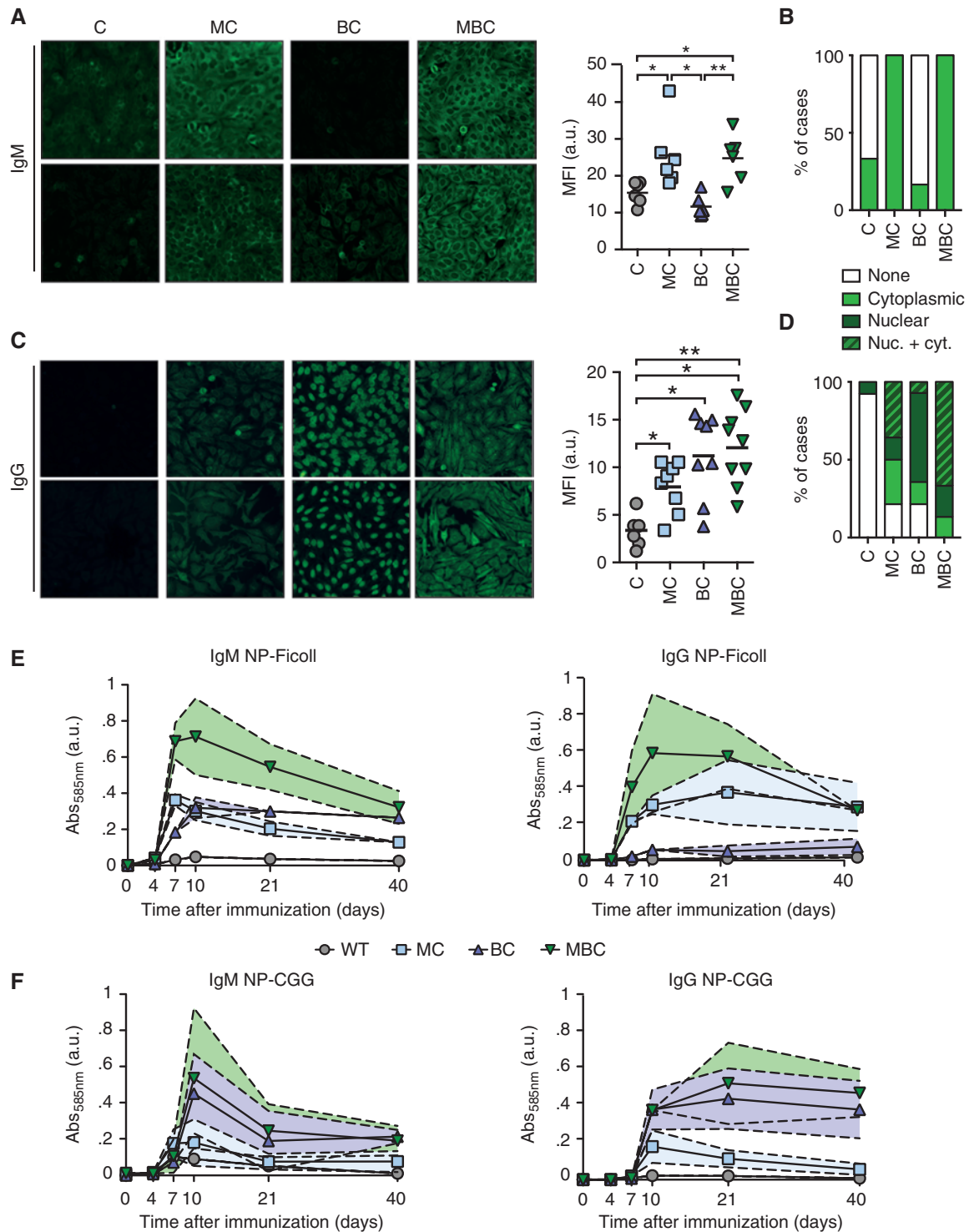
Figure 2. MBC animals show exaggerated immune responses to self- and foreign antigen. **A,** Self-reactive antibodies of the IgM isotype were visualized by a Kallestad HEp-2 assay adapted to the murine system, and mean fluorescence intensities (MFI) were quantified ($n = 6$ per genotype, two exemplary cases per genotype are shown). **B,** Quantification of the observed staining patterns. **C,** Autoreactive IgG immunoglobulins were visualized by an adapted Kallestad HEp-2 assay, and mean fluorescence intensity (MFI) values were quantified (WT, $n = 7$; MC, $n = 8$; BC, $n = 8$; MBC, $n = 9$; two exemplary cases per genotype are shown). **D,** Quantification of the observed staining patterns. **E** and **F,** WT, MC, BC, and MBC animals ($n = 3$) were immunized i.p. with either NP-Ficoll (50 μg) or NP-CGG (50 μg) at day 0, and the NP-specific IgM and IgG levels in the sera of animals were measured at days 0, 4, 7, 10, 21, and 40 after immunization by ELISA. Envelopes represent SEM. *, $P \leq 0.05$ and **, $P \leq 0.01$; Welch unpaired two-tailed t test.
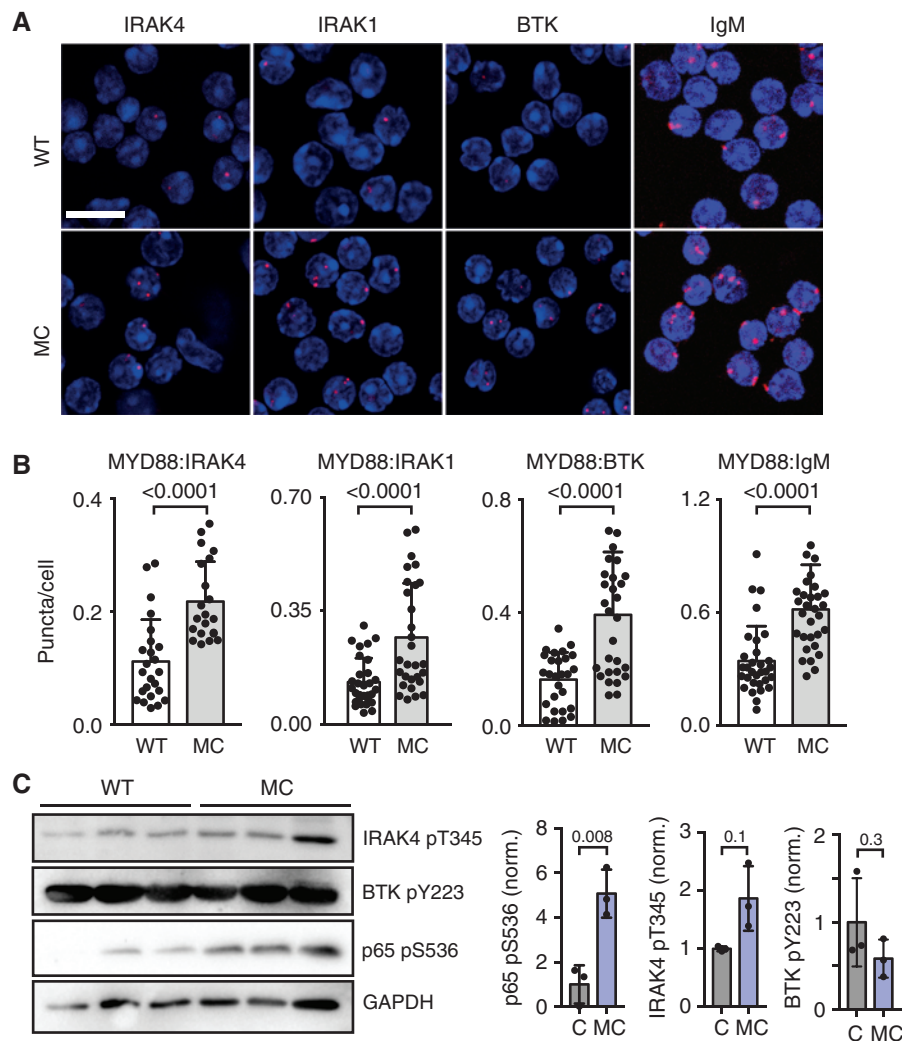
Figure 3. *Myd88* p.L252P mutation enhances the formation of the My-T–BCR supercomplex. **A,** Exemplary images of PLA assays for MYD88 proximity with IRAK4, IRAK1, BTK, and IgM, respectively. Blue, DAPI; red, PLA signal. Scale bar, 10 μm. **B,** Quantification of the data shown in **A**. Each dot represents the average number of PLA signals per cell and experimental well. The mean and SEM of at least three independent experiments are depicted. Significant differences between samples were calculated by Welch unpaired *t* test. **C,** Lysates were generated from CD43-depleted splenocytes from 10-week-old MC and WT. Immunoblots were generated for the indicated targets. Blots were quantified using ImageJ.

interactome of WT and mutant MYD88. In these experiments, we detected significantly more complexes involving MYD88 and IRAK1, as well as the Myddosome component IRAK4, in unstimulated MC B cells compared with WT controls (Fig. 3A and B). Moreover, naïve B cells from MC animals also displayed significantly more protein complexes consisting of MYD88 and the BCR signaling components IgM and BTK compared with WT controls (Fig. 3A and B). To further substantiate the functional relevance of the increased MYD88-centered complex formation in MC-derived B cells, we next performed immunoblots probing the Myddosome formation–induced autophosphorylation site Thr-345 in IRAK4, the phospho-Tyr-223 residue in BTK, and the IKK2-dependent phospho-Ser-536 site in the NF-κB subunit p65 in unstimulated MC and WT B cells (Fig. 3C). In these experiments (*n* = 3 independent B-cell isolations from distinct animals), we observed significantly increased p65 phosphorylation on Ser-536 in

MC compared with WT B cells (Fig. 3C). Although there was a trend toward increased IRAK4 autophosphorylation on Thr-345 in MC B cells, this did not reach statistical significance (Fig. 3C). Similarly, there was no differential BTK Tyr-223 phosphorylation in MC versus WT B cells (Fig. 3C). Altogether, these observations suggest that mutant MYD88 may constitutively nucleate a signaling hub, which links BCR and TLR signaling components, even in nontransformed B cells. This constitutive protein complex formation is further associated with increased p65 Ser-536 phosphorylation in MC B cells.

Myd88[p.L252P] and *BCL2* Cooperate in ABC-DLBCL Lymphomagenesis *In Vivo*

We next aimed to determine the effect of B-cell–specific *Myd88*[p.L252P] and/or *Rosa26*[BCL2.IRES.GFP] expression on overall survival and to determine the cause of death in these mice. We previously reported that MC animals display a significantly

reduced overall survival, compared with WT mice and that MBC animals live significantly shorter than MC mice (20). However, it remained unclear whether BC animals display a different overall survival than MC mice. Thus, we performed a direct head-to-head comparison of MC, BC, and MBC animals. As shown in Fig. 4A, BC mice show a significantly reduced overall survival compared with MC animals. Furthermore, and in line with previous results, MBC mice died significantly earlier than MC and BC animals (Fig. 4A). We further determined the cause of death in MC, BC, and MBC mice. Although MBC mice developed life-limiting lymphoma with 83% penetrance, MC and BC mice developed lymphoma in only 20% and 50%, respectively (Fig. 4B). The malignant lesions observed in MBC animals were largely located sub-diaphragmatically in mesenteric lymph nodes, but rarely in mediastinal and submandibular lymph nodes (Supplementary Fig. S3A and S3B). We did not detect any obvious central nervous system manifestations. Although spleens were frequently enlarged, we failed to detect evidence for infiltration by clonal lymphoma. Instead, we observed the germinal center expansion detailed in Fig. 1D and E. Moreover, spleen weights did not exceed 450 mg, further indicating a reactive nature of the observed splenomegaly (Supplementary Fig. S3B). The average number of distinct lymph node groups involved was 1.7 (Supplementary Fig. S3C). Immunophenotyping revealed that BC- and MBC-derived lymphomas were almost exclusively B220$^-$ and largely CD138$^+$ (Fig. 4B and C). We note that the CD138 staining pattern displayed some intertumoral heterogeneity, which is illustrated in Supplementary Fig. S3D, where six distinct lymph node manifestations derived from six distinct animals are displayed. The CD138 staining intensity varied between different areas of the same lymphoma manifestation. Moreover, when analyzed at higher magnification, we observed clearly distinct CD138 staining intensity in adjacent cells. It is important to note that the same lymphoma areas stained uniformly positive for GFP, which is only expressed in cells that have expressed the $Cd19^{Cre}$ allele during their lifetime and therefore belong to the B-cell lineage (Supplementary Fig. S3D). Altogether, these data suggest a postgerminal center plasmablastic differentiation pattern of MBC lymphomas, whereas lymphomas developing in MC mice retained expression of the B-cell marker B220 and were CD138^{neg} (Fig. 4B and C). The proliferation index in MBC lymphomas was 42.7% (±17.3%, $n = 19$). MC and BC lymphomas displayed similar proliferation indices of 39.1 (±14.5%, $n = 4$) and 35.9% (±14.3%, $n = 5$), respectively (Fig. 4C; Supplementary Fig. S3E). Next to lymphomas, MC, BC, and MBC mice displayed the

indicated percentage of cases that had to be sacrificed, due to nonclonal B-cell lymphoproliferation or scratch wounds (Fig. 4B). Particularly, the latter may represent the manifestation of an exacerbated autoimmunity phenotype. To determine whether lesions histologically classified as lymphoma truly represent clonal expansions, we next performed RNA-based BCR sequencing (adapted from ref. 42). Although the BCR repertoire in the spleens of WT animals was highly polyclonal, as expected, MBC lesions showed a strongly reduced variation, with the majority of cases being dominated by a single or only a few parallel clones (Fig. 4D and E). Perhaps not surprisingly, the BCR sequence of isolated stable cell lines corresponded to a dominant clone found in the primary lesion (Fig. 4D).

Cell lines derived from MBC lymphomas could be established *in vitro* and were transplantable into $Rag1^{-/-}$ recipient animals. Upon transplantation, these MBC-derived cell lines formed lymphomas that were indistinguishable from the original lymphomas with respect to morphology, immune phenotype, and proliferation index (Fig. 4F).

To further benchmark our mouse model against human ABC-DLBCL lymphomas, we next used 3′-RNA sequencing (RNA-seq) to assess the transcriptomes derived from MBC lymphomas. Lymphomas derived from $Kmt2d^{fl/fl};VavP\text{-}Bcl2;$ $Ighg1^{Cre/WT}$ (KBC) mice, which develop follicular lymphoma and GCB-DLBCL–like disease, served as a reference control (43). To specifically ask whether the transcriptome data derived from MBC and KBC lymphomas cocluster with transcriptome data derived from human GCB- or ABC-DLBCL, we performed a gene set enrichment analysis (GSEA) for gene signatures that have previously been shown to effectively distinguish human GCB- from ABC-DLBCL (11) and found a significant enrichment of the GCB and ABC signatures in KBC and MBC tumors, respectively (Fig. 4G). In addition to KBC lesions, we also benchmarked our MBC tumors against the MYC/PI3K-driven $R26^{LSL.Myc/LSL.P110*};$ $Ighg1^{Cre/WT}$ (MPC) Burkitt lymphoma model (44), which constitutes an additional germinal center–derived aggressive lymphoma model (Supplementary Fig. S3F). We observed that MPC lymphomas displayed a significant enrichment of GCB gene expression signatures, whereas MBC lymphomas were enriched, albeit not significantly in this analysis, for ABC signatures (Supplementary Fig. S3F).

Next to transcriptome profiling, we also performed whole-exome sequencing of 17 MBC cases to ask whether the pattern of spontaneous mutations in these lymphomas also resembles the genomic aberrations detected in human DLBCL cases. As benchmarks, we employed two recently

Figure 4. MBC animals develop ABC-DLBCL–like tumors. **A,** Survival curves of WT ($n = 10$), MC ($n = 104$, median 101.9 weeks), BC ($n = 74$, median 68.7 weeks), and MBC animals ($n = 107$, median 42.3 weeks). **B,** Quantification of the terminal phenotype of MC ($n = 15$), BC ($n = 12$) and MBC animals ($n = 30$). **C,** Exemplary illustration of hematoxylin and eosin (H/E), B220, CD138, and Ki67 stainings of MC, BC, and MBC tumors. **D,** BCR sequencing–based clonality analysis of WT spleens and two MBC primary tumors ("M552 tumor" and "M108 tumor") and derived cell lines. Each circle represents a unique BCR sequence, with the circle area representing the clone size. Clones differing in one base are connected by lines to clusters. Clusters consisting of ≥10% of reads are highlighted by color, and the exact percentages are given. **E,** Summary of the clonalities observed in MC ($n = 3$), BC ($n = 5$), and MBC lesions ($n = 25$) compared with the polyclonal scenario observed in WT spleens ($n = 3$). **F,** Comparison of the IHC phenotype of two primary tumors and transplanted tumors. For transplantation, stable cell lines derived from the primary tumors M108 and M552 were injected intraperitoneally into $Rag1^{-/-}$ recipients. **G,** GSEA for ABC- and GCB-DLBCL signatures (11) on MBC ($n = 4$) and KBC (ref. 43; $n = 6$) tumors. **H,** Whole-exome sequencing was performed on 17 MBC tumors. Identified mutated genes (see also Supplementary Table S1) were plotted for the mutation frequencies of the orthologous human genes in two published DLBCL whole-exome sequencing datasets (9, 11). **I,** Cytokine levels in the sera of lymphoma-bearing MBC animals ($n = 15$) were measured and compared with WT levels ($n = 7$). Solid lines represent the mean and envelope the SD. Cytokines with significant differences between MBC and WT are highlighted in red. *, $P \le 0.05$; **, $P \le 0.01$; ***, $P \le 0.001$; and ****, $P \le 0.0001$. **A,** Log-rank test. **G** and **I,** Welch unpaired two-tailed t test adjusted for multiple comparisons. Scale bars, 50 μm.
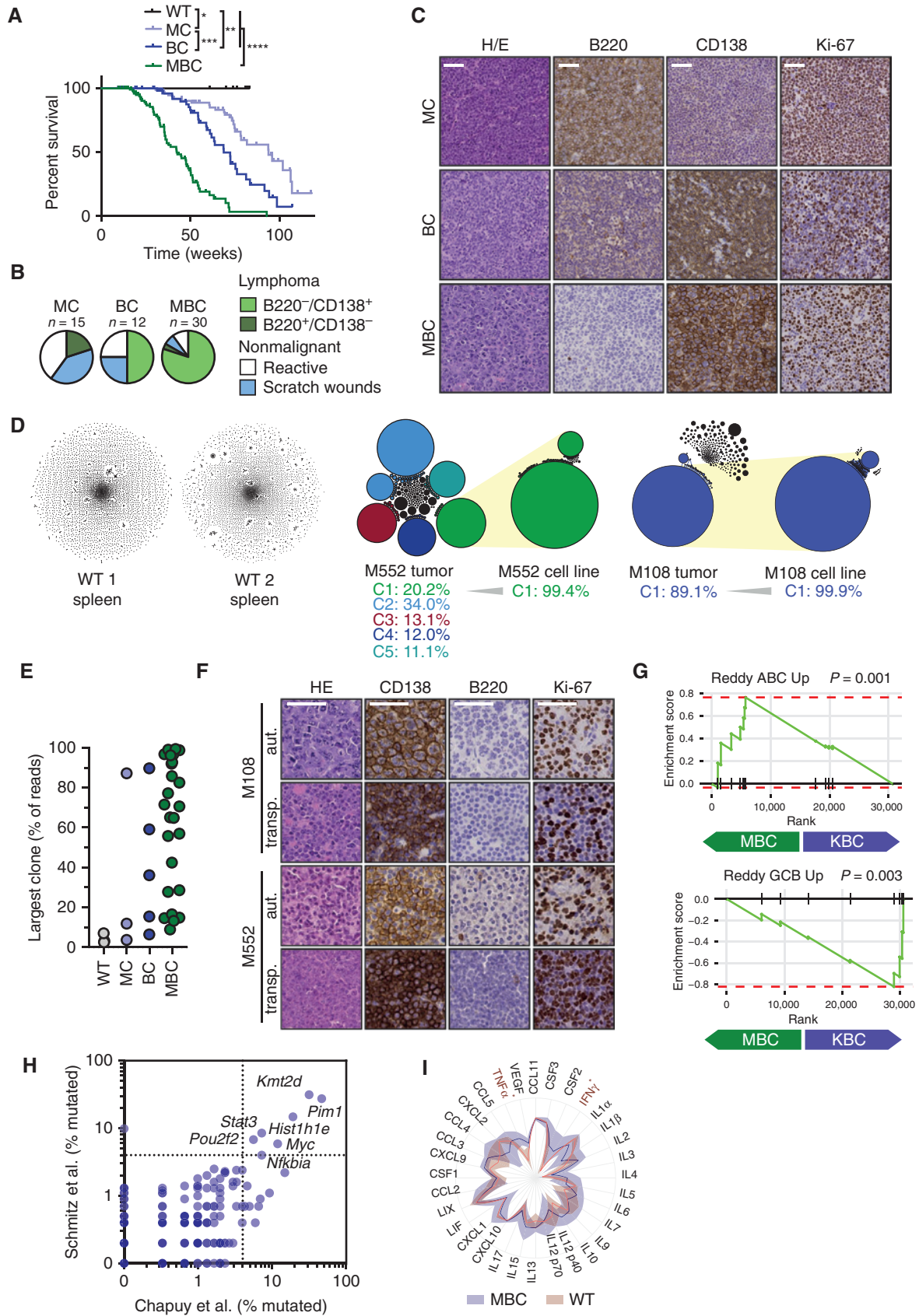
published datasets reporting the mutational profiles of 878 human DLBCL cases (9, 10). We detected a number of mutations in our MBC lymphomas, including aberrations in *Pim1, Myc, Kmt2d, Nfkbia, Stat3, Pou2f2,* and *Hist1h1e* (Fig. 4H; Supplementary Table S1), which were also frequently mutated in both human DLBCL datasets (9, 11).

We also assessed the serum abundance of 32 distinct cytokines in lymphoma-bearing MBC mice and age-matched WT controls using multiplexed cytokine arrays. We observed significantly higher levels of IFNγ and TNFα in sera of lymphoma-bearing MBC mice, compared with controls (Fig. 4I; Supplementary Fig. S4A). In line with these observations, increased TNFα and IL10 plasma levels were recently shown to correlate with poor prognosis in DLBCL (45). Moreover, the *TNFA* single-nucleotide polymorphism 308G→A was shown to be associated with increased constitutive and inducible TNFα expression and increased risk of DLBCL development (46–49). Furthermore, TNFα was shown to induce an inhibitory gene expression signature in CD4+ T cells during chronic viral infection, indicating that TNFα may affect the ratio of CD4+:CD8+ T cells (50). Conversely, IFNγ was shown to act on CD8+ T cells to enhance their abundance, mobility, and cytotoxicity during viral infection and experimental graft rejection (51, 52). Thus, our cytokine profiling data may indicate that lymphoma-bearing MBC mice display signs of a proinflammatory environment favoring the activity of CD8+ T cells.

To further gauge whether cytokines were produced by the lymphoma cells themselves or rather the nonmalignant components of the lymphoma microenvironment, we compared gene expression profiles of bulk primary MBC lymphoma samples and stable cell lines derived from MBC lymphomas. The relative expression levels of *Ccl11, Il1a, Il6, Il12b, Cxcl1, Cxcl5, Ccl2, Csf1, Cxcl9, Ccl5,* and *Ifng* were significantly lower in the three analyzed cell lines compared with the primary lymphoma material, suggesting that these cytokines are, at least partially, synthesized by nonmalignant cells within the microenvironment. In contrast, we found that several cytokines, including *Il2, Il10,* and *Il15* (out of which particularly IL2 and IL15 were previously shown to promote B-cell proliferation; refs. 53, 54), were expressed at high levels by the lymphoma cell lines. Moreover, *Tnf* was expressed at high levels by two of the three cell lines (Supplementary Fig. S4B). However, it is important to note that mRNA expression levels do not always correlate with protein expression (55). Thus, the data presented here have to be interpreted with care.

MBC-Derived Lymphomas Display an Actionable BCL2 Inhibitor Sensitivity

Our data indicate that the MBC model accurately mimics human ABC-DLBCL biology with regard to morphology, as well as genomic and transcriptomic profiles. Thus, we next aimed to employ this model as a preclinical tool. To this end, we initially performed cellular viability assays to determine drug sensitivity. We specifically assessed the sensitivity of four distinct MBC-derived lymphoma cell lines (M191, M190, M108, and M552), as well as two human ABC-DLBCL (U2932 and RI1) and two human GCB-DLBCL cell lines (SUDHL10 and OCILY7) toward the IRAK4 inhibitor ND-2158, the IKK2 inhibitor LY-2409881, and the BCL2 inhibitor venetoclax. These experiments revealed that murine MBC–derived cells, as well as the human ABC-DLBCL cell lines included in our screen were sensitive against IKK2, IRAK4, and BCL2 inhibition (Fig. 5A–C). Reminiscent of previously published data (56, 57), we found the two GCB cell lines investigated here to be resistant against BCL2 blockade (Fig. 5A). However, it is important to note that several human GCB-DLBCL cell lines, such as HF, RC, McA, and OCI-LY19 cells, have been reported to be highly sensitive to BCL2 inhibition (58). Thus, our observations, which are limited to two human GCB cell lines, should not be generalized to all GCB-DLBCL cases. Of note, BH3 profiling (59) confirmed that human ABC-DLBCL cell lines and murine MBC–derived cell lines were BCL2 dependent, whereas the limited number of human GCB-DLBCL cell lines displayed a more prominent sensitivity against MCL1 inhibition (Fig. 5D).

As cell viability assays do not distinguish between cell death and growth arrest, we next performed flow cytometry–based apoptosis measurements, using Annexin V/propidium iodide (PI) costaining. Venetoclax and LY-2409881 effectively induced apoptosis in the MBC lines (Fig. 5E and F). Moreover, venetoclax induced massive apoptosis in both human ABC-DLBCL cell lines, whereas LY-2409881–induced apoptosis was prominent in RI1 and relatively mild in U2932 ABC-DLBCL cells (Fig. 5E and F). ND-2158 treatment did not lead to a significant induction of apoptosis in any of the investigated cell lines. Altogether, these data indicate that venetoclax, ND-2158, and LY-2409881 display therapeutic efficacy in the human and murine ABC-DLBCL cell line models investigated in this study. However, only venetoclax and LY-2409881 appear to induce apoptosis, whereas ND-2158 likely reduces proliferation (Fig. 5G; Supplementary Fig. S5A).

Of note, in an extension of this focused candidate approach to discover potentially actionable aberrations in GCB and ABC cell lines, we also conducted a larger discovery screen on human GCB (OCILY7, SUDHL10) and ABC cell lines (RI1, U2932), as well as three MBC-derived murine lymphoma cell lines. We specifically determined the IC$_{50}$ values of 167 additional distinct drug compounds (Supplementary Fig. S5B; Supplementary Table S2). Fitting with our transcriptome data, RI1 and U2932 cells coclustered with the MBC cell lines.

Figure 5. MBC tumors are responsive to BCL2 inhibition by venetoclax. **A–C,** Murine MBC and MYC cell lines as well as human ABC and GCB DLBCL cell lines were treated with increasing doses of ABT-199 (0–300 nmol/L), LY-2409881 (0–15 μmol/L), or ND-2158 (0–5 μmol/L), and cell viability was measured after 96 hours by CellTiter-Glo assay. The mean of a minimum of three independent experiments is shown, with each experiment consisting of three technical replicates. Error bars represent the SEM. **D,** BH3 profiling (56) of MBC, ABC, MYC, and GCB-DLBCL cell lines. Cells were exposed to either BH3 peptides or small-molecule inhibitors for 1 hour. The coloring indicates the fraction of Cytochrome C releasing (i.e., apoptotic) cells after exposure measured by flow cytometry. **E–G,** Apoptosis was measured by flow cytometric analysis of the Annexin V/PI double-positive population 48 hours after treatment of the cell lines M191, M108, M552, MYC-14, RYS-202, U2932, RI1, SUDHL10, and OCILY7 with 300 nmol/L ABT-199, 5 μmol/L ND-2158, or 5 μmol/L LY-2409881. **H,** 10^7 M108 cells were injected i.p. into *RAG1$^{-/-}$* recipients. Two weeks after transplantation, animals were treated with ABT-199 (200 mg/kg daily, oral gavage), ND-2158 (150 mg/kg, i.p., daily), or LY-2409881 (100 mg/kg, i.p., daily) or were left untreated, and survival after transplantation was recorded. *, $P \leq 0.05$; **, $P \leq 0.01$; and ***, $P \leq 0.001$. **E–G,** Welch unpaired two-tailed *t* test adjusted for multiple comparisons. **H,** Log-rank test.
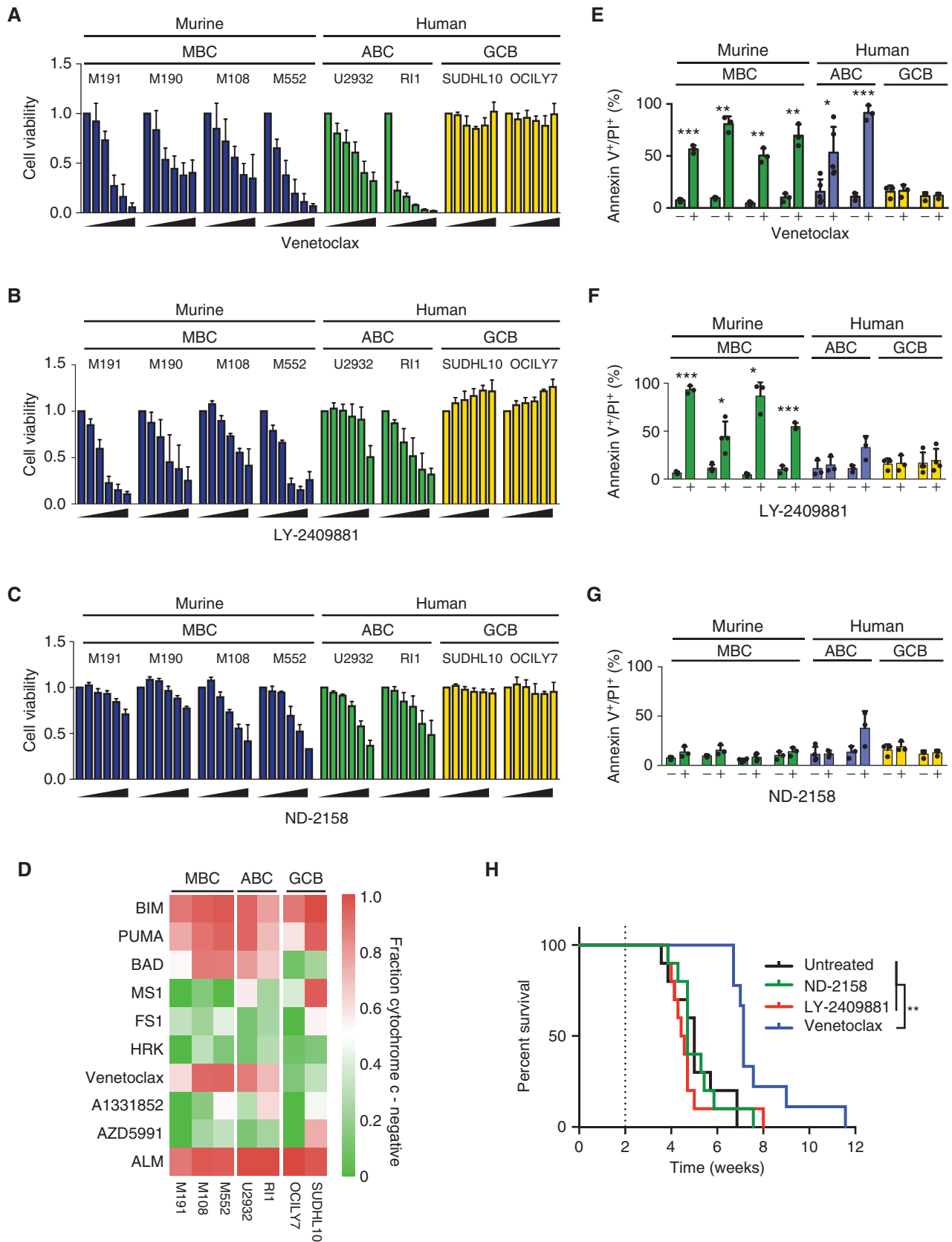
To ask whether the therapeutic efficacy of venetoclax, ND-2158, and LY-2409881 was reproducible *in vivo*, we next performed preclinical drug sensitivity studies in a transplant model. To this end, we transplanted 10^7 murine M108 cells i.p. into $Rag1^{-/-}$ recipient animals. Treatment was initiated 14 days after transplantation. Of note, in a series of preparatory experiments, we had verified that 4 of 4 transplanted animals developed necropsy-verified clonal lymphoma 14 days following transplantation. Animals were treated with venetoclax (200 mg/kg, daily, orally), ND-2158 (150 mg/kg, daily, i.p.), or LY-2409881 (100 mg/kg, daily, i.p.) or were left untreated. As shown in Kaplan–Meier format in Fig. 5H, venetoclax induced a significantly increased overall survival (50.0 ± 4.5 days after transplantation following completion of a 3-week treatment course) compared with vehicle control (32.5 ± 5.9 days). Somewhat surprisingly, ND-2158 did not produce a significant survival gain in these experiments. All ND-2158–treated animals succumbed to lymphoma, indicating a lack of *in vivo* activity of this compound at the chosen dose in our model. Similarly, LY-2409881 did not lead to significant survival gains in this model. We note, however, that LY-2409881–treated animals uniformly reached predefined termination criteria (weight loss >10%, hunched posture, ragged fur, apathy). Importantly, we did not detect lymphoma in any of the LY-2409881–treated animals at the time of sacrifice, indicating that LY-2409881 may display preclinical activity, which is masked by life-limiting toxicity. This proinflammatory adverse effect of LY-2409881 is in line with previously reported toxicities of IKK inhibitors (60). Collectively, our preclinical data indicate that venetoclax may display activity against a subset of *BCL2*-altered ABC-DLBCL lymphomas, whereas our data suggest that ND-2158 and LY-2409881 may not be candidates for further development in this entity due to lack of preclinical efficacy or toxicity.

Human ABC-DLBCL and Murine MBC–Derived Lymphomas Display an Actionable PD-L1 Expression

Immune checkpoint blockade is emerging as a potential route for therapeutic intervention in relapsed/refractory DLBCL (61). For instance, the anti–PD-1 monoclonal antibody nivolumab achieved an overall response rate of 36% in patients with DLBCL in a phase I, open-label, dose-escalation, cohort-expansion study (62). Moreover, NF-κB has been shown to be a potent inducer of PD-L1 expression (63). As increased NF-κB activity is a hallmark of ABC-DLBCL, we next assessed the *CD274* mRNA (encoding for PD-L1) expression levels in a

publicly available dataset comprised of 775 (while 1,001 samples were exome sequenced in this study, only 775 were RNA sequenced) human DLBCL cases (11). This analysis revealed that *CD274* and *PDCD1* (encoding for PD-1) were significantly overexpressed in ABC- compared with GCB-DLBCL, whereas *CD86* was expressed at significantly higher levels in GCB- compared with ABC-DLBCL (Fig. 6A). No entity-specific differences were observed in the expression levels of *PDCD1LG2* (encoding for PD-L2) and *CTLA4* (Fig. 6A). These data are in line with recently reported analyses, which demonstrate that cytogenetic aberrations affecting the *CD273/CD274* locus were more frequently observed in the non-GCB subtype of DLBCL (64). To verify that human ABC-DLBCL displays increased PD-L1 protein expression compared with GCB-DLBCL, we next performed IHC on 38 human DLBCL cases. As shown in Fig. 6B, we observed a significantly higher fraction of PD-L1–positive cases among the ABC-DLBCL samples compared with GCB-DLBCL. Moreover, in a series of primary central nervous system lymphomas, we found PD-L1 expression in 22 of 23 cases (Fig. 6C). Intriguingly, the single PD-L1–negative case harbored a noncanonical *MYD88*p.P267L. Among the PD-L1–expressing cases, we found 16 harboring a *MYD88*p.L265P mutation, whereas the remaining 5 cases were *MYD88* WT. These data suggest that ABC-DLBCL cases may be sensitive to immune checkpoint blockade by disrupting the PD-1/PD-L1 axis.

In addition to the PD-1/PD-L1 axis, BCL2 has emerged as a therapeutic target in DLBCL during the last years. The BCL2 inhibitor venetoclax produces response rates of approximately 18% in relapsed/refractory DLBCL (65). To ask whether there might be a biological rationale for combining these agents, we reassessed the available dataset consisting of 775 human DLBCL cases (11). This analysis revealed that 22% of DLBCL cases display a higher than average combined expression of *CD274* and *BCL2*, and that of these cases, 71% are of the ABC subtype (Supplementary Fig. S6A). In contrast, only 29% of cases with a lower than average expression of both *CD274* and *BCL2* were ABC tumors. Building on the observation that human ABC-DLBCL cases frequently coexpressed *CD274* and *BCL2*, and given that our MBC model phenocopies the clinical scenario of ABC-DLBCL, we next asked whether combined BCL2 and PD-1 inhibition may display synergistic cytotoxic activity in this model. For that purpose, we generated a cohort of MBC animals in which lymphoma development was surveilled by longitudinal MRI scans. Upon lymphoma detection, defined by a lesion larger than 75 μL with detectable volume increase in two consecutive

Figure 6. α–PD-1 treatment is an effective strategy for MBC tumors. **A,** Expression levels of the indicated genes were compared between ABC (*n* = 310)- and GCB (*n* = 328)-DLBCL cases in a previously published RNA-seq dataset (11). **B,** Thirty-eight human DLBCL samples were categorized into the ABC and GCB subtypes employing the Hans algorithm (101), and PD-L1 was stained immunohistochemically. Grades 0 and 1 were classified as negative/low expression and 2 to 5 as medium/high expression. **C,** Expression of PD-L1 in primary central nervous system lymphoma samples was analyzed by IHC. MBC animals were monitored for lymphoma development by MRI, and upon tumor detection, treatment was initiated with either ABT-199 (200 mg/kg daily by oral gavage for 3 weeks), α–PD-1 antibody (250 μg twice weekly for 8 weeks), or a combination of both. Exemplary MRI scans 3 weeks after treatment initiation illustrated in **D** and **E** show best tumor volume change within 8 weeks of untreated (*n* = 4), ABT-199–treated (*n* = 6), α–PD-1–treated (*n* = 5), or combination-treated (*n* = 7) MBC. **F,** Survival after tumor detection of untreated (*n* = 4), ABT-199–treated (*n* = 6), α–PD-1–treated (*n* = 5), or combination-treated (*n* = 7) MBC animals. **G,** Timescale of sample collection from α–PD-1–treated MBC tumors. **H,** Mass cytometric analysis of untreated and α–PD-1–treated tumors. Cells were gated for CD45+DNA+ (not illustrated) and CD3+CD4+ as well as CD3+CD8+ events were selected for further analysis. The adjusted *P* value and log$_2$ fold change between α–PD-1 (*n* = 4) and untreated samples (*n* = 14) for each marker (individually for the CD4+ and CD8+ populations) are depicted in **I**, and significant markers are highlighted. **J,** CD3+/CD4+ and CD3+/CD8+ population sizes are given as percentages of the DNA+/CD45+ population. **K,** Differentially expressed markers in the CD3+/CD4+ and CD3+/CD8+ populations. *, $P \leq 0.05$; **, $P \leq 0.01$; and ****, $P \leq 0.0001$. **A, I,** and **K,** Welch unpaired two-tailed *t* test. **B,** Fisher exact test. **F,** Log-rank test. Scale bars, 50 μm.
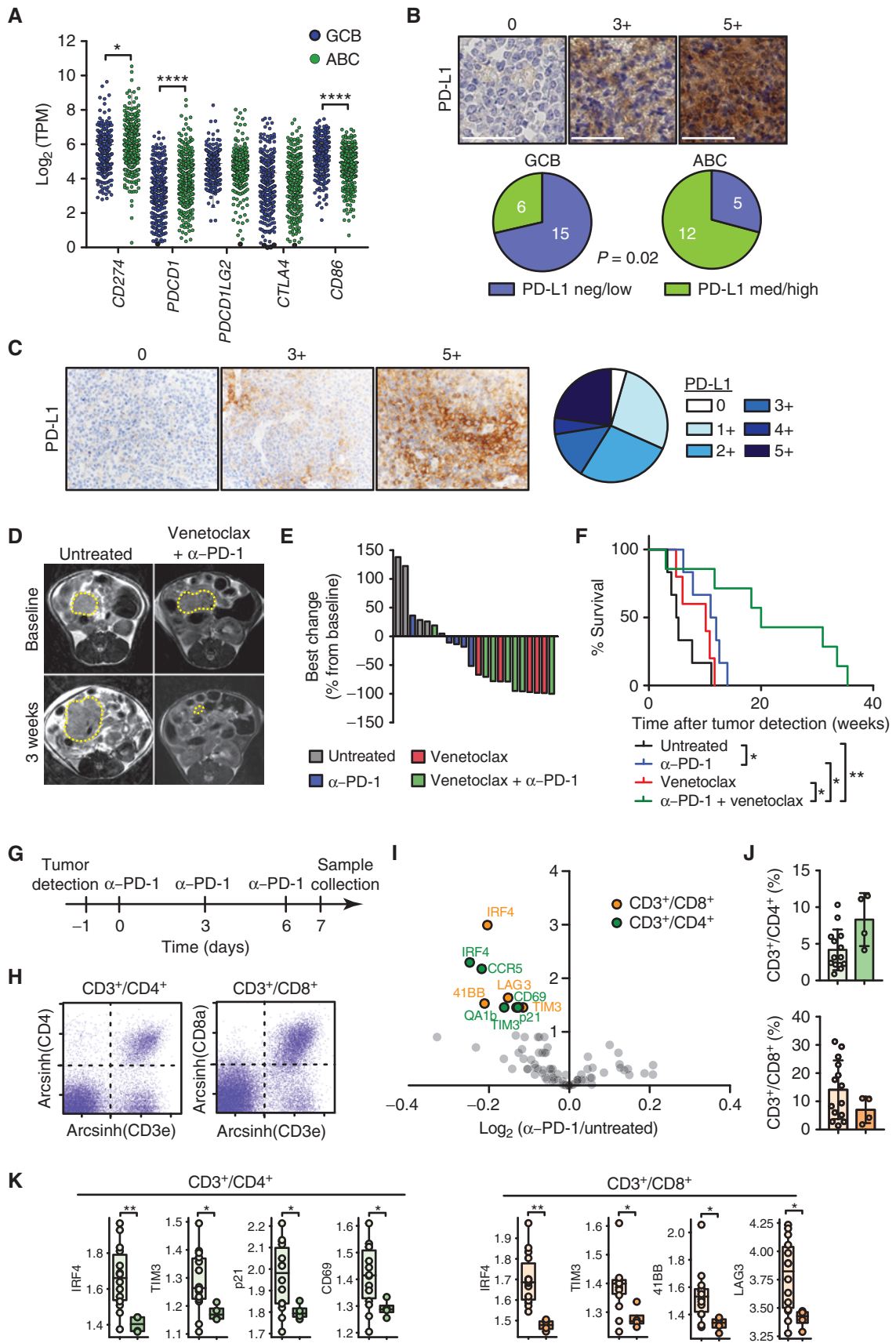
scans, animals were randomized in a 1:1:1:1 fashion to receive either vehicle solution (control), venetoclax (200 mg/kg, orally, daily, days 1–21), the anti–PD-1 antibody RMP1-14 (10 mg/kg, i.p., twice weekly, until death), or combined venetoclax plus RMP1-14. Therapy response was longitudinally assessed through weekly MRI scans, which enabled us to gauge depth of remission and duration of response (Fig. 6D and E; Supplementary Fig. S6B). Although both single-agent RMP1-14 and venetoclax produced objective responses in the MBC model (Fig. 6E), these responses were not durable (Supplementary Fig. S6B). The median survival of RMP1-14– or venetoclax-treated mice was 11.5 and 10.1 weeks, respectively, compared with 5.1 weeks in untreated animals. Although the survival difference between untreated and venetoclax-treated mice failed to reach statistical significance, RMP1-14 induced a significant survival gain, compared with untreated controls (Fig. 6F).

The significant single-agent activity of RMP1-14 prompted us to further explore the effects of PD-1 blockade on the composition and activation status of the cells within the lymphoma microenvironment. For that purpose, we employed mass cytometry from lymphoma tissue derived from RMP1-14–treated (250 µg/dose, days 1, 4, and 7, i.p.) or untreated animals (Fig. 6G–K). Our analysis revealed that PD-1 blockade in MBC lymphoma–bearing animals induced distinct phenotypic changes in lymphoma-infiltrating CD4+ and CD8+ T cells, which are in line with reversal of an exhausted phenotype of lymphoma-infiltrating T cells upon treatment (Fig. 6H and I). Although the CD4+ and CD8+ T-cell population sizes did not show significant changes (Fig. 6J), we particularly detected a significant reduction in IRF4 and TIM3 expression in both CD4+ and CD8+ T cells upon RMP1-14 exposure (Fig. 6I and K). Moreover, CD8+ T cells displayed significantly reduced 4-1BB and LAG3 expression following PD-1 blockade. Further, CD4+ T cells displayed reduced CD69 expression upon RMP1-14 exposure (Fig. 6I and K). These data are in line with a reinstated antilymphoma immune response following PD-1 blockade, as LAG3, TIM3, and CD69 are well-established exhaustion markers in CD4+ and CD8+ T cells (66–70). Similarly, IRF4 was shown to induce exhaustion of CD8+ T cells, during chronic stimulation (71). In addition, 4-1BB is an established marker of exhausted CD8+ T cells (72, 73). Lastly, the p53 target gene *Cdkn1a* (p21) is a potent CDK inhibitor involved in p53-mediated cell-cycle arrest (74). Reduced expression of *Cdkn1a* in CD4+ T cells following PD-1 blockade thus might be in line with restored proliferation potential. Altogether, these data suggest that PD-1 blockade in lymphoma-bearing MBC mice promotes a phenotypic switch away from an exhausted CD4+ and CD8+ T-cell state in treatment-naïve lymphomas. We note that a parallel assessment of serum cytokine levels (*n* = 32 distinct cytokines) in RMP1-14– and vehicle-treated animals did not reveal any significant differences (Supplementary Fig. S7).

In addition to our assessment of single-agent activities, we also analyzed the effect of combined venetoclax plus RMP1-14, which resulted in a significant overall survival gain (median overall survival 20 weeks) compared with untreated animals or mice exposed to the single agents (Fig. 6D–F; Supplementary Fig. S6B). Altogether, these functional *in vivo* experiments indicate that combined BCL2 and PD-1 block-

ade may represent a viable treatment strategy for a molecularly defined subset of ABC-DLBCL cases.

DISCUSSION

Here, we characterized a mouse model of *Myd88*- and *BCL2*-driven DLBCL. In essence, we show that *Myd88* p.L252P and *BCL2* cooperate in DLBCL lymphomagenesis. The resulting lymphomas display gene expression profiles that are strikingly similar to human ABC-DLBCL (Fig. 4G; Supplementary Fig. S3F). Moreover, in addition to the engineered aberrations in *Myd88* and *BCL2*, these lymphomas spontaneously acquire single-nucleotide variants that are also detectable in human DLBCL, including mutations in *Pim1, Myc, Pou2f2, Nfkbia*, and *Kmt2d* (Fig. 4H; Supplementary Table S1).

We also assessed the effects of *Myd88* p.L252P expression in nontransformed B cells. We specifically analyzed spontaneous, MYD88-centered protein complex formation in naïve B cells and found significantly more complexes involving MYD88 together with IRAK1, IRAK4, IgM, and BTK compared with WT controls (Fig. 3). These *ex vivo* experiments suggest that MYD88p.L252P constitutively nucleates a signaling complex, physically linking BCR and TLR signaling molecules in nontransformed B cells. These data are in line with the recently reported presence of the so-called My-T–BCR complex in ABC-DLBCL lymphoma cell lines (40). Moreover, these data are supported by a recent report indicating that BTK localizes in a protein complex with MYD88 in p.L265P-expressing OCI-Ly3 DLBCL cells (75).

Further investigation into the impact of *Myd88* p.L252P expression in nontransformed B cells revealed the presence of autoreactive antibodies in MC, BC, and MBC animals (Fig. 2A–D). Particularly the robust detection of autoreactive antibodies in MC animals was surprising, as it suggests that B-cell–specific expression of *Myd88* p.L252P is tolerated *in vivo*. This observation is in contrast to the results of a recently reported transplantation experiment where mature B cells were first transduced with *MYD88* p.L265P and subsequently transplanted into *Rag1*−/− recipients (76). In these experiments, *MYD88* p.L265P was sufficient to initiate a spontaneous proliferation burst in mature B cells *in vitro* and *in vivo* (76). Nevertheless, the *MYD88* p.L265P–induced aberrant clonal growth was rapidly limited in a *Bim*-dependent manner (76). However, it is important to note that an overexpression system was used in those experiments, whereas we employ *Myd88* expression from its endogenous locus *in vivo* (Fig. 1A). Moreover, as we use *Cd19*Cre to mediate recombination, the entire B-cell pool in our experimental system carries the *Myd88* p.L252P mutation (Fig. 1A). Thus, B-cell competition effects are very limited in our mouse model.

The observation of an increased presence of autoreactive IgM and IgG antibodies in lymphoma-prone MBC mice (Fig. 2A–D) is intriguing, as this might suggest a role for autoantigens in promoting DLBCL lymphomagenesis. A role for BCR stimulation in lymphomagenesis has long been postulated (77). For instance, there is ample evidence indicating that chronic infections, such as hepatitis C (HCV) or *Helicobacter pylori*, are associated with the development of splenic marginal zone lymphoma (SMZL) and mucosa-associated lymphoid tissue lymphoma, respectively (78). Moreover, in

HCV-associated SMZL, a single BCR specific to a glyco-protein in the viral envelope has been identified, strongly suggesting that HCV itself contributes to driving SMZL BCR signaling (78). Next to infection-driven BCR signaling, our detection of autoreactive antibodies in MBC animals is in line with the hypothesis that the constant engagement of the BCR by a self-antigen might account for the sustained nature of chronic active BCR signaling (79). In fact, BCR stimulation by self-antigens has been correlated with lymphomagenesis. Epidemiologic analyses revealed associations between B-cell–activating autoimmune diseases, such as Sjögren's syndrome and systemic lupus erythematosus, with increased DLBCL risk after controlling for all other risk factors (80). Furthermore, analyses of V_H gene segment in DLBCL revealed that segment V_H4-34 is utilized in approximately 30% of ABC-DLBCL cases (79). Experiments in cell line models of ABC-DLBCL with chronic active BCR signaling provided further evidence for autoreactivity of the V_H4-34 segment. The viability of the V_H4-34–positive ABC cell line HBL1 depended on the V region–mediated ability of its BCR to bind to self-glycoproteins on its own cell surface (79). Moreover, chronic active BCR signaling in the ABC-DLBCL cell line OCI-Ly10 is driven by BCR recognition of an antigen in the debris of apoptotic cells (79). OCI-Ly10 was shown to be dependent on BCR specificity mediated by charged amino acids within CDR2 and CDR3 of the V_H3-7 region (79). Lastly, the survival of the ABC-DLBCL cell line TMD8 was shown to depend on homotypic interactions with its own FR2 domain, which sustained chronic active BCR signaling (79). These data indicate that a diverse array of self-antigens is responsible for maintaining the survival of ABC-DLBCL cells. Building on these data, it is intriguing to speculate that in our MBC model, the enlarged pool of B cells that are activated by self-antigen and in which anergy is repressed by MYD88-driven TLR signaling might increase the pool of cells that are prone for malignant transformation.

We also employed our MBC model as a preclinical tool that mimics central features of ABC-DLBCL (surface marker profile, expression profile, driver mutations, and spontaneously developing mutational profile). Particularly the analysis of murine and human tissue specimens and transcription profiles revealed that ABC-DLBCL cases display higher *CD274* levels than GCB-DLBCL cases. These observations are in line with a previous report in which the authors demonstrated an increased *Cd274* expression in the murine $C\gamma1^{Cre/WT}$;*Ikk2CAGFP*$^{LSL/LSL}$;*Prdm1*$^{fl/fl}$– and $C\gamma1^{Cre/WT}$;*Tp53*$^{fl/fl}$;*Ikk2CAGFP*$^{LSL/LSL}$;*Prdm1*$^{fl/fl}$–derived lymphoma cells, compared with $C\gamma1^{Cre/WT}$;*YFP*$^{LSL/WT}$ GCB cells (81). There is further substantial evidence that mechanistically supports the high PD-L1 expression levels in our MBC model: IFNγ and Myd88-dependent TLR signaling was recently shown to drive PD-L1 expression in multiple myeloma cells (82). Intriguingly, we found significantly higher IFNγ levels in the serum of MBC mice compared with WT serum (Fig. 4I). Moreover, an *in silico* analysis revealed that a sizeable fraction of human DLBCL cases (22%) harbor high *BCL2* and *CD274* expression levels. To particularly target this population, we assessed the preclinical efficacy of combined BCL2 and PD-1 blockade. Although both single agents displayed only mild activity in the MBC model, combined venetoclax

and RMP1-14 led to significantly increased tumor volume control and overall survival benefit compared with the single agents or vehicle. These results are in line with previous reports demonstrating that the anti–PD-1 antibody RPM1-14 as a single agent did not lead to a significant overall survival benefit in $C\gamma1^{Cre/WT}$;*Tp53*$^{fl/fl}$;*Ikk2CAGFP*$^{LSL/LSL}$;*Prdm1*$^{fl/fl}$ lymphoma–bearing mice compared with untreated controls, whereas combined anti–PD-1/anti-CD20 blockade synergistically increased the overall survival in these animals (81).

Our observations provide further evidence for the clinical development of BCL2 and PD-1/PD-L1 inhibitors in the clinical arena. In this context, it is important to reiterate that single-agent venetoclax was recently shown to achieve an overall response rate (ORR) of 18% in relapsed/refractory DLBCL (65). Similarly, single-agent nivolumab achieved an ORR of 36% in DLBCL (62). Our data now indicate that patients with DLBCL displaying high-level PD-L1 and BCL2 exist and that these patients may be particularly well suited to receive combined BCL2 and PD-1 blockade. This strategy may be particularly useful in relapsed/refractory ABC-DLBCL, or those patients who are not eligible for intensive consolidation regimens, involving autologous stem cell support. In our experiments, venetoclax was used at 200 mg/kg daily, which is a dose that is typically used for *in vivo* experiments in mice (83, 84). Although venetoclax at 200 mg/kg daily did not induce any obvious toxicity in our experiments, it is important to note that this dose exceeds the doses that are clinically applied to human patients (typically 5–20 mg/kg, depending on venetoclax dosing regimen and body weight). Altogether, we provide a detailed molecular analysis of the MBC model, including the comparison with *Kmt2d/BCL2*-driven lymphomas and a large series of human DLBCL cases. These experiments indicate that the MBC model reflects key aspects of human ABC-DLBCL. Moreover, we employ the MBC model to derive a combination strategy involving PD-1 and BCL2 blockade for the treatment of *MYD88-* and *BCL2*-altered aggressive lymphomas.

METHODS

Experimental Mice

The generation of the $Cd19^{Cre}$, $Myd88^{cond.p.L252P}$, and $Rosa26^{LSL.BCL2-IRES-GFP}$ alleles has been described previously (20, 85). For survival analyses, animals that succumbed to disease or had to be killed due to satisfied termination criteria were recorded as events. Animals that died from genotype-unrelated criteria in rare cases (appendicitis, abnormal teeth, injuries inflicted by cage mates) were censored. For transplantation experiments, 10^7 cells were transplanted i.p. into $Rag1^{-/-}$ recipients. In autochthonous treatment studies, onset of lymphoma was defined by a lesion larger than 75 μL detectable by MRI, with a detectable volume increase in two consecutive scans. In transplantation studies, onset of clonal lymphoma was determined in a preceding experiment. ABT-199 was administered as a suspension in 60% Phosal 50PG, 30% polyethylene glycol 400, and 10% ethanol by oral gavage at 200 mg/kg daily. ND-2158 was dissolved in 10% β-cyclodextrin at 15 mg/mL and administered i.p. at 150 mg/kg. The anti–PD-1 antibody RMP1-14 (BioXCell) was administered i.p. 3 days per week (250 μg/administration).

All animals were housed in a specific pathogen–free facility, and animal breedings and experiments were approved by the local animal care committee and the relevant authorities (Landesamt für

Natur, Umwelt und Verbraucherschutz Nordrhein-Westfalen, AZ: 84-02.04.2014.A146, 84-02.04.2017.A131, 81-02.04.2019.A009).

MR Imaging

MR imaging was performed as described previously (20). In brief, mice were anesthetized with 2.5% isoflurane and scanned on a 3.0T MRI system (Igenia, Philips) with a small rodent solenoid coil (diameter 40 mm, Philips Research Europe). Axial T2-weighted images of the abdomen were acquired (TSE factor: 10, TR: 2674 ms, TE: 65 ms, slice thickness: 1.0 mm). Images were exported in DICOM format, and spleen and tumor volumes were measured by segmentation using the Horos software.

Immunohistochemistry

Formalin-fixed and paraffin-embedded tissues from mice were cut into 4 μm sections and stained for BCL6 (Santa Cruz Biotechnology, clone C-19), B220 (BD, clone RA3-6B2), CD138 (BD, Cat. No. 553712), Ki67 (Cell Marque), CD3 (Thermo Fisher, clone RM-9107), CD4 (Abcam, Cat. No. ab183685), CD8 (Abcam, Cat. No. ab203035), and biotinylated PNA (Vector Laboratories, B-1075-5). Germinal centers were quantified from BCL6 and PNA stainings using the software ImageJ. Ki67 and CD3 positivity was quantified using the ImmunoRatio plugin for ImageJ (86).

Human samples were cut into 4 μm sections and stained for CD10 (NCL-L-CD10-279, Novocastra), IRF4 (Dako, Cat. No. M7259), BCL6 (Dako, Cat. No. M7211), BCL2 (Dako, Cat. No. M0877), PD-L1 (Dako, clone 28-8), CD3 (Bio-Rad, clone 145-2C11), CD4 (Abcam, clone EPR19514), and CD8 (Abcam, Cat. No. ab203035). Human PD-L1 stainings were graded according to the Cologne Score (87).

Flow Cytometry

For immunotypisation, splenocytes were stained with fluorophore-coupled primary antibodies against CD23 PE, (Ebioscience, clone B3B4), CD93 (PE-Cy7, Biolegend, clone AA4.1), CD21/35 (APC, BD, clone 7G6), CD45 (APC-Cy7, BD, clone 30-F11), B220 (Pacific-Blue, BD, clone RA3-6B2), CD138 (PE-Cy7, Biolegend, Cat. No. 142514), and MHCII (AF700, Biolegend, clone M5-1142) and measured on a Gallios flow cytometer (Beckman Coulter). Data were analyzed with the software Kaluza (Beckman Coulter). The gating strategy is depicted in Supplementary Fig. S8.

For Annexin V/PI measurements, cells were cultured at an initial density of 10^6 cells/mL and treated with the indicated compounds and doses for 48 hours. Cells were then washed and stained with an FITC-coupled antibody against Annexin V (diluted 1:600, BD, Cat. No. 550474) and PI (0.5 mg/mL). Cells were analyzed on a flow cytometer (Gallios, Beckman Coulter) after 15 minutes of incubation, and the double-positive population was measured using the software Kaluza (Beckman Coulter).

Serum Gel Electrophoresis

Serum protein electrophoresis was performed with HYDRAGEL IF 2/4 agarose gels (Sebia) on the HYDRASIS electrophoresis system (Sebia). Therefore, 4 μL serum was diluted 8 μL HYDRAGEL IF diluent (Sebia), electrophoretically separated, and stained with acid violet according to the manufacturer's instructions.

HEp-2 Assay

Serum was diluted 1:40 in PBS, and 30 μL per sample were added on a Kallestad HEp-2 slide (Bio-Rad, Cat. No. 26101), incubated for 20 minutes in a wet chamber, and washed with PBS for 10 minutes. The samples were then stained with Alexa Fluor 488–coupled secondary antibodies against either murine IgM (Thermo Fisher, Cat. No. A-21042) or IgG (Thermo Fisher, Cat. No. A-11001) for 20 minutes, washed, and covered. Fluorescence intensities were quantified from

stainings produced in the same run by analyzing images generated with identical exposure times by ImageJ.

Immunization Experiments

Animals were injected i.p. with 50 μg of either NP-Ficoll (Biocat, Cat. No. F-1420-10-BS) dissolved in 200 μL PBS or NP-CGG (Biocat, Cat. No. N-5055E-1-BS) dissolved in 100 μL PBS + 100 μL Imject Alum (Thermo Scientific, Cat. No. 77161). Note that 30 μL of blood was drawn from the tail vein at the indicated days. Antibody levels against NP in the collected sera were measured by ELISA. High-protein–binding plates were coated with NP-BSA (5 μg/mL) overnight. Plates were washed with 0.05% PBS-T and blocked with 1% BSA. The samples were prediluted with 1% BSA in PBS at 1:10,000 or higher and incubated on the plate for 2 hours at room temperature. Plates were washed with PBS-T and secondary antibody against murine IgG (Antibodies-online, Cat. No. ABIN376241) or IgM (Novus, Cat. No. NB7497). After 20 minutes, the reaction was stopped by 1 mol/L phosphoric acid, and the plates were read on a plate reader (Tecan).

Immunoblotting

Single-cell suspensions were generated by pressing spleens through a cell strainer (70 μm), and naïve B cells were purified using a CD43-depletion kit (Miltenyi, 130-049-801). Cells were lysed in 4% SDS containing phosphatase and protease inhibitors (Merck, 4906845001 and 05892970001). Protein concentration was measured by BCA assay (Thermo Fisher, 23225), and concentration was adjusted to 800 μg/mL before the addition of Laemmli buffer. Note that 20 μL per sample were loaded onto 10% polyacrylamide gels and blotted onto a PVDF membrane. Membranes were blocked (5% BSA in TBST) and stained overnight with primary antibody (pp65, Cell Signaling Technology, 3033; pIRAK4, Abnova, MAB2538; pBTK, Cell Signaling Technology, 5082; GAPDH, Cell Signaling Technology, 5174). Membranes were washed and incubated with horseradish peroxidase–coupled secondary antibody for 1 hour at room temperature. After washing, membranes were incubated with ECL solution (Amersham) and imaged on a ChemiDoc (Bio-Rad). Densitometric analysis was performed using ImageJ.

Clonality Analysis

RNA was isolated from cryopreserved tumor tissue using a commercial kit (Qiagen, Cat. No. 74104), and clonality analysis was performed using an adaption of a published BCR clonality analysis approach (42). The cDNA was then synthesized using a reverse transcriptase generating poly-dC overlaps (SMARTScribe, Takara, Cat. No. 639537), allowing for template switching and adapter ligation, which contains a unique barcode (UMI). For first-strand synthesis, primers specific for the constant regions of *Ighg*, *Ighm*, and *Igha* were used. Two rounds of nested PCR were performed, resulting in an amplification product containing the *V(D)J* junctions, which was then sequenced. Purified PCR amplicons were end-repaired, A-tailed, and adapter ligated with unique dual indices using the Illumina TruSeq nano kit and protocol but without further PCR amplification. After validation (2200 TapeStation; Agilent Technologies) and quantification (Qubit System; Invitrogen), amplicon libraries were individually quantified using the KAPA Library Quantification kit (Peqlab) and the 7900HT Sequence Detection System (Applied Biosystems) and subsequently spiked-in larger pools of libraries. The pools were sequenced on an Illumina NovaSeq6000 sequencing instrument using a paired-end 2×100 bp protocol. The samples were then error corrected using the published MIGEC algorithm (42). UMIs present with less than three reads were discarded. To quantify clone sizes, we next assessed the abundance of individual UMIs. Clones differing by one base were connected to clusters, and the size of these clusters was quantified as the sum of the individual clone sizes. BCR

repertoires were visualized using the software Gephi (https://gephi.org/). Primer sequences and barcode-sample mapping are given in Supplementary Table S3.

Determination of SHM Frequency in CD138+ Cells

CD138-positive cells were selected using a magnetic antibody-based cell separation kit (Miltenyi, 130-098-257). RNA was isolated from these cells using a commercial kit (Qiagen). Full-length B-cell receptor sequencing was performed as published by Turchaninova and colleagues (21). Primer sequences and barcode-sample mapping are given in Supplementary Table S3. Note that 600 ng of RNA were used for cDNA synthesis, and a cDNA equivalent of 500 plasma cells was used for further PCR amplification steps. Amplicon sequencing was then performed on a MiSeq (asymmetric 400+100-nt paired-end sequencing), with eight samples on a full lane. Processing of the sequencing data was performed according to the protocol using the MIGEC software (21, 42). Mapping of the identified BCR sequences was done using the MiXCR (for isotype information) and MiGMAP (for determination of differing bases from germline sequence; ref. 88).

3′-RNA-Seq

RNA was isolated from cryopreserved tumor tissue using a commercial kit (Qiagen, Cat. No. 74104). Note that 3′mRNA libraries were generated from total RNA using the Lexogen QuantSeq Kit according to the standard protocol. After validation (2200 TapeStation; Agilent Technologies) and quantification (Qubit System; Invitrogen), pools of cDNA libraries were generated. The pools were quantified using the KAPA Library Quantification Kit (Peqlab) and the 7900HT Sequence Detection System (Applied Biosystems) and subsequently sequenced on an Illumina HiSeq4000 sequencer using a 1×50 bp protocol. Reads were mapped to the murine genome (mm10) and quantified using Salmon. Data were normalized, and statistics were calculated using DESeq2 (89). To perform GSEA for published human gene sets, the murine genes were mapped to their human orthologs using the biomaRt package for R (90). Gene set enrichment analysis was then performed using the FGSEA package (91). To analyze the published human RNA-seq dataset (11), reads were mapped to the human transcriptome (GRCh38) and quantified using Salmon (92).

CyTOF Analysis

Single-cell suspensions were generated from untreated and anti–PD-1–treated tumors (RMP1-14–treated, 250 µg on days 1, 4, and 7 after tumor detection by MRI, i.p., collected on day 8) by pressing the tissue through a 70-µm cell strainer. Cell suspensions were frozen in FCS/10% DMSO at −80°C for collective staining and measurement. Samples were barcoded using a commercial kit following the manufacturer's instructions (Fluidigm, 201060). Cells were then pooled and stained with a set of surface and intracellular markers following standard protocol. Antibodies (clone or manufacturer and order number in case of polyclonal): IRF4 (IRF4.3E4), QA1b (6A8.6F10.1A6), p16 (2D9A12), TIM-3 (RMT3-23), CD179 (MFL3), LAG-3 (631501), p21 (WA-1), CTLA-4 (UC10-4B9), CCR6 (29-2L17), CD45R (RA3-6B2), CD4 (RM4-5), CD19 (6D5), CD8a (53-6.7), CD279 (R&D, AF1021), CD95 (R&D, AF435), BCL6 (K112-91), CD3e (145-2C11), 4-1BB (158332), NK1.1 (PK136), CD69 (H1.2F3), FOXP3 (FJK-16s), ICOS (7E.17G9), and CD45 (30-F11). Cell acquisition was done on a Helios mass cytometer (Fluidigm). Debarcoding, normalization, and compensation were performed with the R package CATALYST (93). CD3+/CD8+ and CD3+/CD4+ cells were gated, mean signal intensities between the two groups were compared for each marker, and significance was calculated by unpaired two-sided Welch t test and adjusted for multiple hypothesis testing (Benjamini and Hochberg).

Whole-Exome Sequencing

DNA was isolated from MBC tumors with high clonal fractions. Mouse exomes were individually prepared using 200 ng of DNA, the standard protocol SureSelectXT Automated Target Enrichment for Illumina Paired-End Multiplexed Sequencing, and the Agilent Bravo automated liquid handling platform. After validation (2200 TapeStation; Agilent Technologies) and quantification (Qubit System; Invitrogen), pools of libraries were generated. The pools were quantified using the KAPA Library Quantification Kit (Peqlab) and the 7900HT Sequence Detection System (Applied Biosystems) and subsequently sequenced on an Illumina NovaSeq6000 sequencing instrument using a paired-end 2×100 bp protocol. We aligned raw sequencing reads to the mouse reference genome (mm10) by using the BWA mem aligner (version 0.7.13-r1126). Concordant read pairs that represent possible PCR duplicates were masked out after alignment. Furthermore, all overlapping regions between the read pairs are considered only once in the analysis. Due to a lack of matched normals for all tumor specimens, we generated a representative nontumor sample by combining normals matching to two tumor samples. This combined normal is used for mutation calling with the latest version of our in-house cancer genome analysis pipeline (94). To correct for genotypes that are not captured by representative normal, we filtered out called mutations that were exactly the same in two or more tumor samples.

Multiplex Cytokine Assay

Mouse serum was collected by retro-orbital or tail-vein bleeding. Serum levels of cytokines and chemokines were determined using the Mouse 31-Plex Cytokine/Chemokine Array (Eve Technologies).

Cell Lines

Human cell lines were purchased from DSMZ. Cell line identity was verified by short tandem repeat (STR) analysis. Cell lines were cultivated in RPMI with 20% FCS and 1% penicillin/streptomycin. Murine cell lines were established from primary tumors and cultivated in DMSO containing 4.5 g/L glucose, with the following supplements: 10% FCS, 2 mmol/L L-glutamine, 1 mmol/L sodium pyruvate, 10 mmol/L HEPES, nonessential amino acids, 1% penicillin/streptomycin, and 50 µmol/L beta-mercaptoethanol. No *Mycoplasma* testing was performed.

Cell Viability Assays

Five thousand cells per well were treated with the indicated drugs and doses (dissolved in DMSO, DMSO concentrations were adjusted). After 96 hours of incubation, viability was measured by CellTiter-Glo assay (Promega, Cat. No. G7572) diluted 1:6 in PBS and the luminescence was measured (Infinite M1000 pro, Tecan). The values were normalized to untreated controls on each plate.

High-Throughput Cell Line Screening

High-throughput screening was performed on the mouse and human lymphomas cells, as described earlier with minor modifications (95–97). Briefly, the DMSO-dissolved compound library (MedChemExpress) was dispensed with increasing concentrations of the inhibitors in six dilution steps (0.008–25 µmol/L) on a white 1,536-well plate (Corning) using digital dispenser (D300e, Tecan), which ensures precise and robotic compound application in randomized fashion. The compound selection consisted of FDA/European Medicines Agency–approved classical chemotherapeutic drugs and targeted agents, as well as molecules that are currently in clinical trials at various stages, and several investigational compounds (see Supplementary Table S2 for the detailed list). The printed plates were sealed with parafilm, followed by packing in vacuum-sealed bags to avoid evaporation during storage at −80°C. The cells (>90% viability) were seeded on the thawed predispensed inhibitor plates using an automated Multidrop Combi

Reagent Dispenser (Thermo Fisher Scientific). Differential responses were monitored with ATP-dependent CellTiter-Glo Luminescent cell viability kit (Promega) after 72 hours of inhibitor exposure using Microplate reader (Spark 10M, Tecan). The outer three wells of the plate were excluded from analysis to circumvent the evaporation effect on the plate edges. Dose–response curves ($n = 3$) for the inhibitors were determined by plotting raw data (normalized to controls) with nonlinear regression [log(inhibitor) vs. normalized response] variable slope function (GraphPad Prism Inc.). Average drug response values ($n = 3$) normalized to the mean IC_{50} for each individual compound over all lines were plotted for the Heatmap visualization, followed by unsupervised hierarchical clustering (R package gplots).

PLA

B cells were isolated from spleens of 15- to 20-week-old WT and MC mice by MACS sorting according to protocol [CD43 (Ly-48) MicroBeads, Miltenyi Biotec, Cat. No. 130-049-801]. PLA was performed with the Duolink-In-Situ-Orange kit (Sigma, Cat. No. DUO92007), as previously published (98). In brief, cells were plated on a 10-well polylysine-coated, microscope slide (Thermo Scientific, three wells per genotype, condition, and experiment), allowed to adhere for 30 minutes at 37°C, and subsequently fixed with 1% PFA at room temperature for 20 minutes. Cells were then blocked and permeabilized with 0.5% Saponin in Duolink Blocking buffer (Sigma). For PLA probes against specific targets, the following primary antibodies were used: anti-Myd88 (Abcam), anti-BTK (Novus Biologicals, Cat. No. NBP1-78295SS), anti-IRAK1 (Novus Biologicals, Cat. No. NBP1-77068SS), anti-IRAK4 (Invitrogen, Cat. No. 700026), and anti-IgM (Jackson Laboratories, Cat. No. 115-007-020). Primary antibodies were labeled with Duolink In-Situ Probemaker Plus (Sigma, DUO92009) or Minus (Sigma, Cat. No. DUO92010) according to protocol. Fixed cells were incubated with Plus and Minus probes overnight at 4°C. Ligation, rolling circle amplification, and mounting of cells were performed according to protocol. Three images per well, each capturing at least 120 cells, were acquired on a Leica SP8 confocal microscope using the Leica LAS X software. Nuclei and PLA signals were counted using BlobFinder version 3.0.0 (99).

BH3 Profiling

BH3 profiling was performed using the iBH3 plate–based method as previously published (56). In brief, cell lines were seeded at a density of 1×10^6 cells/mL 24 hours before profiling. Four million cells of each cell line were pelleted at $300 \times g$ for 5 minutes and resuspended in 2 mL MEB-P25 [150 mmol/L Mannitol, 10 mmol/L HEPES-KOH, pH 7.5, 150 mmol/L KCl, 1 mmol/L EGTA, 1 mmol/L EDTA, 0.1% BSA, 5 mmol/L Succinate, 0.25% Polaxamer 188 (Fisher, MT61161RM)]. Cells were permeabilized with digitonin (Sigma, D5628) exposed to BH3 peptides for 60 minutes at 25°C, and mitochondrial Cytochrome C release was measured by flow cytometry using an FITC-conjugated antibody (BioLegend, 983502). BH3 peptides were synthesized by New England Peptide using published sequences (100). The Bcl-XL–selective inhibitor A-1331852 (Selleckchem, S7801), the Bcl-2–selective inhibitor ABT-199 (Selleckchem, S8048), and the MCL inhibitor AZD5991 (Selleckchem, S8643) were used at a concentration of 10 µmol/L. Results were only deemed valid where cell cytochrome C release in the presence of DMSO control was <10% and cytochrome C release in the presence of 50 µg/mL (25 µmol/L) Alamethicin (Enzo, BML-A150-0005) was >90%. Figure 5D represents the mean of three independent experiments.

Data Accessibility

Murine exome and 3′-RNA-seq data are available at the Sequence Read Archive under the accession number PRJNA668334. The BCR repertoire sequencing data are available under PRJNA672930. A dataset consisting of DNA and RNA-seq data generated by the lab of Sandeep S. Dave (11) was reanalyzed for this work and is accessible at the European Genome-phenome Archive (accession number EGAD00001003600). Some analyses conducted in this work are based on previously published supplementary data by the labs of Margaret A. Shipp and Louis M. Staudt (9, 10).

Authors' Contributions

R. Flümann: Investigation, visualization, methodology, writing–original draft. T. Rehkämper: Investigation, visualization. P. Nieper: Investigation, visualization, methodology. P. Pfeiffer: Investigation. A. Holzem: Investigation. S. Klein: Investigation. S. Bhatia: Investigation, methodology. M. Kochanek: Investigation. I. Kisis: Investigation, methodology. B.W. Pelzer: Investigation, methodology. H. Ahlert: Methodology. J. Hauer: Methodology. A. da Palma Guerreiro: Methodology. J.A. Ryan: Supervision, methodology. M. Reimann: Resources, investigation. A. Riabinska: Resources. J. Wiederstein: Investigation, methodology. M. Krüger: Resources, supervision, funding acquisition, methodology. M. Deckert: Investigation, visualization. J. Altmüller: Investigation. A.R. Klatt: Investigation. L.P. Frenzel: Supervision, methodology. L. Pasqualucci: Resources, investigation. W. Béguelin: Resources, investigation. A.M. Melnick: Resources, investigation. S. Sander: Resources, investigation. M. Montesinos-Rongen: Resources, investigation. A. Brunn: Investigation. P. Lohneis: Investigation. R. Büttner: Resources, supervision, methodology. H. Kashkar: Supervision. A. Borkhardt: Supervision, methodology. A. Letai: Supervision, methodology. T. Persigehl: Resources. M. Peifer: Investigation, methodology. C.A. Schmitt: Conceptualization, resources, supervision. H.C. Reinhardt: Conceptualization, resources, supervision, funding acquisition, investigation, methodology, writing–original draft, project administration, writing–review and editing. G. Knittel: Conceptualization, data curation, formal analysis, supervision, validation, investigation, visualization, methodology, writing–original draft, project administration, writing–review and editing.

REFERENCES

1. Swerdlow SH, Campo E, Pileri SA, Harris NL, Stein H, Siebert R, et al. The 2016 revision of the World Health Organization classification of lymphoid neoplasms. Blood 2016;127:2375–90.
2. Alizadeh AA, Eisen MB, Davis RE, Ma C, Lossos IS, Rosenwald A, et al. Distinct types of diffuse large B-cell lymphoma identified by gene expression profiling. Nature 2000;403:503–11.
3. Shaffer AL 3rd, Young RM, Staudt LM. Pathogenesis of human B cell lymphomas. Annu Rev Immunol 2012;30:565–610.
4. Lenz G, Wright G, Dave SS, Xiao W, Powell J, Zhao H, et al. Stromal gene signatures in large-B-cell lymphomas. N Engl J Med 2008;359: 2313–23.
5. Rosenwald A, Wright G, Chan WC, Connors JM, Campo E, Fisher RI, et al. The use of molecular profiling to predict survival after chemotherapy for diffuse large-B-cell lymphoma. N Engl J Med 2002;346: 1937–47.
6. Basso K, Dalla-Favera R. Germinal centres and B cell lymphomagenesis. Nat Rev Immunol 2015;15:172–84.
7. Knittel G, Liedgens P, Korovkina D, Pallasch CP, Reinhardt HC. Rewired NFkappaB signaling as a potentially actionable feature of activated B-cell-like diffuse large B-cell lymphoma. Eur J Haematol 2016; 97:499–510.
8. Grondona P, Bucher P, Schulze-Osthoff K, Hailfinger S, Schmitt A. NF-kappaB activation in lymphoid malignancies: genetics, signaling, and targeted therapy. Biomedicines 2018;6:38.
9. Chapuy B, Stewart C, Dunford AJ, Kim J, Kamburov A, Redd RA, et al. Molecular subtypes of diffuse large B cell lymphoma are associated with distinct pathogenic mechanisms and outcomes. Nat Med 2018;24:679–90.
10. Schmitz R, Wright GW, Huang DW, Johnson CA, Phelan JD, Wang JQ, et al. Genetics and pathogenesis of diffuse large B-cell lymphoma. N Engl J Med 2018;378:1396–407.
11. Reddy A, Zhang J, Davis NS, Moffitt AB, Love CL, Waldrop A, et al. Genetic and functional drivers of diffuse large B cell lymphoma. Cell 2017;171:481–94.
12. Pfreundschuh M, Kuhnt E, Trumper L, Osterborg A, Trneny M, Shepherd L, et al. CHOP-like chemotherapy with or without rituximab in young patients with good-prognosis diffuse large-B-cell lymphoma: 6-year results of an open-label randomised study of the MabThera International Trial (MInT) Group. Lancet Oncol 2011;12: 1013–22.
13. Pfreundschuh M, Schubert J, Ziepert M, Schmits R, Mohren M, Lengfelder E, et al. Six versus eight cycles of bi-weekly CHOP-14 with or without rituximab in elderly patients with aggressive CD20+ B-cell lymphomas: a randomised controlled trial (RICOVER-60). Lancet Oncol 2008;9:105–16.
14. Gisselbrecht C, Glass B, Mounier N, Singh Gill D, Linch DC, Trneny M, et al. Salvage regimens with autologous transplantation for relapsed large B-cell lymphoma in the rituximab era. J Clin Oncol 2010;28:4184–90.

15. Horwitz SM, Negrin RS, Blume KG, Breslin S, Stuart MJ, Stockerl-Goldstein KE, et al. Rituximab as adjuvant to high-dose therapy and autologous hematopoietic cell transplantation for aggressive non-Hodgkin lymphoma. Blood 2004;103:777–83.
16. Kewalramani T, Zelenetz AD, Nimer SD, Portlock C, Straus D, Noy A, et al. Rituximab and ICE as second-line therapy before autologous stem cell transplantation for relapsed or primary refractory diffuse large B-cell lymphoma. Blood 2004;103:3684–8.
17. Tilly H, Gomes da Silva M, Vitolo U, Jack A, Meignan M, Lopez-Guillermo A, et al. Diffuse large B-cell lymphoma (DLBCL): ESMO Clinical Practice Guidelines for diagnosis, treatment and follow-up. Ann Oncol 2015;26:v116–25.
18. Ngo VN, Young RM, Schmitz R, Jhavar S, Xiao W, Lim KH, et al. Oncogenically active MYD88 mutations in human lymphoma. Nature 2011;470:115–9.
19. Weber ANR, Cardona Gloria Y, Cinar O, Reinhardt HC, Pezzutto A, Wolz OO. Oncogenic MYD88 mutations in lymphoma: novel insights and therapeutic possibilities. Cancer Immunol Immunother 2018;67:1797–807.
20. Knittel G, Liedgens P, Korovkina D, Seeger JM, Al-Baldawi Y, Al-Maarri M, et al. B cell-specific conditional expression of Myd88p. L252P leads to the development of diffuse large B cell lymphoma in mice. Blood 2016;127:2732–41.
21. Turchaninova MA, Davydov A, Britanova OV, Shugay M, Bikos V, Egorov ES, et al. High-quality full-length immunoglobulin profiling with unique molecular barcoding. Nat Protoc 2016;11:1599–616.
22. He B, Qiao X, Cerutti A. CpG DNA induces IgG class switch DNA recombination by activating human B cells through an innate pathway that requires TLR9 and cooperates with IL-10. J Immunol 2004;173:4479–91.
23. Pone EJ, Zhang J, Mai T, White CA, Li G, Sakakura JK, et al. BCR-signalling synergizes with TLR-signalling for induction of AID and immunoglobulin class-switching through the non-canonical NF-kappaB pathway. Nat Commun 2012;3:767.
24. Ueda Y, Liao D, Yang K, Patel A, Kelsoe G. T-independent activation-induced cytidine deaminase expression, class-switch recombination, and antibody production by immature/transitional 1 B cells. J Immunol 2007;178:3593–601.
25. Guinamard R, Okigaki M, Schlessinger J, Ravetch JV. Absence of marginal zone B cells in Pyk-2-deficient mice defines their role in the humoral response. Nat Immunol 2000;1:31–6.
26. Leadbetter EA, Rifkin IR, Hohlbaum AM, Beaudette BC, Shlomchik MJ, Marshak-Rothstein A. Chromatin-IgG complexes activate B cells by dual engagement of IgM and Toll-like receptors. Nature 2002;416: 603–7.
27. Viglianti GA, Lau CM, Hanley TM, Miko BA, Shlomchik MJ, Marshak-Rothstein A. Activation of autoreactive B cells by CpG dsDNA. Immunity 2003;19:837–47.
28. Marshak-Rothstein A. Toll-like receptors in systemic autoimmune disease. Nat Rev Immunol 2006;6:823–35.
29. Lau CM, Broughton C, Tabor AS, Akira S, Flavell RA, Mamula MJ, et al. RNA-associated autoantigens activate B cells by combined B cell antigen receptor/Toll-like receptor 7 engagement. J Exp Med 2005; 202:1171–7.
30. Rifkin IR, Leadbetter EA, Beaudette BC, Kiani C, Monestier M, Shlomchik MJ, et al. Immune complexes present in the sera of autoimmune mice activate rheumatoid factor B cells. J Immunol 2000;165:1626–33.
31. Hande S, Notidis E, Manser T. Bcl-2 obstructs negative selection of autoreactive, hypermutated antibody V regions during memory B cell development. Immunity 1998;8:189–98.
32. Notidis E, Hande S, Manser T. Enforced expression of Bcl-2 selectively perturbs negative selection of dual reactive antibodies. Dev Immunol 2001;8:223–34.
33. Kuo P, Bynoe MS, Wang C, Diamond B. Bcl-2 leads to expression of anti-DNA B cells but no nephritis: a model for a clinical subset. Eur J Immunol 1999;29:3168–78.
34. Nisitani S, Tsubata T, Murakami M, Okamoto M, Honjo T. The bcl-2 gene product inhibits clonal deletion of self-reactive B lymphocytes

in the periphery but not in the bone marrow. J Exp Med 1993;178: 1247–54.

35. Strasser A, Whittingham S, Vaux DL, Bath ML, Adams JM, Cory S, et al. Enforced BCL2 expression in B-lymphoid cells prolongs antibody responses and elicits autoimmune disease. Proc Natl Acad Sci U S A 1991;88:8661–5.

36. Marquina R, Diez MA, Lopez-Hoyos M, Buelta L, Kuroki A, Kikuchi S, et al. Inhibition of B cell death causes the development of an IgA nephropathy in (New Zealand white x C57BL/6)F(1)-bcl-2 transgenic mice. J Immunol 2004;172:7177–85.

37. Mandik-Nayak L, Nayak S, Sokol C, Eaton-Bassiri A, Madaio MP, Caton AJ, et al. The origin of anti-nuclear antibodies in bcl-2 transgenic mice. Int Immunol 2000;12:353–64.

38. Mond JJ, Lees A, Snapper CM. T cell-independent antigens type 2. Annu Rev Immunol 1995;13:655–92.

39. Jegerlehner A, Maurer P, Bessa J, Hinton HJ, Kopf M, Bachmann MF. TLR9 signaling in B cells determines class switch recombination to IgG2a. J Immunol 2007;178:2415–20.

40. Phelan JD, Young RM, Webster DE, Roulland S, Wright GW, Kasbekar M, et al. A multiprotein supercomplex controlling oncogenic signalling in lymphoma. Nature 2018;560:387–91.

41. Soderberg O, Leuchowius KJ, Gullberg M, Jarvius M, Weibrecht I, Larsson LG, et al. Characterizing proteins and their interactions in cells and tissues using the in situ proximity ligation assay. Methods 2008;45:227–32.

42. Shugay M, Britanova OV, Merzlyak EM, Turchaninova MA, Mamedov IZ, Tuganbaev TR, et al. Towards error-free profiling of immune repertoires. Nat Methods 2014;11:653–5.

43. Zhang J, Dominguez-Sola D, Hussein S, Lee JE, Holmes AB, Bansal M, et al. Disruption of KMT2D perturbs germinal center B cell development and promotes lymphomagenesis. Nat Med 2015;21:1190–8.

44. Sander S, Calado DP, Srinivasan L, Kochert K, Zhang B, Rosolowski M, et al. Synergy between PI3K signaling and MYC in Burkitt lymphomagenesis. Cancer Cell 2012;22:167–79.

45. Lech-Maranda E, Bienvenu J, Broussais-Guillaumot F, Warzocha K, Michallet AS, Robak T, et al. Plasma TNF-alpha and IL-10 level-based prognostic model predicts outcome of patients with diffuse large B-cell lymphoma in different risk groups defined by the International Prognostic Index. Arch Immunol Ther Exp 2010;58: 131–41.

46. Rothman N, Skibola CF, Wang SS, Morgan G, Lan Q, Smith MT, et al. Genetic variation in TNF and IL10 and risk of non-Hodgkin lymphoma: a report from the InterLymph Consortium. Lancet Oncol 2006;7:27–38.

47. Wilson AG, Symons JA, McDowell TL, McDevitt HO, Duff GW. Effects of a polymorphism in the human tumor necrosis factor alpha promoter on transcriptional activation. Proc Natl Acad Sci U S A 1997;94:3195–9.

48. Heesen M, Kunz D, Bachmann-Mennenga B, Merk HF, Bloemeke B. Linkage disequilibrium between tumor necrosis factor (TNF)-alpha-308 G/A promoter and TNF-beta NcoI polymorphisms: association with TNF-alpha response of granulocytes to endotoxin stimulation. Crit Care Med 2003;31:211–4.

49. Bouma G, Crusius JB, Oudkerk Pool M, Kolkman JJ, von Blomberg BM, Kostense PJ, et al. Secretion of tumour necrosis factor alpha and lymphotoxin alpha in relation to polymorphisms in the TNF genes and HLA-DR alleles. Relevance for inflammatory bowel disease. Scand J Immunol. 1996;43:456–63.

50. Beyer M, Abdullah Z, Chemnitz JM, Maisel D, Sander J, Lehmann C, et al. Tumor-necrosis factor impairs CD4(+) T cell-mediated immunological control in chronic viral infection. Nat Immunol 2016;17: 593–603.

51. Bhat P, Leggatt G, Waterhouse N, Frazer IH. Interferon-gamma derived from cytotoxic lymphocytes directly enhances their motility and cytotoxicity. Cell Death Dis 2017;8:e2836.

52. Whitmire JK, Tan JT, Whitton JL. Interferon-gamma acts directly on CD8+ T cells to increase their abundance during virus infection. J Exp Med 2005;201:1053–9.

53. Armitage RJ, Macduff BM, Eisenman J, Paxton R, Grabstein KH. IL-15 has stimulatory activity for the induction of B cell proliferation and differentiation. J Immunol 1995;154:483–90.

54. Gearing A, Thorpe R, Bird C, Spitz M. Human B cell proliferation is stimulated by interleukin 2. Immunol Lett 1985;9:105–8.

55. Maier T, Guell M, Serrano L. Correlation of mRNA and protein in complex biological samples. FEBS Lett 2009;583:3966–73.

56. Deng J, Carlson N, Takeyama K, Dal Cin P, Shipp M, Letai A. BH3 profiling identifies three distinct classes of apoptotic blocks to predict response to ABT-737 and conventional chemotherapeutic agents. Cancer Cell 2007;12:171–85.

57. Souers AJ, Leverson JD, Boghaert ER, Ackler SL, Catron ND, Chen J, et al. ABT-199, a potent and selective BCL-2 inhibitor, achieves antitumor activity while sparing platelets. Nat Med 2013;19:202–8.

58. Pham LV, Huang S, Zhang H, Zhang J, Bell T, Zhou S, et al. Strategic therapeutic targeting to overcome venetoclax resistance in aggressive B-cell lymphomas. Clin Cancer Res 2018;24:3967–80.

59. Certo M, Del Gaizo Moore V, Nishino M, Wei G, Korsmeyer S, Armstrong SA, et al. Mitochondria primed by death signals determine cellular addiction to antiapoptotic BCL-2 family members. Cancer Cell 2006;9:351–65.

60. Prescott JA, Cook SJ. Targeting IKKbeta in cancer: challenges and opportunities for the therapeutic utilisation of IKKbeta inhibitors. Cells 2018;7:115.

61. Juarez-Salcedo LM, Sandoval-Sus J, Sokol L, Chavez JC, Dalia S. The role of anti-PD-1 and anti-PD-L1 agents in the treatment of diffuse large B-cell lymphoma: the future is now. Crit Rev Oncol Hematol 2017;113:52–62.

62. Lesokhin AM, Ansell SM, Armand P, Scott EC, Halwani A, Gutierrez M, et al. Nivolumab in patients with relapsed or refractory hematologic malignancy: preliminary results of a phase Ib study. J Clin Oncol 2016;34:2698–704.

63. Chen J, Jiang CC, Jin L, Zhang XD. Regulation of PD-L1: a novel role of pro-survival signalling in cancer. Ann Oncol 2016;27:409–16.

64. Georgiou K, Chen L, Berglund M, Ren W, de Miranda NF, Lisboa S, et al. Genetic basis of PD-L1 overexpression in diffuse large B-cell lymphomas. Blood 2016;127:3026–34.

65. Davids MS, Roberts AW, Seymour JF, Pagel JM, Kahl BS, Wierda WG, et al. Phase I first-in-human study of venetoclax in patients with relapsed or refractory non-Hodgkin lymphoma. J Clin Oncol 2017;35:826–33.

66. Grosso JF, Kelleher CC, Harris TJ, Maris CH, Hipkiss EL, De Marzo A, et al. LAG-3 regulates CD8+ T cell accumulation and effector function in murine self- and tumor-tolerance systems. J Clin Invest 2007; 117:3383–92.

67. Macon-Lemaitre L, Triebel F. The negative regulatory function of the lymphocyte-activation gene-3 co-receptor (CD223) on human T cells. Immunology 2005;115:170–8.

68. Tang R, Rangachari M, Kuchroo VK. Tim-3: a co-receptor with diverse roles in T cell exhaustion and tolerance. Semin Immunol 2019;42:101302.

69. Mita Y, Kimura MY, Hayashizaki K, Koyama-Nasu R, Ito T, Motohashi S, et al. Crucial role of CD69 in anti-tumor immunity through regulating the exhaustion of tumor-infiltrating T cells. Int Immunol 2018;30:559–67.

70. Yi JS, Cox MA, Zajac AJ. T-cell exhaustion: characteristics, causes and conversion. Immunology 2010;129:474–81.

71. Man K, Gabriel SS, Liao Y, Gloury R, Preston S, Henstridge DC, et al. Transcription factor IRF4 promotes CD8(+) T cell exhaustion and limits the development of memory-like T cells during chronic infection. Immunity 2017;47:1129–41.

72. Menk AV, Scharping NE, Rivadeneira DB, Calderon MJ, Watson MJ, Dunstane D, et al. 4-1BB costimulation induces T cell mitochondrial function and biogenesis enabling cancer immunotherapeutic responses. J Exp Med 2018;215:1091–100.

73. Williams JB, Horton BL, Zheng Y, Duan Y, Powell JD, Gajewski TF. The EGR2 targets LAG-3 and 4-1BB describe and regulate dysfunctional antigen-specific CD8+ T cells in the tumor microenvironment. J Exp Med 2017;214:381–400.

74. Torgovnick A, Heger JM, Liaki V, Isensee J, Schmitt A, Knittel G, et al. The Cdkn1a(SUPER) mouse as a tool to study p53-mediated tumor suppression. Cell Rep 2018;25:1027–39.

75. Yang G, Zhou Y, Liu X, Xu L, Cao Y, Manning RJ, et al. A mutation in MYD88 (L265P) supports the survival of lymphoplasmacytic cells by activation of Bruton tyrosine kinase in Waldenstrom macroglobulinemia. Blood 2013;122:1222–32.

76. Wang JQ, Jeelall YS, Beutler B, Horikawa K, Goodnow CC. Consequences of the recurrent MYD88(L265P) somatic mutation for B cell tolerance. J Exp Med 2014;211:413–26.

77. Dameshek W, Schwartz RS. Leukemia and auto-immunization-some possible relationships. Blood 1959;14:1151–8.

78. Young RM, Phelan JD, Wilson WH, Staudt LM. Pathogenic B-cell receptor signaling in lymphoid malignancies: new insights to improve treatment. Immunol Rev 2019;291:190–213.

79. Young RM, Wu T, Schmitz R, Dawood M, Xiao W, Phelan JD, et al. Survival of human lymphoma cells requires B-cell receptor engagement by self-antigens. Proc Natl Acad Sci U S A 2015;112: 13447–54.

80. Cerhan JR, Kricker A, Paltiel O, Flowers CR, Wang SS, Monnereau A, et al. Medical history, lifestyle, family history, and occupational risk factors for diffuse large B-cell lymphoma: the InterLymph Non-Hodgkin Lymphoma Subtypes Project. J Natl Cancer Inst Monogr 2014; 2014:15–25.

81. Pascual M, Mena-Varas M, Robles EF, Garcia-Barchino MJ, Panizo C, Hervas-Stubbs S, et al. PD-1/PD-L1 immune checkpoint and p53 loss facilitate tumor progression in activated B-cell diffuse large B-cell lymphomas. Blood 2019;133:2401–12.

82. Liu J, Hamrouni A, Wolowiec D, Coiteux V, Kuliczkowski K, Hetuin D, et al. Plasma cells from multiple myeloma patients express B7-H1 (PD-L1) and increase expression after stimulation with IFN-{gamma} and TLR ligands via a MyD88-, TRAF6-, and MEK-dependent pathway. Blood 2007;110:296–304.

83. O'Steen S, Green DJ, Gopal AK, Orozco JJ, Kenoyer AL, Lin Y, et al. Venetoclax synergizes with radiotherapy for treatment of B-cell lymphomas. Cancer Res 2017;77:3885–93.

84. Tarantelli C, Lange M, Gaudio E, Cascione L, Spriano F, Kwee I, et al. Copanlisib synergizes with conventional and targeted agents including venetoclax in B- and T-cell lymphoma models. Blood Adv 2020;4:819–29.

85. Rickert RC, Roes J, Rajewsky K. B lymphocyte-specific, Cre-mediated mutagenesis in mice. Nucleic Acids Res 1997;25:1317–8.

86. Tuominen VJ, Ruotoistenmaki S, Viitanen A, Jumppanen M, Isola J. ImmunoRatio: a publicly available web application for quantitative image analysis of estrogen receptor (ER), progesterone receptor (PR), and Ki-67. Breast Cancer Res 2010;12:R56.

87. Scheel AH, Dietel M, Heukamp LC, Johrens K, Kirchner T, Reu S, et al. [Predictive PD-L1 immunohistochemistry for non-small cell lung cancer: current state of the art and experiences of the first German harmonization study]. Pathologe 2016;37:557–67.

88. Bolotin DA, Poslavsky S, Mitrophanov I, Shugay M, Mamedov IZ, Putintseva EV, et al. MiXCR: software for comprehensive adaptive immunity profiling. Nat Methods 2015;12:380–1.

89. Pang XP, Hershman JM, Chung M, Pekary AE. Characterization of tumor necrosis factor-alpha receptors in human and rat thyroid cells and regulation of the receptors by thyrotropin. Endocrinology 1989;125:1783–8.

90. Durinck S, Spellman PT, Birney E, Huber W. Mapping identifiers for the integration of genomic datasets with the R/Bioconductor package biomaRt. Nat Protoc 2009;4:1184–91.

91. Korotkevich G, Sukhov V, Sergushichev A. Fast gene set enrichment analysis. BioRxiv 060012 [Preprint]. 2019. Available from: https://doi.org/10.1101/060012.

92. Patro R, Duggal G, Love MI, Irizarry RA, Kingsford C. Salmon provides fast and bias-aware quantification of transcript expression. Nat Methods 2017;14:417–9.

93. Chevrier S, Crowell HL, Zanotelli VRT, Engler S, Robinson MD, Bodenmiller B. Compensation of signal spillover in suspension and imaging mass cytometry. Cell Syst 2018;6:612–20.

94. Ackermann S, Cartolano M, Hero B, Welte A, Kahlert Y, Roderwieser A, et al. A mechanistic classification of clinical phenotypes in neuroblastoma. Science 2018;362:1165–70.

95. Bhatia S, Diedrich D, Frieg B, Ahlert H, Stein S, Bopp B, et al. Targeting HSP90 dimerization via the C terminus is effective in imatinib-resistant CML and lacks the heat shock response. Blood 2018;132:307–20.

96. Dietrich S, Oles M, Lu J, Sellner L, Anders S, Velten B, et al. Drug-perturbation-based stratification of blood cancer. J Clin Invest 2018;128:427–45.

97. Pemovska T, Kontro M, Yadav B, Edgren H, Eldfors S, Szwajda A, et al. Individualized systems medicine strategy to tailor treatments for patients with chemorefractory acute myeloid leukemia. Cancer Discov 2013;3:1416–29.

98. Klasener K, Maity PC, Hobeika E, Yang J, Reth M. B cell activation involves nanoscale receptor reorganizations and inside-out signaling by Syk. Elife 2014;3:e02069.

99. Allalou A, Wahlby C. BlobFinder, a tool for fluorescence microscopy image cytometry. Comput Methods Programs Biomed 2009;94:58–65.

100. Ryan J, Letai A. BH3 profiling in whole cells by fluorimeter or FACS. Methods 2013;61:156–64.

101. Hans CP, Weisenburger DD, Greiner TC, Gascoyne RD, Delabie J, Ott G, et al. Confirmation of the molecular classification of diffuse large B-cell lymphoma by immunohistochemistry using a tissue microarray. Blood 2004;103:275–82.

American Association for Cancer Research®

An Autochthonous Mouse Model of *Myd88*- and *BCL2*-Driven Diffuse Large B-cell Lymphoma Reveals Actionable Molecular Vulnerabilities

Ruth Flümann, Tim Rehkämper, Pascal Nieper, et al.

Updated version	Access the most recent version of this article at: doi: 10.1158/2643-3230.BCD-19-0059
Supplementary Material	Access the most recent supplemental material at: http://bloodcancerdiscov.aacrjournals.org/content/suppl/2020/10/31/2643-3230.BCD-19-0059.DC1

E-mail alerts	Sign up to receive free email-alerts related to this article or journal.
Reprints and Subscriptions	To order reprints of this article or to subscribe to the journal, contact the AACR Publications Department at pubs@aacr.org.
Permissions	To request permission to re-use all or part of this article, use this link http://bloodcancerdiscov.aacrjournals.org/content/early/2020/12/01/2643-3230.BCD-19-0059. Click on "Request Permissions" which will take you to the Copyright Clearance Center's (CCC) Rightslink site.

5   Discussion

In this project we characterized a mouse model of *Myd88*- and *BCL2*- driven DLBCL. In this model, an allele was generated that allows the conditional expression of *Myd88* p.L252P, which is localized at the orthologous position of human *Myd88* p.L265P[118]. The expression of the mutant is induced upon B-cell specific Cre-mediated recombination[61]. We observed that upon *CD19:Cre* activation the mutant *Myd88* p.L252P leads to a loss of self-tolerance and exaggerated responses to thymus-independent antigen (TI antigen)[118]. Together with the B-cell-specific overexpression of human *BCL2* cDNA, *Myd88* p.L252P cooperates in DLBCL lymphomagenesis[118]. Gene expression profiling clearly shows that the resulting lymphomas reveal a profile very similar to the human MCD/C5-DLBCL (Figure 4G; Supplementary Fig. S3F)[118]. Furthermore, these murine lymphomas spontaneously acquire mutations in *Pim1, Myc, Pouf2f, Nfkbia,* and *Kmt2d* (Fig. 4H; Supplementary Table S1)[118] that are also detectable in human DLBCL.

To gather a better understanding of how the *Myd88* p.L252P mutation leads to lymphomagenesis, we investigated the effects of *Myd88* p.L252P expression in non-transformed B-cells. Therefore, we analyzed the formation of MYD88-centered protein complexes in naïve B-cells. As shown in Figure 3, MYD88 forms significantly more complexes with IRAK1, IRAK4, IgM and BTK compared to the WT control[118]. This finding suggests that MYD88[p.L252P] is constantly forming signaling complexes linking BCR and TLR signaling molecules even in non-transformed cells. This finding is in line with the recently published presence of the so called My-T-BCR complex in ABC-DLBCL lymphoma cell lines[106]. Furthermore, these data are underlined by a recent report that suggests the localization of BTK in a protein complex with MYD88 in p.L252P-expressing OCI-Ly3 DLBCL cell lines[118,119].

The impact of *MYD88* p.L252P expression and *BCL2* overexpression on non-transformed cells further shows the presence of autoreactive antibodies in MC, BC, and MBC animals (Fig. 2A-D)[118]. While all three animals showed increased levels of autoantibodies compared to the wildtype, the staining patterns were different (Fig. 2A-D). *BCL2* overexpression resulted mainly in the appearance of IgG anti-nuclear antibodies, whereas MC animals showed a cytoplasmic pattern, predominantly of the IgM isotype (Fig. 2A-F). These differences are likely to reflect the distinct roles of MYD88 and BCL2 in B-cell activation.

Activation of a B-cell requires an antigen binding by the B-cell-receptor. Antigens are classified in two main groups, thymus independent antigens (TI antigen) and thymus-dependent antigens (TD antigen)[47,63]. TI antigens are non-protein molecules and they cannot cooperate with MHC-II molecules and are therefore unable to stimulate T-cell help[47]. TI antigens are for example repetitive, large molecular weight structures that are able to induce cross-linking of BCR molecules (TI-2 antigens)[47]. The cross-linking can activate the B-cell and initiate humoral immune response without T-cell help[47,120,121]. It has been suggested that a second signal is

needed for B-cell activation by TI-2 antigens [120]. This second signal would prevent multivalent cellular components to activate B cells by cross-linking[63].

While TI-2 antigens result in clonal B-cell activation the other subgroup of TI antigens, TI-1 antigens, can cause a polyclonal activation because the recognizing receptors are TLRs[120,122]. Furthermore, these TI-1 antigens can provide the stimulating second signal needed for B-cell activation[47]. MAMPs recognized by TLRs can be a further option for a second signal to B-cells that recognize non-peptide bacterial antigens, allowing for the production of anti-bacterial IgM antibodies[123].

The structures bound by self-reactive IgM antibodies in MC mice might resemble a bacterial antigen in different ways (Fig. 2A). First, due to the "self" nature of the antigen and the non-protein structure there is no T-cell help available[63]. Secondly the BCR crosslinking is able to activate the BCR-pathway[63]. Lastly, the TLR signaling is active due to the presence of MAMPs or as a result of the *Myd88* p.L252P mutation[63].

Especially the reproduceable detection of autoreactive antibodies in MC animals was surprising, as it clearly suggests that the expression of *Myd88* p.L252P alone is tolerated *in vivo*[118]. The *in vivo* tolerance of *Myd88* p.L252P as shown is in contrast to a recently reported transplantation experiment where mature B-cells were transduced with *MYD88* p.L265P and transplanted into *Rag1*$^{-/-}$ recipients[100]. In this experiment *MYD88* p.L265P initiated a proliferation burst in mature B-cells, *in vivo* and *in vitro*[100]. However the proliferation burst and NFκB activation were countered by the induction of TNFAIP3 and limited in a Bim-dependent manner[100]. Hence, it is important to emphasize that an overexpression system by transduction was used in the experiments, whereas the *Myd88* p.L252P expression in our model is from the endogenous locus *in vivo* (Fig. 1A)[61,118]. Furthermore, in our model the entire B-cell pool carries the *Myd88* p.L252P mutation as it is activated by Cd19^{Cre} (Fig. 1A)[118]. Therefore, B-cell competition is limited in our mouse model.

For a long time it is postulated that the stimulation of the BCR might play a role in lymphomagenesis[124]. Hepatitis C (HCV) or *Helicobacter pylori* are proven to be associated with the development of splenic marginal zone lymphoma (SMZL) and mucosa-associated lymphoid tissue lymphoma[125]. The observation that there is an increased presence of autoreactive IgG and IgM antibodies in lymphomas of MBC mice (Fig. 2 A-D) is in line with that[118]. Moreover, it is shown that in HCV-associated SMZL, a single BCR specific to a glycoprotein in the viral envelope was detected, that suggests that the virus contributes to BCR signaling in SMZL[125]. This example of infection-driven BCR signaling given, our detection of autoreactive antibodies in MBC mice is in line with the hypothesis that permanent engagement of the BCR by a self-antigen might be the reason for chronic active BCR signaling[88,118]. In fact, BCR stimulation by self-antigens is correlated with lymphomagenesis. As shown by an epidemiologic analysis DLBCL is associated with B-cell activating autoimmune diseases, such

as Sjögren´s syndrome or systemic lupus erythematosus[126]. Furthermore, analyses of V_H gene segment in DLBCL revealed that segment V_H4-34 is utilized in around 30% of ABC-DLBCL cases[88,118]. Further, human cell line models of ABC-DLBCL with chronic active BCR signaling provided further evidence for autoreactivity of the V_H4-34 segment[118]. In the OCI-Ly10 cell line, for example, the chronic active BCR signaling is driven by BCR recognition of an antigen in the debris of apoptotic cells[88,118]. The ABC-DLBCL cell line HBL1 on the other hand showed to be dependent on self-glycoproteins on its own cell surface[88,118]. Lastly, the cell line TMD8 depends on homotypic interactions with its own FR2 domain, which then leads to chronic active BCR signaling[88]. The discussed examples of three DLBCL cell lines indicate that the chronic active BCR signaling is based on a large amount of self-antigens[118]. These self-antigens might be responsible for maintaining the survival of the ABC-DLBCL cells. Based on these data, one can speculate that in our MBC mouse model, the enlarged pool of B- cells that are activated by self-antigen and in which anergy is repressed by MYD88-driven TLR signaling, might increase the pool of cells that could possibly transform malignant[118].

We also established our MBC mouse model as a preclinical tool for MCD/C5-DLBCL. The lymphomas derived from that model as well as the cell lines mimic central features of the human MCD/C5-DLBCL or former ABC-DLBCL like surface marker profiles, expression profiles, driver mutations and spontaneously developing mutational profile[118]. Especially the analysis and comparison of human and murine tissue specimens and transcription profiles revealed that ABC-DLBCL cases display higher CD274 (encoding PD-L1) levels than GCB-DLBCL cases[118]. These findings are supported by a previously published study in which Cd274 expression in murine $C\gamma1^{Cre/WT};Ikk2CAGFP^{LSL/LSL};Prdm1^{fl/fl-}$ and $C\gamma1^{Cre/WT};Tp53fl/fl;Ikk2CAGFP^{LSL/LSL};Prdm1^{fl/fl-}$ derived murine lymphoma cells, which overexpress the NFκB activator IKK2, compared with $C\gamma1^{Cre/WT};YFP^{LSL/WT}$ GCB cells is increased[127]. In our mouse model there is further evidence that mechanistically supports the high PD-L1 expression levels: It was recently shown that IFNy and MYD88-dependent TLR signaling drives the *PD-L1* expression levels in multiple myeloma cells[128]. Fittingly the IFNy levels in the serum of MBC mice compared to WT serum (Figure 4I) showed to be significantly higher[118].

In addition to that an *in silico* analysis showed that there is a fraction of 22% in human DLBCL cases that harbor high *BCL2* levels and a high expression of *CD274*[118]. To check for a possible treatment regimen, we performed a combined BCL2 and PD-1 blockade in our MBC mice. It shows that the single agents only have a mild activity in the MBC mice, but the combined therapy with the BCL2-inhibitor venetoclax and the aPD1-antibody RMP1-14 proofed to show a benefit in overall survival and tumor volume control. As others have shown before, the single agent RPM1-14 has no significant survival benefit in lymphoma bearing mice, but in combination with an anti-CD20 blockade it shows synergistic effects[129]. This study goes in line

with our observations, as we could not observe a survival benefit with the single blockade of PD-1[118].

To sum up, the further clinical development of a combined BCL2 and PD-1 blockade is underlined by our observations. It is important to note that the single agent use of venetoclax and nivolumab in refractory/relapsed DLBCL recently showed an overall response rate of 18% and 36%[130,131], respectively. Our project and preclinical use of MBC mice for a combined therapy with BCL2 and PD-1 blockade now indicate that a combined therapy might be well suited for relapsed/refractory DLBCL patients with high BCL2 and PD-1 levels. Also, we could show that there is a fraction of patient of around 20% that show these high levels[118]. Furthermore, the treatment regimen with a combination of BCL2 and PD-1 blockade would be a great chance for our patients that are not eligible for intensive consolidation regimens.

Altogether we could provide a detailed molecular analysis of the MBC model and its use as a preclinical tool. Our experiments indicate that our MBC derived lymphoma reflect key aspects of the human MCD/C5-DLBCL. Moreover, we could point out a reasonable combined therapy approach for the treatment of *MYD88* and *BCL2* high expressing lymphomas.

6   Bibliography

1.   Torre LA, Bray F, Siegel RL, Ferlay J, Lortet-Tieulent J, Jemal A. Global cancer statistics, 2012. *CA: a cancer journal for clinicians* 2015; **65**(2): 87-108.
2.   Bray F, Jemal A, Grey N, Ferlay J, Forman D. Global cancer transitions according to the Human Development Index (2008-2030): a population-based study. *The Lancet Oncology* 2012; **13**(8): 790-801.
3.   Luo J, Solimini NL, Elledge SJ. Principles of cancer therapy: oncogene and non-oncogene addiction. *Cell* 2009; **136**(5): 823-37.
4.   Weinstein IB, Joe A. Oncogene addiction. *Cancer Res* 2008; **68**(9): 3077-80; discussion 80.
5.   Roberts PJ, Der CJ. Targeting the Raf-MEK-ERK mitogen-activated protein kinase cascade for the treatment of cancer. *Oncogene* 2007; **26**(22): 3291-310.
6.   Sharma SV, Bell DW, Settleman J, Haber DA. Epidermal growth factor receptor mutations in lung cancer. *Nature reviews Cancer* 2007; **7**(3): 169-81.
7.   Lenz G, Staudt LM. Aggressive lymphomas. *The New England journal of medicine* 2010; **362**(15): 1417-29.
8.   Armitage JO. My treatment approach to patients with diffuse large B-cell lymphoma. *Mayo Clinic proceedings* 2012; **87**(2): 161-71.
9.   Pfreundschuh M, Kuhnt E, Trumper L, et al. CHOP-like chemotherapy with or without rituximab in young patients with good-prognosis diffuse large-B-cell lymphoma: 6-year results of an open-label randomised study of the MabThera International Trial (MInT) Group. *The Lancet Oncology* 2011; **12**(11): 1013-22.
10.   Schmitz N, Nickelsen M, Ziepert M, et al. Conventional chemotherapy (CHOEP-14) with rituximab or high-dose chemotherapy (MegaCHOEP) with rituximab for young, high-risk patients with aggressive B-cell lymphoma: an open-label, randomised, phase 3 trial (DSHNHL 2002-1). *The Lancet Oncology* 2012; **13**(12): 1250-9.
11.   Chiappella A, Martelli M, Angelucci E, et al. Rituximab-dose-dense chemotherapy with or without high-dose chemotherapy plus autologous stem-cell transplantation in high-risk diffuse large B-cell lymphoma (DLCL04): final results of a multicentre, open-label, randomised, controlled, phase 3 study. *The Lancet Oncology* 2017; **18**(8): 1076-88.
12.   Basso K, Dalla-Favera R. Germinal centres and B cell lymphomagenesis. *Nature reviews Immunology* 2015; **15**(3): 172-84.
13.   Rosenwald A, Wright G, Chan WC, et al. The use of molecular profiling to predict survival after chemotherapy for diffuse large-B-cell lymphoma. *The New England journal of medicine* 2002; **346**(25): 1937-47.
14.   Reddy A, Zhang J, Davis NS, et al. Genetic and Functional Drivers of Diffuse Large B Cell Lymphoma. *Cell* 2017; **171**(2): 481-94.e15.
15.   Schmitz R, Wright GW, Huang DW, et al. Genetics and Pathogenesis of Diffuse Large B-Cell Lymphoma. *The New England journal of medicine* 2018; **378**(15): 1396-407.
16.   Chapuy B, Stewart C, Dunford AJ, et al. Molecular subtypes of diffuse large B cell lymphoma are associated with distinct pathogenic mechanisms and outcomes. *Nature medicine* 2018; **24**(5): 679-90.
17.   Hajdu SI. A note from history: landmarks in history of cancer, part 1. *Cancer* 2011; **117**(5): 1097-102.
18.   Ribatti D. An historical note on the cell theory. *Exp Cell Res* 2018; **364**(1): 1-4.
19.   Weinberg RA. The biology of cancer: Garland Science, Taylor and Francis Group; 2014.

20.   Hajdu SI. A note from history: landmarks in history of cancer, part 3. *Cancer* 2012; **118**(4): 1155-68.

21.   Hajdu SI, Vadmal M. A note from history: Landmarks in history of cancer, Part 6. *Cancer* 2013; **119**(23): 4058-82.

22.   Hanahan D, Weinberg RA. The hallmarks of cancer. *Cell* 2000; **100**(1): 57-70.

23.   Hanahan D, Weinberg RA. Hallmarks of cancer: the next generation. *Cell* 2011; **144**(5): 646-74.

24.   Tomasetti C, Li L, Vogelstein B. Stem cell divisions, somatic mutations, cancer etiology, and cancer prevention. *Science (New York, NY)* 2017; **355**(6331): 1330-4.

25.   Greaves M, Maley CC. Clonal evolution in cancer. *Nature* 2012; **481**(7381): 306-13.

26.   Landau DA, Carter SL, Stojanov P, et al. Evolution and impact of subclonal mutations in chronic lymphocytic leukemia. *Cell* 2013; **152**(4): 714-26.

27.   Carter SL, Cibulskis K, Helman E, et al. Absolute quantification of somatic DNA alterations in human cancer. *Nat Biotechnol* 2012; **30**(5): 413-21.

28.   Gerlinger M, Swanton C. How Darwinian models inform therapeutic failure initiated by clonal heterogeneity in cancer medicine. *Br J Cancer* 2010; **103**(8): 1139-43.

29.   Druker BJ, Tamura S, Buchdunger E, et al. Effects of a selective inhibitor of the Abl tyrosine kinase on the growth of Bcr-Abl positive cells. *Nature medicine* 1996; **2**(5): 561-6.

30.   Lee CS, Rattu MA, Kim SS. A review of a novel, Bruton's tyrosine kinase inhibitor, ibrutinib. *J Oncol Pharm Pract* 2016; **22**(1): 92-104.

31.   Ventura A, Kirsch DG, McLaughlin ME, et al. Restoration of p53 function leads to tumour regression in vivo. *Nature* 2007; **445**(7128): 661-5.

32.   Martins CP, Brown-Swigart L, Evan GI. Modeling the therapeutic efficacy of p53 restoration in tumors. *Cell* 2006; **127**(7): 1323-34.

33.   Xue W, Zender L, Miething C, et al. Senescence and tumour clearance is triggered by p53 restoration in murine liver carcinomas. *Nature* 2007; **445**(7128): 656-60.

34.   Romano G. Development of safer gene delivery systems to minimize the risk of insertional mutagenesis-related malignancies: a critical issue for the field of gene therapy. *ISRN Oncol* 2012; **2012**: 616310.

35.   Vassilev LT, Vu BT, Graves B, et al. In vivo activation of the p53 pathway by small-molecule antagonists of MDM2. *Science (New York, NY)* 2004; **303**(5659): 844-8.

36.   Konopleva M, Martinelli G, Daver N, et al. MDM2 inhibition: an important step forward in cancer therapy. *Leukemia* 2020; **34**(11): 2858-74.

37.   Reinhardt HC, Jiang H, Hemann MT, Yaffe MB. Exploiting synthetic lethal interactions for targeted cancer therapy. *Cell Cycle* 2009; **8**(19): 3112-9.

38.   Kaelin WG, Jr. The concept of synthetic lethality in the context of anticancer therapy. *Nature reviews Cancer* 2005; **5**(9): 689-98.

39.   Bryant HE, Schultz N, Thomas HD, et al. Specific killing of BRCA2-deficient tumours with inhibitors of poly(ADP-ribose) polymerase. *Nature* 2005; **434**(7035): 913-7.

40.   Farmer H, McCabe N, Lord CJ, et al. Targeting the DNA repair defect in BRCA mutant cells as a therapeutic strategy. *Nature* 2005; **434**(7035): 917-21.

41.   Arora S, Balasubramaniam S, Zhang H, et al. FDA Approval Summary: Olaparib Monotherapy or in Combination with Bevacizumab for the Maintenance Treatment of Patients with Advanced Ovarian Cancer. *Oncologist* 2021; **26**(1): e164-e72.

42.   VanderWeele DJ, Hussain M. PARP inhibitors in prostate cancer: practical guidance for busy clinicians. *Clin Adv Hematol Oncol* 2020; **18**(12): 808-15.

43. Knittel G, Rehkämper T, Korovkina D, et al. Two mouse models reveal an actionable PARP1 dependence in aggressive chronic lymphocytic leukemia. *Nat Commun* 2017; **8**(1): 153.

44. Knittel G, Liedgens P, Korovkina D, Pallasch CP, Reinhardt HC. Rewired NFkappaB signaling as a potentially actionable feature of activated B-cell-like diffuse large B-cell lymphoma. *European journal of haematology* 2016; **97**(6): 499-510.

45. Shaffer AL, 3rd, Young RM, Staudt LM. Pathogenesis of human B cell lymphomas. *Annual review of immunology* 2012; **30**: 565-610.

46. Swerdlow SH, Campo E, Pileri SA, et al. The 2016 revision of the World Health Organization classification of lymphoid neoplasms. *Blood* 2016; **127**(20): 2375-90.

47. Murphy K, Weaver C. Janeway´s Immunobiology. New York, NY: Garland Science; 2017.

48. Damle RN, Wasil T, Fais F, et al. Ig V gene mutation status and CD38 expression as novel prognostic indicators in chronic lymphocytic leukemia. *Blood* 1999; **94**(6): 1840-7.

49. Hamblin TJ, Davis Z, Gardiner A, Oscier DG, Stevenson FK. Unmutated Ig V(H) genes are associated with a more aggressive form of chronic lymphocytic leukemia. *Blood* 1999; **94**(6): 1848-54.

50. Alizadeh AA, Eisen MB, Davis RE, et al. Distinct types of diffuse large B-cell lymphoma identified by gene expression profiling. *Nature* 2000; **403**(6769): 503-11.

51. Wright G, Tan B, Rosenwald A, Hurt EH, Wiestner A, Staudt LM. A gene expression-based method to diagnose clinically distinct subgroups of diffuse large B cell lymphoma. *Proceedings of the National Academy of Sciences of the United States of America* 2003; **100**(17): 9991-6.

52. Dave SS, Fu K, Wright GW, et al. Molecular diagnosis of Burkitt's lymphoma. *The New England journal of medicine* 2006; **354**(23): 2431-42.

53. Isaacson PG, Du MQ. MALT lymphoma: from morphology to molecules. *Nature reviews Cancer* 2004; **4**(8): 644-53.

54. Basso K, Liso A, Tiacci E, et al. Gene expression profiling of hairy cell leukemia reveals a phenotype related to memory B cells with altered expression of chemokine and adhesion receptors. *The Journal of experimental medicine* 2004; **199**(1): 59-68.

55. Rui L, Schmitz R, Ceribelli M, Staudt LM. Malignant pirates of the immune system. *Nature immunology* 2011; **12**(10): 933-40.

56. Venturutti L, Melnick AM. The dangers of déjà vu: memory B cells as the cells of origin of ABC-DLBCLs. *Blood* 2020; **136**(20): 2263-74.

57. Venturutti L, Teater M, Zhai A, et al. TBL1XR1 Mutations Drive Extranodal Lymphoma by Inducing a Pro-tumorigenic Memory Fate. *Cell* 2020; **182**(2): 297-316.e27.

58. Hua C, Zorn S, Jensen JP, et al. Consequences of the t(14;18) chromosomal translocation in follicular lymphoma: deregulated expression of a chimeric and mutated BCL-2 gene. *Oncogene research* 1988; **2**(3): 263-75.

59. Schatz DG, Oettinger MA, Baltimore D. Pillars article: the V(D)J recombination activating gene, RAG-1. 1989. *Journal of immunology (Baltimore, Md : 1950)* 2008; **180**(1): 5-18.

60. Strasser A, Whittingham S, Vaux DL, et al. Enforced BCL2 expression in B-lymphoid cells prolongs antibody responses and elicits autoimmune disease. *Proceedings of the National Academy of Sciences of the United States of America* 1991; **88**(19): 8661-5.

61. Knittel G, Liedgens P, Korovkina D, et al. B-cell-specific conditional expression of Myd88p.L252P leads to the development of diffuse large B-cell lymphoma in mice. *Blood* 2016; **127**(22): 2732-41.

62. Klein U, Goossens T, Fischer M, et al. Somatic hypermutation in normal and transformed human B cells. *Immunological reviews* 1998; **162**: 261-80.

63. Knittel G. An autochthonous mouse model of MYD88 p.L265P- and BCL2-driven diffuse large B cell lymphoma. Cologne: University of Cologne; 2018.

64. Hans CP, Weisenburger DD, Greiner TC, et al. Confirmation of the molecular classification of diffuse large B-cell lymphoma by immunohistochemistry using a tissue microarray. *Blood* 2004; **103**(1): 275-82.

65. Choi WW, Weisenburger DD, Greiner TC, et al. A new immunostain algorithm classifies diffuse large B-cell lymphoma into molecular subtypes with high accuracy. *Clinical cancer research : an official journal of the American Association for Cancer Research* 2009; **15**(17): 5494-502.

66. Tilly H, Gomes da Silva M, Vitolo U, et al. Diffuse large B-cell lymphoma (DLBCL): ESMO Clinical Practice Guidelines for diagnosis, treatment and follow-up. *Annals of oncology : official journal of the European Society for Medical Oncology* 2015; **26 Suppl 5**: v116-25.

67. Ngo VN, Young RM, Schmitz R, et al. Oncogenically active MYD88 mutations in human lymphoma. *Nature* 2011; **470**(7332): 115-9.

68. Davis RE, Ngo VN, Lenz G, et al. Chronic active B-cell-receptor signalling in diffuse large B-cell lymphoma. *Nature* 2010; **463**(7277): 88-92.

69. Davis RE, Brown KD, Siebenlist U, Staudt LM. Constitutive nuclear factor kappaB activity is required for survival of activated B cell-like diffuse large B cell lymphoma cells. *The Journal of experimental medicine* 2001; **194**(12): 1861-74.

70. Willis TG, Jadayel DM, Du MQ, et al. Bcl10 is involved in t(1;14)(p22;q32) of MALT B cell lymphoma and mutated in multiple tumor types. *Cell* 1999; **96**(1): 35-45.

71. Savage KJ, Monti S, Kutok JL, et al. The molecular signature of mediastinal large B-cell lymphoma differs from that of other diffuse large B-cell lymphomas and shares features with classical Hodgkin lymphoma. *Blood* 2003; **102**(12): 3871-9.

72. Ni H, Ergin M, Huang Q, et al. Analysis of expression of nuclear factor kappa B (NF-kappa B) in multiple myeloma: downregulation of NF-kappa B induces apoptosis. *British journal of haematology* 2001; **115**(2): 279-86.

73. Bargou RC, Leng C, Krappmann D, et al. High-level nuclear NF-kappa B and Oct-2 is a common feature of cultured Hodgkin/Reed-Sternberg cells. *Blood* 1996; **87**(10): 4340-7.

74. Staudt LM. Oncogenic activation of NF-kappaB. *Cold Spring Harbor perspectives in biology* 2010; **2**(6): a000109.

75. Razani B, Reichardt AD, Cheng G. Non-canonical NF-kappaB signaling activation and regulation: principles and perspectives. *Immunological reviews* 2011; **244**(1): 44-54.

76. Gilmore TD. Introduction to NF-kappaB: players, pathways, perspectives. *Oncogene* 2006; **25**(51): 6680-4.

77. Vallabhapurapu S, Karin M. Regulation and function of NF-kappaB transcription factors in the immune system. *Annual review of immunology* 2009; **27**: 693-733.

78. Catz SD, Johnson JL. Transcriptional regulation of bcl-2 by nuclear factor kappa B and its significance in prostate cancer. *Oncogene* 2001; **20**(50): 7342-51.

79. Tracey L, Perez-Rosado A, Artiga MJ, et al. Expression of the NF-kappaB targets BCL2 and BIRC5/Survivin characterizes small B-cell and aggressive B-cell lymphomas, respectively. *The Journal of pathology* 2005; **206**(2): 123-34.

80. Baldwin AS. Control of oncogenesis and cancer therapy resistance by the transcription factor NF-kappaB. *The Journal of clinical investigation* 2001; **107**(3): 241-6.

81. Reth M. Antigen receptor tail clue. *Nature* 1989; **338**(6214): 383-4.

82. Saijo K, Schmedt C, Su IH, et al. Essential role of Src-family protein tyrosine kinases in NF-kappaB activation during B cell development. *Nature immunology* 2003; **4**(3): 274-9.

83. Rowley RB, Burkhardt AL, Chao HG, Matsueda GR, Bolen JB. Syk protein-tyrosine kinase is regulated by tyrosine-phosphorylated Ig alpha/Ig beta immunoreceptor tyrosine activation motif binding and autophosphorylation. *The Journal of biological chemistry* 1995; **270**(19): 11590-4.

84. Dal Porto JM, Gauld SB, Merrell KT, Mills D, Pugh-Bernard AE, Cambier J. B cell antigen receptor signaling 101. *Molecular immunology* 2004; **41**(6-7): 599-613.

85. Hashimoto A, Okada H, Jiang A, et al. Involvement of guanosine triphosphatases and phospholipase C-gamma2 in extracellular signal-regulated kinase, c-Jun NH2-terminal kinase, and p38 mitogen-activated protein kinase activation by the B cell antigen receptor. *The Journal of experimental medicine* 1998; **188**(7): 1287-95.

86. Shinohara H, Yasuda T, Aiba Y, et al. PKC beta regulates BCR-mediated IKK activation by facilitating the interaction between TAK1 and CARMA1. *The Journal of experimental medicine* 2005; **202**(10): 1423-31.

87. Deane JA, Fruman DA. Phosphoinositide 3-kinase: diverse roles in immune cell activation. *Annual review of immunology* 2004; **22**: 563-98.

88. Young RM, Wu T, Schmitz R, et al. Survival of human lymphoma cells requires B-cell receptor engagement by self-antigens. *Proceedings of the National Academy of Sciences of the United States of America* 2015; **112**(44): 13447-54.

89. Akira S, Takeda K. Toll-like receptor signalling. *Nature reviews Immunology* 2004; **4**(7): 499-511.

90. Compagno M, Lim WK, Grunn A, et al. Mutations of multiple genes cause deregulation of NF-kappaB in diffuse large B-cell lymphoma. *Nature* 2009; **459**(7247): 717-21.

91. Loiarro M, Volpe E, Ruggiero V, et al. Mutational analysis identifies residues crucial for homodimerization of myeloid differentiation factor 88 (MyD88) and for its function in immune cells. *The Journal of biological chemistry* 2013; **288**(42): 30210-22.

92. Lin SC, Lo YC, Wu H. Helical assembly in the MyD88-IRAK4-IRAK2 complex in TLR/IL-1R signalling. *Nature* 2010; **465**(7300): 885-90.

93. Gay NJ, Symmons MF, Gangloff M, Bryant CE. Assembly and localization of Toll-like receptor signalling complexes. *Nature reviews Immunology* 2014; **14**(8): 546-58.

94. Ferrao R, Zhou H, Shan Y, et al. IRAK4 dimerization and trans-autophosphorylation are induced by Myddosome assembly. *Molecular cell* 2014; **55**(6): 891-903.

95. Ye H, Arron JR, Lamothe B, et al. Distinct molecular mechanism for initiating TRAF6 signalling. *Nature* 2002; **418**(6896): 443-7.

96. Wang C, Deng L, Hong M, Akkaraju GR, Inoue J, Chen ZJ. TAK1 is a ubiquitin-dependent kinase of MKK and IKK. *Nature* 2001; **412**(6844): 346-51.

97. Li Q, Lu Q, Bottero V, et al. Enhanced NF-kappaB activation and cellular function in macrophages lacking IkappaB kinase 1 (IKK1). *Proceedings of the National Academy of Sciences of the United States of America* 2005; **102**(35): 12425-30.

98. Ntoufa S, Vilia MG, Stamatopoulos K, Ghia P, Muzio M. Toll-like receptors signaling: A complex network for NF-kappaB activation in B-cell lymphoid malignancies. *Seminars in cancer biology* 2016; **39**: 15-25.

99. Kawai T, Akira S. TLR signaling. *Seminars in immunology* 2007; **19**(1): 24-32.

100. Wang JQ, Jeelall YS, Beutler B, Horikawa K, Goodnow CC. Consequences of the recurrent MYD88(L265P) somatic mutation for B cell tolerance. *The Journal of experimental medicine* 2014; **211**(3): 413-26.

101. Puente XS, Pinyol M, Quesada V, et al. Whole-genome sequencing identifies recurrent mutations in chronic lymphocytic leukaemia. *Nature* 2011; **475**(7354): 101-5.

102. Treon SP, Xu L, Yang G, et al. MYD88 L265P somatic mutation in Waldenstrom's macroglobulinemia. *The New England journal of medicine* 2012; **367**(9): 826-33.

103. Landau DA, Tausch E, Taylor-Weiner AN, et al. Mutations driving CLL and their evolution in progression and relapse. *Nature* 2015; **526**(7574): 525-30.

104. Poulain S, Roumier C, Decambron A, et al. MYD88 L265P mutation in Waldenstrom macroglobulinemia. *Blood* 2013; **121**(22): 4504-11.

105. Avbelj M, Wolz OO, Fekonja O, et al. Activation of lymphoma-associated MyD88 mutations via allostery-induced TIR-domain oligomerization. *Blood* 2014; **124**(26): 3896-904.

106. Phelan JD, Young RM, Webster DE, et al. A multiprotein supercomplex controlling oncogenic signalling in lymphoma. *Nature* 2018; **560**(7718): 387-91.

107. Aster JC, Longtine JA. Detection of BCL2 rearrangements in follicular lymphoma. *Am J Pathol* 2002; **160**(3): 759-63.

108. Czabotar PE, Lessene G, Strasser A, Adams JM. Control of apoptosis by the BCL-2 protein family: implications for physiology and therapy. *Nat Rev Mol Cell Biol* 2014; **15**(1): 49-63.

109. Nakano K, Vousden KH. PUMA, a novel proapoptotic gene, is induced by p53. *Molecular cell* 2001; **7**(3): 683-94.

110. Oda E, Ohki R, Murasawa H, et al. Noxa, a BH3-only member of the Bcl-2 family and candidate mediator of p53-induced apoptosis. *Science (New York, NY)* 2000; **288**(5468): 1053-8.

111. McDonnell TJ, Korsmeyer SJ. Progression from lymphoid hyperplasia to high-grade malignant lymphoma in mice transgenic for the t(14; 18). *Nature* 1991; **349**(6306): 254-6.

112. Huang JZ, Sanger WG, Greiner TC, et al. The t(14;18) defines a unique subset of diffuse large B-cell lymphoma with a germinal center B-cell gene expression profile. *Blood* 2002; **99**(7): 2285-90.

113. Strasser A, Harris AW, Bath ML, Cory S. Novel primitive lymphoid tumours induced in transgenic mice by cooperation between myc and bcl-2. *Nature* 1990; **348**(6299): 331-3.

114. Green TM, Young KH, Visco C, et al. Immunohistochemical double-hit score is a strong predictor of outcome in patients with diffuse large B-cell lymphoma treated with rituximab plus cyclophosphamide, doxorubicin, vincristine, and prednisone. *J Clin Oncol* 2012; **30**(28): 3460-7.

115. Johnson NA, Slack GW, Savage KJ, et al. Concurrent expression of MYC and BCL2 in diffuse large B-cell lymphoma treated with rituximab plus cyclophosphamide, doxorubicin, vincristine, and prednisone. *J Clin Oncol* 2012; **30**(28): 3452-9.

116. Kersten K, de Visser KE, van Miltenburg MH, Jonkers J. Genetically engineered mouse models in oncology research and cancer medicine. *EMBO Mol Med* 2017; **9**(2): 137-53.

117. Cheon DJ, Orsulic S. Mouse models of cancer. *Annu Rev Pathol* 2011; **6**: 95-119.

118. Flümann R, Rehkämper T, Nieper P, et al. An Autochthonous Mouse Model of Myd88- and BCL2-Driven Diffuse Large B-cell Lymphoma Reveals Actionable Molecular Vulnerabilities. *Blood Cancer Discov* 2021; **2**(1): 70-91.

119. Yang G, Zhou Y, Liu X, et al. A mutation in MYD88 (L265P) supports the survival of lymphoplasmacytic cells by activation of Bruton tyrosine kinase in Waldenström macroglobulinemia. *Blood* 2013; **122**(7): 1222-32.

120. Vos Q, Lees A, Wu ZQ, Snapper CM, Mond JJ. B-cell activation by T-cell-independent type 2 antigens as an integral part of the humoral immune response to pathogenic microorganisms. *Immunological reviews* 2000; **176**: 154-70.

121. Fagarasan S, Honjo T. T-Independent immune response: new aspects of B cell biology. *Science (New York, NY)* 2000; **290**(5489): 89-92.

122. Mond JJ, Lees A, Snapper CM. T cell-independent antigens type 2. *Annual review of immunology* 1995; **13**: 655-92.

123. Alugupalli KR, Akira S, Lien E, Leong JM. MyD88- and Bruton's tyrosine kinase-mediated signals are essential for T cell-independent pathogen-specific IgM responses. *Journal of immunology (Baltimore, Md : 1950)* 2007; **178**(6): 3740-9.

124. Dameshek W, Schwartz RS. Leukemia and auto-immunization- some possible relationships. *Blood* 1959; **14**: 1151-8.

125. Young RM, Phelan JD, Wilson WH, Staudt LM. Pathogenic B-cell receptor signaling in lymphoid malignancies: New insights to improve treatment. *Immunological reviews* 2019; **291**(1): 190-213.

126. Cerhan JR, Kricker A, Paltiel O, et al. Medical history, lifestyle, family history, and occupational risk factors for diffuse large B-cell lymphoma: the InterLymph Non-Hodgkin Lymphoma Subtypes Project. *J Natl Cancer Inst Monogr* 2014; **2014**(48): 15-25.

127. Pascual M, Mena-Varas M, Robles EF, et al. PD-1/PD-L1 immune checkpoint and p53 loss facilitate tumor progression in activated B-cell diffuse large B-cell lymphomas. *Blood* 2019; **133**(22): 2401-12.

128. Liu J, Hamrouni A, Wolowiec D, et al. Plasma cells from multiple myeloma patients express B7-H1 (PD-L1) and increase expression after stimulation with IFN-{gamma} and TLR ligands via a MyD88-, TRAF6-, and MEK-dependent pathway. *Blood* 2007; **110**(1): 296-304.

129. O'Steen S, Green DJ, Gopal AK, et al. Venetoclax Synergizes with Radiotherapy for Treatment of B-cell Lymphomas. *Cancer Res* 2017; **77**(14): 3885-93.

130. Davids MS, Roberts AW, Seymour JF, et al. Phase I First-in-Human Study of Venetoclax in Patients With Relapsed or Refractory Non-Hodgkin Lymphoma. *J Clin Oncol* 2017; **35**(8): 826-33.

131. Lesokhin AM, Ansell SM, Armand P, et al. Nivolumab in Patients With Relapsed or Refractory Hematologic Malignancy: Preliminary Results of a Phase Ib Study. *J Clin Oncol* 2016; **34**(23): 2698-704.

7   Appendix

7.1   List of Figures

Franks Copy Shop

Münster, Germany